

Adaptive Multipath-Based SLAM for Distributed MIMO Systems

Xuhong Li*, *Member, IEEE*, Benjamin J. B. Deutschmann*, *Student Member, IEEE*, Erik Leitinger, *Member, IEEE*, Florian Meyer, *Member, IEEE*

Abstract—Localizing users and mapping the environment using radio signals is a key task in emerging applications such as reliable low-latency communications, location-aware security, and safety-critical navigation. Recently introduced multipath-based simultaneous localization and mapping (SLAM) methods can jointly localize a mobile agent and map reflective surfaces in radio frequency (RF) environments. Most existing approaches assume that map features and their corresponding RF propagation paths are statistically independent, conditioned on the state of the mobile agent. This assumption neglects inherent dependencies that arise when a single reflective surface contributes to multiple propagation paths or when an agent communicates with multiple base stations. Existing approaches that aim to fuse information across propagation paths are further limited by their inability to perform ray tracing in RF environments with nonconvex geometries.

In this paper, we propose a Bayesian multipath-based SLAM method for distributed multiple-input multiple-output (MIMO) systems that addresses these limitations. In particular, we exploit amplitude statistics to establish adaptive, time-varying detection probabilities. Based on the resulting “soft” ray-tracing strategy, the proposed method can fuse information across propagation paths in RF environments with nonconvex geometries. A Bayesian estimation framework for the joint estimation of map features and agent state is developed by applying the message passing rules of the sum-product algorithm (SPA) to a factor graph representation of the proposed statistical model. We further introduce a new initialization procedure for reflective surfaces that enables the introduction of new surface states even when measurements arise solely from double-bounce paths. The proposed method is validated using both synthetic and real RF measurements obtained in challenging scenarios with nonconvex geometries and obstructed line-of-sight conditions. The results demonstrate that it provides accurate localization and mapping performance and approaches the posterior Cramér–Rao lower bound.

I. INTRODUCTION

Ensuring reliable communication and sensing in harsh propagation environments, such as urban canyons and indoor spaces, remains a fundamental and challenging problem. Multipath-based simultaneous localization and mapping (SLAM) [1]–[9] in 5G and 6G networks has therefore attracted significant attention as a promising solution. Existing

Xuhong Li is with the Department of Electrical and Information Technology, Lund University, Sweden (email: xuhong.li@eit.lth.se). This work was performed at University of California San Diego, CA, USA. Benjamin J. B. Deutschmann and Erik Leitinger are with the Institute of Communication Networks and Satellite Communications, Graz University of Technology, Austria (email: {benjamin.deutschmann, erik.leitinger}@tugraz.at). Florian Meyer is with the Department of Electrical and Computer Engineering and the Scripps Institution of Oceanography, University of California San Diego, CA, USA (email: flmeyer@ucsd.edu). This work was supported by the Knut and Alice Wallenberg Foundation, by the Ericsson Research Foundation, by AMBIENT-6G project of the European Commission under Grant No. 101192113, and by the National Science Foundation (NSF) under CAREER Award No. 2146261.

Xuhong Li and Benjamin J. B. Deutschmann contributed equally as co-first authors to this work.

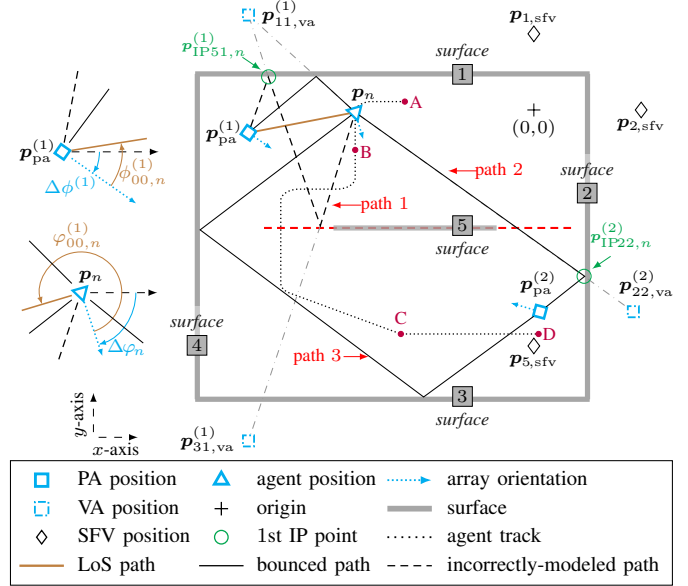


Fig. 1: Exemplary distributed multiple-input multiple-output (MIMO) (D-MIMO) radio frequency (RF) propagation scenario with five reflective surfaces $s \in \{1, \dots, 5\}$, two physical anchors (PAs) $p_{pa}^{(j)}$, and one mobile agent p_n . Reflective surfaces are represented by surface feature vectors (SFVs) $p_{s,svf}$, i.e., mirror images of a common origin $(0, 0)$ with respect to the surfaces. Reflected paths are modeled by virtual anchors (VAs) $p_{ss',va}^{(j)}$. The intersection point of each path with the first reflective surface is denoted by $p_{IP_{ss',n}}^{(j)}$. This intersection point determines the angle-of-departure (AoD). Array orientations, AoD, and angle-of-arrival (AoA) at PA 1 and the agent, respectively, are shown on the left side of the figure. The red dashed line indicates the infinite extent of surface 5 as assumed in previously proposed methods, e.g., [7]. In the absence of surface extent information, such an environmental model may introduce nonexistent paths such as path 1, while failing to account for existing paths such as paths 2 and 3, since the infinite extent of surface 5 would block these paths.

multipath-based SLAM methods are typically categorized as feature-based SLAM, in which propagation paths arising from RF signals interacting with environmental objects are modeled individually using independent map features, such as VAs and point scatterers. The VA is a commonly used feature type representing mirror images of PAs (e.g., base stations (BSs)) with respect to planar surfaces, thereby modeling specular RF reflections. In general, the number of features and their positions are unknown and time-varying. Multipath-based SLAM jointly estimates the mobile agent state and the locations of distinct features, either using measurements of multipath components (MPCs) that are extracted from received RF signals via parametric channel estimation [10]–[15], or directly from RF signals [9].

A. State-of-the-Art Methods

A common assumption in state-of-the-art multipath-based SLAM methods is that VAs corresponding to individual propagation paths are conditionally independent given the state of the agent. This assumption is restrictive, as multiple propagation paths may originate from interactions with the same environmental feature. In particular, a reflective surface (e.g., a wall) is an extended object that can simultaneously generate single-bounce as well as higher-order multi-bounce paths, all of which may significantly contribute to the received signal.

Recent work addresses this limitation by considering the mapping of extended objects [16] and by exploiting data fusion across MPCs in multipath-based SLAM [7], [17]–[21], demonstrating notable performance improvements. In particular, [17], [18], [22] propose methods that fuse information across single-bounce paths and cooperating agents. Furthermore, [20], [23] introduce statistical models that jointly account for diffuse MPCs arising from rough or non-ideal reflective surfaces, while [7] develops the master virtual anchors (MVAs) model for representing reflective surfaces that enables data fusion across paths up to double-bounce reflections and PAs.

A simple geometric model for a reflective surface, as used in [7], represents the surface as an infinite straight line characterized by its position and orientation, as well as binary decisions on the availability of propagation paths obtained via conventional “hard” ray tracing. While this model has been demonstrated to be effective in certain indoor experiments, it is essentially limited to convex room geometries. This is because in scenarios with nonconvex geometries, the infinite nature of the reflective surface represented by the SFVs “blocks” physically possible propagation path in the hard ray tracing process, making it impossible to reliably decide on the availability of propagation paths. An extension to nonconvex room geometries requires either (i) modeling and estimating the shape and size of the surface represented by the MVA; (ii) inferring the time-varying availability of propagation paths associated with each MVA. Approach (i) would introduce significant additional complexity and require dense measurements across the surface to yield reliable extent estimates [18], [20]. For this reason, we focus on approach (ii) in this paper.

State-of-the-art methods for localization and tracking using MPCs [24], [25] perform the estimation of complex path amplitudes that determine the detection probability of propagation paths and measurement variances related to each surface within a joint sequential Bayesian framework. The joint formulation enables reliable and adaptive feature detection even in the presence of measurement impairments such as clutter and missed detections.

B. Contributions

This paper introduces an adaptive multipath-based SLAM algorithm (AM-SLAM) for distributed MIMO (D-MIMO) systems that jointly estimates the position and orientation of the mobile agent, detects and localizes reflective surfaces, and is applicable to arbitrary room geometries.

A key novelty of the proposed approach is the introduction of a normalized amplitude and a binary existence variable for each potential first- and second-order propagation path, enabling the inference of the time-varying availability and strength of each path within a unified Bayesian framework. The method operates on MPC parameter estimates, e.g., distances, AoAs, AoDs, and normalized amplitudes, obtained in a pre-processing stage. Reflective surfaces are modeled by surface feature vectors (SFVs), formerly referred to as MVAs [7]¹, which characterize their positions and orientations. Based on the SFVs, the corresponding VAs can be derived to model either single- or double-bounce propagation paths via geometric transformations.

We introduce a new statistical model with hierarchical features, in which SFV states reside at the upper level of the hierarchy and propagation paths at the lower level. Each SFV gives rise to multiple propagation paths. As in our previous work [24], [25], the states of the propagation paths are their complex amplitudes, which determine both the detection probability of the paths and the associated measurement variances. Both SFV states and path amplitude states are augmented with existence variables that enable inference of their existence probabilities. The proposed hierarchical feature model facilitates estimation of the number of SFVs and enables “soft” ray tracing. In particular, by explicitly modeling propagation paths and inferring their existence, the method can capture nonconvex room geometries. Another key aspect is that new SFVs can be initialized even when the corresponding reflective surface yields measurements only from double-bounce paths. This capability contrasts with [7] and is enabled by an improved initialization procedure for new SFVs.

The proposed method performs probabilistic data association (DA) and sequential estimation of the states of the mobile agent, SFVs, and VAs by running sum-product algorithm (SPA) on a factor graph (FG) representation of the proposed statistical model. Numerical results, based on both synthetic and real data, compare the proposed method with state-of-the-art reference methods [1], [3], [26] as well as the posterior Cramér–Rao lower bounds (PCRLBs). The results demonstrate that the proposed method significantly improves both localization and mapping accuracy, achieving state-of-the-art performance. The key contributions of this paper can be summarized as follows.

- We introduce a statistical model for multipath-based SLAM based on SFVs that can represent the presence and strength of each propagation path.
- We develop the FG and a SPA for multipath-based SLAM D-MIMO systems with adaptive data fusion across propagation paths suitable for nonconvex room geometries.
- We design a proposal probability density function (PDF) that relies on both single- and double-bounce propagation paths, enabling effective introduction of new surfaces.

¹We adopt the term SFV instead of MVA for improved generality, as the proposed model can accommodate additional surface parameters, such as spatial extent or other properties describing the surface.

- We validate our method using synthetic and real measurements and compare performance against two state-of-the-art methods [1], [3], [26] and the PCRLBs.

This work advances over the previous work on multipath-based SLAM exploiting a SFV model [7] by (i) incorporating amplitude statistics into the joint statistical model for adaptive path detection and fusion; (ii) extending to a D-MIMO setup; (iii) improving the proposal PDF for new SFVs; (iv) providing the PCRLBs as a performance benchmark; and (v) validating the performance using both synthetic and real measurements in challenging dynamic scenarios. Note that the detailed derivations and the necessary references for the Bayesian models and the corresponding SPA are provided in the supplementary material [27] to ensure clarity and completeness of the methodology.

Notations: Column vectors and matrices are denoted as lowercase and uppercase bold letters. Random variables are displayed in sans serif, upright fonts as for example \mathbf{x} and \mathbf{x} and their realizations in serif, italic font as for example x and \mathbf{x} . $f(\mathbf{x})$ denotes the PDF or probability mass function (PMF) of a continuous or discrete random vector. $(\cdot)^T$ denotes matrix transpose. $\|\cdot\|$ is the Euclidean norm. $|\cdot|$ represents the cardinality of a set. $f(\mathbf{a}|\mathbf{b})$ denotes the conditional PDF of random vector \mathbf{a} conditioned on random vector \mathbf{b} . $f_N(z|a, b)$ denotes Gaussian PDF with mean a and variance b^2 . $\angle(\mathbf{a}, \mathbf{b}, o) \triangleq \text{atan2}(\mathbf{a}, \mathbf{b}) - o$ calculates the angle between the two points \mathbf{a} and \mathbf{b} w.r.t. the reference angle o .

II. GEOMETRICAL MODEL OF THE ENVIRONMENT

We consider a D-MIMO system operating in a dynamic scenario and consisting of J distributed static base stations (i.e., PAs) and a mobile agent, as shown in Fig. 1. For the sake of brevity, we assume a two-dimensional (2D) scenario with horizontal-only RF signal propagation. At each discrete time n , all J PAs with known positions $\mathbf{p}_{\text{pa}}^{(j)} = [p_{\text{pa},x}^{(j)} p_{\text{pa},y}^{(j)}]^T \in \mathbb{R}^{2 \times 1}$ and $j \in \{1, \dots, J\}$ transmit RF signals and the mobile agent at an unknown, time-varying position $\mathbf{p}_n = [p_{n,x} p_{n,y}]^T \in \mathbb{R}^{2 \times 1}$ acts as a receiver. Time and frequency synchronization between the PAs and the agent are assumed to be perfect.² Each PA is equipped with a H_{tx} -element antenna array with known orientation $\Delta\phi^{(j)}$, and the mobile agent is equipped with a H_{rx} -element antenna array with unknown orientation $\Delta\varphi_n$. The positions $\mathbf{p}_{\text{pa}}^{(j)}$ and \mathbf{p}_n refer to the center of gravity of the arrays.

A. SFV-Based Model of the Environment

The RF signal propagation environment consists of S static reflective surfaces which are indexed by $s \in \mathcal{S} \triangleq \{1, \dots, S\}$ and modeled by SFVs at positions $\mathbf{p}_{s,\text{sfv}} \in \mathbb{R}^{2 \times 1}$ denoting the mirror images of the origin $[0, 0]^T$ on the surfaces. Propagation paths that are specularly reflected can be modeled by VAs at positions $\mathbf{p}_{ss',\text{va}}^{(j)} \in \mathbb{R}^{2 \times 1}$ denoting the mirror images of the j th

PA on these surfaces, where the index tuple $(s, s') \in \mathcal{D} \triangleq \{(s, s') \in \mathcal{S} \times \mathcal{S}\}$ denotes the signal interaction order from the s' th surface to the s th surface before reaching the agent. Following [7], we consider paths experiencing maximal double bounces³. The two sets $\mathcal{D}_S \triangleq \{(s, s) \in \mathcal{S} \times \mathcal{S}\}$ with $|\mathcal{D}_S| = S$ and $\mathcal{D}_D \triangleq \{(s, s') \in \mathcal{S} \times \mathcal{S} | s \neq s'\}$ with $|\mathcal{D}_D| = S(S-1)$ contain the index tuples for single-bounce and double-bounce VAs, respectively. Therefore, the maximum number of VAs for PA j is given by $|\mathcal{D}| = S + S(S-1)$ and $\mathcal{D} = \mathcal{D}_S \cup \mathcal{D}_D$. For conveniently addressing PA-related notations, we also define $\mathbf{p}_{\text{pa}}^{(j)} = \mathbf{p}_{00,\text{va}}^{(j)}$ and $\tilde{\mathcal{D}} = (0, 0) \cup \mathcal{D}$. The positions of a single-bounce VA $\mathbf{p}_{ss',\text{va}}^{(j)}$ and a double-bounce VA $\mathbf{p}_{ss',\text{va}}^{(j)}$ can be transformed from $\mathbf{p}_{s,\text{sfv}}$, $\mathbf{p}_{s',\text{sfv}}$ and $\mathbf{p}_{00,\text{va}}^{(j)}$ as $\mathbf{p}_{ss',\text{va}}^{(j)} = h_{\text{va}}(\mathbf{p}_{s,\text{sfv}}, \mathbf{p}_{\text{pa}}^{(j)})$ and $\mathbf{p}_{ss',\text{va}}^{(j)} = h_{\text{va}}(\mathbf{p}_{s,\text{sfv}}, h_{\text{va}}(\mathbf{p}_{s',\text{sfv}}, \mathbf{p}_{\text{pa}}^{(j)}))$, respectively. The inverse transformation from a VA position to a SFV position is given by $\mathbf{p}_{s,\text{sfv}}^{(j)} = h_{\text{sfv}}(\mathbf{p}_{ss',\text{va}}^{(j)}, \mathbf{p}_{\text{pa}}^{(j)})$. Details of the transformations $h_{\text{va}}(\cdot, \cdot)$ and $h_{\text{sfv}}(\cdot, \cdot)$ are provided in [7, Section II-A].

For each propagation path, its distance $d_{ss',n}^{(j)}$, AoD $\phi_{ss',n}^{(j)}$ and AoA $\varphi_{ss',n}^{(j)}$ are modeled by $d_{ss',n}^{(j)} = \|\mathbf{p}_n - \mathbf{p}_{ss',\text{va}}^{(j)}\|$, $\phi_{ss',n}^{(j)} = \angle(\mathbf{p}_{\text{IP}_{ss',n}^{(j)}}, \mathbf{p}_{\text{pa}}, \Delta\phi^{(j)})$ and $\varphi_{ss',n}^{(j)} = \angle(\mathbf{p}_n, \mathbf{p}_{ss',\text{va}}^{(j)}, \Delta\varphi_n)$. The interaction point (IP) $\mathbf{p}_{\text{IP}_{ss',n}^{(j)}}$ of path on the first interacting surface s' is given by

$$\mathbf{p}_{\text{IP}_{ss',n}^{(j)}} = \mathbf{p}_{\text{pa}}^{(j)} + \frac{(\mathbf{p}_{s'}^{\text{w}} - \mathbf{p}_{\text{pa}}^{(j)})^T \mathbf{n}_{s'}^{\text{w}}}{(\mathbf{p}_{ss',n}^{\text{vm}} - \mathbf{p}_{\text{pa}}^{(j)})^T \mathbf{n}_{s'}^{\text{w}}} (\mathbf{p}_{ss',n}^{\text{vm}} - \mathbf{p}_{\text{pa}}^{(j)}) \quad (1)$$

where $\mathbf{p}_{s'}^{\text{w}} = \frac{\mathbf{p}_{s',\text{sfv}}}{2}$, $\mathbf{n}_{s'}^{\text{w}} = \frac{\mathbf{p}_{s',\text{sfv}}}{\|\mathbf{p}_{s',\text{sfv}}\|}$ is the normal vector of the s' th reflective surface, and the virtual mobile agent positions $\mathbf{p}_{ss',n}^{\text{vm}}$ are computed by applying the same transformations for obtaining VAs from SFVs, leading to $\mathbf{p}_{ss',n}^{\text{vm}} = h_{\text{va}}(\mathbf{p}_{s,\text{sfv}}, \mathbf{p}_n)$ for single-bounce paths ($(s, s') \in \mathcal{D}_S$), and $\mathbf{p}_{ss',n}^{\text{vm}} = h_{\text{va}}(\mathbf{p}_{s,\text{sfv}}, h_{\text{va}}(\mathbf{p}_{s',\text{sfv}}, \mathbf{p}_n))$ for double-bounce paths ($(s, s') \in \mathcal{D}_D$). For the j th PA related line-of-sight (LoS) path, its parameters are defined as $d_{00,n}^{(j)}$, $\phi_{00,n}^{(j)} = \angle(\mathbf{p}_n, \mathbf{p}_{\text{pa}}^{(j)}, \Delta\phi^{(j)})$ and $\varphi_{00,n}^{(j)}$.

III. SYSTEM MODEL

At each time n , the state of the mobile agent is given by $\mathbf{x}_n \triangleq [\mathbf{p}_n^T \mathbf{v}_n^T \Delta\varphi_n]^T$ consisting of the position \mathbf{p}_n , the velocity $\mathbf{v}_n = [v_{n,x} v_{n,y}]^T$ and the azimuth array orientation $\Delta\varphi_n$. The agent states for all time steps up to n are denoted as $\mathbf{x}_{1:n} \triangleq [\mathbf{x}_1^T \dots \mathbf{x}_n^T]^T$. Following [7], we account for the unknown number of SFVs at each time step n by introducing potential SFVs (PSFVs) indexed by $s \in \{1, \dots, S_n\}$, where S_n represents the maximum possible number of PSFVs that have been produced at least one measurement so far and S_n increases with time. PSFV states are given as $\mathbf{y}_{s,n} \triangleq [\mathbf{p}_{s,\text{sfv}}^T r_{s,n}]^T$ with $\mathbf{p}_{s,\text{sfv}}$ denoting the position. The existence/nonexistence of the s th PSFV is modeled by a binary random variable $r_{s,n} \in \{1, 0\}$ in the sense that it exists if and only if $r_{s,n} = 1$. Similarly, to account for the unknown and time-varying number of

²The proposed algorithm can be easily extended to three-dimensional (3D) scenarios with both horizontal and vertical propagation and reformulated for the case where the mobile agent acts as a transmitter and the PAs act as receivers, as shown in Section VI-E. It can also be extended to unsynchronized systems in line with [1], [28]–[30].

³Propagation paths up to second-order reflections constitute the primary contribution to the received signals, making this a practical assumption. However, the model can be extended to incorporate higher-order bounce paths, though this introduces a substantial increase in complexity.

VAs associated to each PSFV, we introduce for each VA a single potential ray (PR) with state $\beta_{ss',n}^{(j)} \triangleq [u_{ss',n}^{(j)} r_{ss',n}^{(j)}]^T$ consisting of the normalized amplitude $u_{ss',n}^{(j)}$ and the binary existence variable $r_{ss',n}^{(j)} \in \{1, 0\}$.

We further define the state of the j th PA as $\beta_{00,n}^{(j)} \triangleq [u_{00,n}^{(j)} r_{00,n}^{(j)}]^T$ to account for its time-varying LoS condition to the agent. Fundamentally, a PSFV models a potentially existing environmental object and PRs model signal interacting processes on this object, thus their existence/nonexistence status are related as follows: (i) a nonexistent reflective surface cannot generate any propagation paths, i.e., from $r_{s,n} = 0$ follows $r_{ss',n}^{(j)} = 0 \forall (s, s')$; (ii) an existing surface does not necessarily interact with any RF signals and therefore generate propagation paths, i.e., if $r_{s,n} = 1$, then $r_{ss',n}^{(j)} \in \{1, 0\}$; (iii) a path exists if and only if the interacting surfaces all exist, i.e., from $r_{ss',n}^{(j)} = 1$ follows $r_{s,n} = 1$ and $r_{s',n} = 1$. The aforementioned relations are considered in the pseudo likelihood function (LHF) formulations in Section IV-B.

Formally, the states of nonexistent PSFVs and nonexistent PRs, i.e., $r_{s,n} = 0$ and $r_{ss',n} = 0$, are also considered even though they are irrelevant and have no influence on the detection and state estimation. Therefore, all PDFs defined for PSFV and PR states $f(\mathbf{y}_{s,n}) = f(\mathbf{p}_{s,\text{sfv}}, r_{s,n})$ and $f(\beta_{ss',\text{va}}^{(j)}) = f(u_{ss',n}^{(j)}, r_{ss',n}^{(j)})$, are of the forms $f(\mathbf{p}_{s,\text{sfv}}, 0) = f_{s,n} f_D(\mathbf{y}_{s,n})$ and $f(u_{ss',n}^{(j)}, 0) = f_{ss',n}^{(j)} f_D(u_{ss',n}^{(j)})$, respectively, where $f_D(\cdot)$ is an arbitrary ‘‘dummy PDF’’, and $f_{s,n} \in [0, 1]$ and $f_{ss',n}^{(j)} \in [0, 1]$ are constants representing the probabilities of nonexistence [3], [31], [32].

A. Measurements and New PSFVs

The mobile agent state, PSFV states and PR states relate to the distance measurements $z_{d,m,n}^{(j)}$, the AoD measurements $z_{\phi,m,n}^{(j)}$, the AoA measurements $z_{\varphi,m,n}^{(j)}$, and the normalized amplitude measurements $z_{u,m,n}^{(j)} \in [u_{\text{de}}, \infty)$ via the following LHF, which are assumed to be conditionally independent of each other. The individual LHF of the distance, AoD and AoA measurements are modeled by Gaussian PDFs, given as

$$f_{ss'}^{(j)}(z_{d,m,n}^{(j)}) \triangleq f_N(z_{d,m,n}^{(j)}; d_{ss',n}^{(j)}, \sigma_d(u_{ss',n}^{(j)})), \quad (2)$$

$$f_{ss'}^{(j)}(z_{\phi,m,n}^{(j)}) \triangleq f_N(z_{\phi,m,n}^{(j)}; \phi_{ss',n}^{(j)}, \sigma_\phi(u_{ss',n}^{(j)})), \quad (3)$$

$$f_{ss'}^{(j)}(z_{\varphi,m,n}^{(j)}) \triangleq f_N(z_{\varphi,m,n}^{(j)}; \varphi_{ss',n}^{(j)}, \sigma_\varphi(u_{ss',n}^{(j)})) \quad (4)$$

where the means $d_{ss',n}^{(j)}$, $\phi_{ss',n}^{(j)}$ and $\varphi_{ss',n}^{(j)}$ are calculated according to Section II-A. The variances of the Gaussian PDFs $\sigma_d^2(u_{ss',n}^{(j)})$, $\sigma_\phi^2(u_{ss',n}^{(j)})$ and $\sigma_\varphi^2(u_{ss',n}^{(j)})$ are determined based on their respective Fisher information as in [26], [33], i.e., $\sigma_d^2(u_{ss',n}^{(j)}) = c^2 / (8\pi^2 \beta_{\text{bw}}^2 (u_{ss',n}^{(j)})^2)$, $\sigma_\phi^2(u_{ss',n}^{(j)}) = c^2 / (8\pi^2 f_c^2 (u_{ss',n}^{(j)})^2 D^2(\phi_{ss',n}^{(j)}))$ and $\sigma_\varphi^2(u_{ss',n}^{(j)}) = c^2 / (8\pi^2 f_c^2 (u_{ss',n}^{(j)})^2 D^2(\varphi_{ss',n}^{(j)}))$ with β_{bw}^2 denoting the mean square bandwidth of the transmit signal pulse, $D^2(\cdot)$ is the squared array aperture, c is the speed of light and f_c is the center carrier frequency. The normalized amplitude $u_{ss',n}^{(j)}$ is defined as the square root of the propagation path’s signal-to-noise ratio

(SNR), and directly related to the detection probability $p_d(u_{ss',n}^{(j)})$ of PR (s, s') via the Marcum Q-function as $p_d(u_{ss',n}^{(j)}) = Q_1(u_{ss',n}^{(j)} / \sigma_u(u_{ss',n}^{(j)}), u_{\text{de}} / \sigma_u(u_{ss',n}^{(j)}))$ [24], [34]. The scale parameter $\sigma_u(u_{ss',n}^{(j)})$ is set to the corresponding Fisher information [24], i.e., $\sigma_u(u_{ss',n}^{(j)}) = \frac{1}{2} + \frac{1}{4N_{\text{rx}}N_{\text{s}}}(u_{ss',n}^{(j)})^2$, with N_{s} denoting the number of signal samples per transmit–receive antenna pair at time n . The LHF of the normalized amplitude measurements $z_{u,m,n}^{(j)} > u_{\text{de}}$ are modeled by a truncated Rician PDF [34, Ch. 1.6.7] [24], i.e.,

$$f_{ss'}^{(j)}(z_{u,m,n}^{(j)}) \triangleq f_{\text{TR}}(z_{u,m,n}^{(j)}; u_{ss',n}^{(j)}, \sigma_u(u_{ss',n}^{(j)}), p_d(u_{ss',n}^{(j)}); u_{\text{de}}). \quad (5)$$

Note that (2)–(5) generally apply for LoS paths, single- and double-bounce paths, depending on whether $(s, s') = (0, 0)$, $(s, s') \in \mathcal{D}_{\text{S},n}^{(j)}$ or $(s, s') \in \mathcal{D}_{\text{D},n}^{(j)}$. Using (2) through (5), the LHF for different types of paths are factorized as follows and further used in the pseudo LHF in Section IV-B.

1) LHF for LoS Paths:

$$f_{\text{P}}(z_{m,n}^{(j)} | \mathbf{p}_n, u_{00,n}^{(j)}) = f_{00}^{(j)}(z_{d,m,n}^{(j)}) f_{00}^{(j)}(z_{\phi,m,n}^{(j)}) f_{00}^{(j)}(z_{\varphi,m,n}^{(j)}) f_{00}^{(j)}(z_{u,m,n}^{(j)}). \quad (6)$$

2) LHF for Single-Bounce Paths:

$$f_{\text{S}}(z_{m,n}^{(j)} | \mathbf{p}_n, \mathbf{p}_{s,\text{sfv}}, u_{ss,n}^{(j)}) = f_{ss}^{(j)}(z_{d,m,n}^{(j)}) f_{ss}^{(j)}(z_{\phi,m,n}^{(j)}) f_{ss}^{(j)}(z_{\varphi,m,n}^{(j)}) f_{ss}^{(j)}(z_{u,m,n}^{(j)}). \quad (7)$$

3) LHF for Double-Bounce Paths:

$$f_{\text{D}}(z_{m,n}^{(j)} | \mathbf{p}_n, \mathbf{p}_{s,\text{sfv}}, \mathbf{p}_{s',\text{sfv}}, u_{ss',n}^{(j)}) = f_{ss'}^{(j)}(z_{d,m,n}^{(j)}) f_{ss'}^{(j)}(z_{\phi,m,n}^{(j)}) f_{ss'}^{(j)}(z_{\varphi,m,n}^{(j)}) f_{ss'}^{(j)}(z_{u,m,n}^{(j)}). \quad (8)$$

Before being observed, the measurements $\mathbf{z}_{m,n}^{(j)} \triangleq [z_{d,m,n}^{(j)} z_{\phi,m,n}^{(j)} z_{\varphi,m,n}^{(j)} z_{u,m,n}^{(j)}]^T \in \mathbb{R}^{4 \times 1}$ with $m \in \{1, \dots, M_n^{(j)}\}$ and the measurement number $M_n^{(j)}$ at each PA are considered as random. The joint measurement vectors for all PAs and all times up to n are given by $\mathbf{z}_n^{(j)} \triangleq [\mathbf{z}_{1,n}^{(j)T} \dots \mathbf{z}_{M_n^{(j)},n}^{(j)T}]^T \in \mathbb{R}^{4M_n^{(j)} \times 1}$, $\mathbf{z}_n \triangleq [\mathbf{z}_n^{(1)T} \dots \mathbf{z}_n^{(J)T}]^T$ and $\mathbf{z}_{1:n} \triangleq [\mathbf{z}_1^T \dots \mathbf{z}_n^T]^T$. Note that the measurements are obtained by applying a parametric channel estimation and detection algorithm [10]–[15], [35] to the observed discrete RF signals in the pre-processing stage, where a detection threshold u_{de} is applied to the normalized amplitude, leading to $z_{u,m,n}^{(j)} > u_{\text{de}}$. The measurements $\mathbf{z}_{m,n}^{(j)}$ that do not originate from any SFVs are referred to as false alarms (FAs), which are assumed to be statistically independent of PSFV and PR states and modeled by a Poisson point process with mean number μ_{fa} and LHF $f_{\text{fa}}(z_{m,n}^{(j)})$.

4) *New PSFVs and New PRs*: Newly detected SFVs, i.e., SFVs that generate measurements for the first time, are modeled by a Poisson point process with mean μ_{n} and conditional PDF $f_n(\bar{\mathbf{p}}_{m,\text{sfv}}^{(j)} | \mathbf{x}_n)$. Newly detected SFVs are represented by new PSFV states $\bar{\mathbf{y}}_{m,n}^{(j)} \triangleq [\bar{\mathbf{p}}_{m,\text{sfv}}^{(j)T} \bar{r}_{m,n}^{(j)}]^T$, $m \in \{1, \dots, M_n^{(j)}\}$. Each new PSFV $\bar{\mathbf{y}}_{m,n}^{(j)}$ corresponds to a new PR $\bar{\beta}_{m,n}^{(j)} = [\bar{u}_{mm,n}^{(j)}, \bar{r}_{mm,n}^{(j)}]^T$ and a measurement $\mathbf{z}_{m,n}^{(j)}$.

If and only if $\bar{r}_{m,n}^{(j)} = 1$ and $\bar{r}_{mm,n}^{(j)} = 1$, the measurement $\mathbf{z}_{m,n}$ is claimed to be generated from the new PSFV m . The normalized amplitude states of new PRs are modeled by the PDF $f_n(\bar{u}_{mm}^{(j)})$. The state vectors of all new PSFVs and new PRs at PA j are given by $\bar{\mathbf{y}}_n^{(j)} \triangleq [\bar{\mathbf{y}}_{1,n}^{(j)} \cdots \bar{\mathbf{y}}_{M_n^{(j)},n}^{(j)}]^\top$ and $\bar{\boldsymbol{\beta}}_n^{(j)} \triangleq [\bar{\boldsymbol{\beta}}_{1,n}^{(j)} \cdots \bar{\boldsymbol{\beta}}_{M_n^{(j)},n}^{(j)}]^\top$, respectively.

B. Legacy PSFVs, Legacy PRs and State Transition

PSFVs that have been detected either at a previous time $n' < n$ or at time n but at a previous PA $j' < j$ are referred to as legacy PSFVs with states $\underline{\mathbf{y}}_{s,n}^{(j)} \triangleq [\underline{\mathbf{p}}_{s,\text{sfv}}^{(j)} \underline{\mathbf{r}}_{s,n}^{(j)}]^\top$. Accordingly, PRs that have been detected at a previous time $n' < n$ are referred to as legacy PRs with states $\underline{\boldsymbol{\beta}}_{ss',n}^{(j)} \triangleq [\underline{\mathbf{u}}_{ss',n}^{(j)} \underline{\mathbf{r}}_{ss',n}^{(j)}]^\top$. Assume that measurements are incorporated sequentially across PAs $j \in \{1, \dots, J\}$ at each time n . New PSFVs become legacy PSFVs after the next measurements either of the next PA or at the next time are observed. New PRs of PA j become legacy PRs after the measurements of PA j at the next time are observed. The number of legacy PSFVs is updated according to $S_n^{(j)} = S_{n-1}^{(j)} + M_n^{(j-1)}$ for $j > 1$ or $S_n^{(1)} = S_{n-1}^{(J)} + M_n^{(J)}$. Accordingly, the number of PRs for each PA is given as $|\mathcal{D}_n^{(j)}| = S_n^{(j)} + S_n^{(j)}(S_n^{(j)} - 1)$ with $\mathcal{D}_n^{(j)} \triangleq \{(s, s') \in \mathcal{S}_n^{(j)} \times \mathcal{S}_n^{(j)}\} = \mathcal{D}_{S,n}^{(j)} \cup \mathcal{D}_{D,n}^{(j)}$, and $\tilde{\mathcal{D}}_n^{(j)} = (0, 0) \cup \mathcal{D}_n^{(j)}$. Up to PA j at time n , the vector of all legacy PSFVs is given as $\underline{\mathbf{y}}_n^{(j)} \triangleq [\underline{\mathbf{y}}_n^{(j-1)\top} \bar{\mathbf{y}}_n^{(j-1)\top}]^\top$, and the vector of all PSFVs is given as $\mathbf{y}_n^{(j)} \triangleq [\underline{\mathbf{y}}_n^{(j)\top} \bar{\mathbf{y}}_n^{(j)\top}]^\top$. After the measurements of all J PAs have been incorporated at time n , the total number of PSFVs is $S_n = S_{n-1} + \sum_{j=1}^J M_n^{(j)} = S_n^{(J)} + M_n^{(J)}$, the state of all PSFV states at time n is given by $\mathbf{y}_n \triangleq [\underline{\mathbf{y}}_n^{(J)\top} \bar{\mathbf{y}}_n^{(J)\top}]^\top$ which is further stacked into the vector for all times up to n given by $\mathbf{y}_{1:n} \triangleq [\mathbf{y}_1^\top \cdots \mathbf{y}_n^\top]^\top$.

The agent state, legacy PSFVs states and the legacy PR states are assumed to evolve independently across time n according to state-transition PDFs $f(\mathbf{x}_n | \mathbf{x}_{n-1})$, $f(\underline{\mathbf{y}}_{s,n} | \underline{\mathbf{y}}_{s,n-1})$ and $f(\underline{\boldsymbol{\beta}}_{ss',n}^{(j)} | \underline{\boldsymbol{\beta}}_{ss',n-1}^{(j)})$. In line with [3], [7], [31], the state-transition PDF $f(\underline{\mathbf{y}}_{s,n} | \underline{\mathbf{y}}_{s,n-1}) = f(\underline{\mathbf{p}}_{s,\text{sfv}}, \underline{\mathbf{r}}_{s,n} | \underline{\mathbf{p}}_{s,\text{sfv}}, \underline{\mathbf{r}}_{s,n-1})$ at PA $j = 1$ is defined as

$$f(\underline{\mathbf{p}}_{s,\text{sfv}}, \underline{\mathbf{r}}_{s,n} | \underline{\mathbf{p}}_{s,\text{sfv}}, 1) = \begin{cases} (1 - p_s) f_D(\underline{\mathbf{p}}_{s,\text{sfv}}), & \underline{\mathbf{r}}_{s,n} = 0 \\ p_s f(\underline{\mathbf{p}}_{s,\text{sfv}} | \underline{\mathbf{p}}_{s,\text{sfv}}), & \underline{\mathbf{r}}_{s,n} = 1 \end{cases} \quad (9)$$

for $\underline{\mathbf{r}}_{s,n-1} = 1$. For nonexistent PSFVs at the previous time, i.e., $\underline{\mathbf{r}}_{s,n-1} = 0$, it is defined as

$$f(\underline{\mathbf{p}}_{s,\text{sfv}}, \underline{\mathbf{r}}_{s,n} | \underline{\mathbf{p}}_{s,\text{sfv}}, 0) = \begin{cases} f_D(\underline{\mathbf{p}}_{s,\text{sfv}}), & \underline{\mathbf{r}}_{s,n} = 0 \\ 0, & \underline{\mathbf{r}}_{s,n} = 1. \end{cases} \quad (10)$$

Considering the sequential incorporation of PSFVs states across PAs at each time n , we also define the state-transition PDF $f(\underline{\mathbf{y}}_n^{(j)} | \underline{\mathbf{y}}_{s,n}^{(j-1)}) = f(\underline{\mathbf{p}}_{s,\text{sfv}}^{(j)}, \underline{\mathbf{r}}_{s,n}^{(j)} | \underline{\mathbf{p}}_{s,\text{sfv}}^{(j-1)}, \underline{\mathbf{r}}_{s,n}^{(j-1)})$ for $j > 1$, reads

$$f(\underline{\mathbf{p}}_{s,\text{sfv}}^{(j)}, \underline{\mathbf{r}}_{s,n}^{(j)} | \underline{\mathbf{p}}_{s,\text{sfv}}^{(j-1)}, 1) = \begin{cases} f_D(\underline{\mathbf{p}}_{s,\text{sfv}}^{(j)}), & \underline{\mathbf{r}}_{s,n}^{(j)} = 0 \\ f(\underline{\mathbf{p}}_{s,\text{sfv}}^{(j)} | \underline{\mathbf{p}}_{s,\text{sfv}}^{(j-1)}), & \underline{\mathbf{r}}_{s,n}^{(j)} = 1, \end{cases} \quad (11)$$

$$f(\underline{\mathbf{p}}_{s,\text{sfv}}^{(j)}, \underline{\mathbf{r}}_{s,n}^{(j)} | \underline{\mathbf{p}}_{s,\text{sfv}}^{(j-1)}, 0) = \begin{cases} f_D(\underline{\mathbf{p}}_{s,\text{sfv}}^{(j)}), & \underline{\mathbf{r}}_{s,n}^{(j)} = 0 \\ 0, & \underline{\mathbf{r}}_{s,n}^{(j)} = 1. \end{cases} \quad (12)$$

The state-transition PDF for PRs $f(\underline{\boldsymbol{\beta}}_{ss',n}^{(j)} | \underline{\boldsymbol{\beta}}_{ss',n-1}^{(j)}) = f(\underline{\mathbf{u}}_{ss',n}^{(j)}, \underline{\mathbf{r}}_{ss',n}^{(j)} | \underline{\mathbf{u}}_{ss',n-1}^{(j)}, \underline{\mathbf{r}}_{ss',n-1}^{(j)})$ is given by

$$f(\underline{\mathbf{u}}_{ss',n}^{(j)}, \underline{\mathbf{r}}_{ss',n}^{(j)} | \underline{\mathbf{u}}_{ss',n-1}^{(j)}, \underline{\mathbf{r}}_{ss',n-1}^{(j)} = 1) = \begin{cases} (1 - p_s) f_D(\underline{\mathbf{u}}_{ss',n}^{(j)}), & \underline{\mathbf{r}}_{ss',n}^{(j)} = 0 \\ p_s f(\underline{\mathbf{u}}_{ss',n}^{(j)} | \underline{\mathbf{u}}_{ss',n-1}^{(j)}), & \underline{\mathbf{r}}_{ss',n}^{(j)} = 1 \end{cases} \quad (13)$$

for existing PR at time $n - 1$. For nonexistent PR at the previous time, i.e., $\underline{\mathbf{r}}_{ss',n-1}^{(j)} = 0$, it is obtained as

$$f(\underline{\mathbf{u}}_{ss',n}^{(j)}, \underline{\mathbf{r}}_{ss',n}^{(j)} | \underline{\mathbf{u}}_{ss',n-1}^{(j)}, 0) = \begin{cases} f_D(\underline{\mathbf{u}}_{ss',n}^{(j)}), & \underline{\mathbf{r}}_{ss',n}^{(j)} = 0 \\ 0, & \underline{\mathbf{r}}_{ss',n}^{(j)} = 1. \end{cases} \quad (14)$$

The initial prior PDFs $f(\mathbf{x}_0)$, $f(\underline{\mathbf{y}}_{s,0})$ and $f(\underline{\boldsymbol{\beta}}_{ss',0}^{(j)})$ for $s \in \mathcal{S}_0$, $(s, s') \in \tilde{\mathcal{D}}_0^{(j)}$ and $j \in \{1, \dots, J\}$ at time $n = 0$ are assumed to be known.

C. Data Association Uncertainty

Estimation of multiple PSFV states is complicated by the DA uncertainty, i.e., it is unknown which measurement $\mathbf{z}_{m,n}^{(j)}$ originated from which PA, PSFV, or PSFV pair. Following [7], the associations between measurements and legacy PSFVs are described by the *PSFV-oriented* association variables $\underline{\mathbf{a}}_n^{(j)} \triangleq [\underline{\mathbf{a}}_{00,n}^{(j)} \underline{\mathbf{a}}_{11,n}^{(j)} \cdots \underline{\mathbf{a}}_{S_n^{(j)} S_n^{(j)},n}^{(j)}]^\top$ with entries $\underline{\mathbf{a}}_{ss',n}^{(j)} \triangleq m \in \{1, \dots, M_n^{(j)}\}$ if the legacy PSFV pair ss' generates measurement m , or $\underline{\mathbf{a}}_{ss',n}^{(j)} \triangleq 0$ if the pair ss' does not generate any measurement. Following [3], [31], [36], the associations can be equivalently described by the *measurement-oriented* association variables $\bar{\mathbf{a}}_n^{(j)} \triangleq [\bar{\mathbf{a}}_{1,n}^{(j)} \cdots \bar{\mathbf{a}}_{M_n^{(j)},n}^{(j)}]^\top$ with entries $\bar{\mathbf{a}}_{m,n}^{(j)} \triangleq (s, s') \in \tilde{\mathcal{D}}_n^{(j)}$ if measurement m is generated by legacy PSFV pair ss' , or $\bar{\mathbf{a}}_{m,n}^{(j)} \triangleq 0$ if measurement m is not generated by any legacy PSFV. Note that the association variables are valid for all cases with $(s, s') \in \tilde{\mathcal{D}}_n^{(j)}$. At any time n , we follow the assumption that each PR can generate at most one measurement, and each measurement can be generated by at most one PSFV pair, which is guaranteed by the ‘‘redundant formulation’’ of using $\underline{\mathbf{a}}_n^{(j)}$ together with $\bar{\mathbf{a}}_n^{(j)}$. This is also the key to make the algorithm scalable for large numbers of PSFVs and measurements. The joint association vectors for all PAs and for all times up to n are given by $\underline{\mathbf{a}}_n \triangleq [\underline{\mathbf{a}}_n^{(1)\top} \cdots \underline{\mathbf{a}}_n^{(J)\top}]^\top$, $\bar{\mathbf{a}}_n \triangleq [\bar{\mathbf{a}}_n^{(1)\top} \cdots \bar{\mathbf{a}}_n^{(J)\top}]^\top$, $\underline{\mathbf{a}}_{1:n} \triangleq [\underline{\mathbf{a}}_1^\top \cdots \underline{\mathbf{a}}_n^\top]^\top$ and $\bar{\mathbf{a}}_{1:n} \triangleq [\bar{\mathbf{a}}_1^\top \cdots \bar{\mathbf{a}}_n^\top]^\top$.

IV. PROBLEM FORMULATION AND FACTOR GRAPH

Using all the measurements $\mathbf{z}_{1:n}$ of all PAs and all times up to n , we aim to sequentially detect the existences of PRs and PSFVs, and estimate their states $\underline{\boldsymbol{\beta}}_{ss',n}^{(j)}$, $\underline{\mathbf{y}}_{s,n}$ and the agent state \mathbf{x}_n . This relies on the marginal posterior existence probabilities $f(r_{ss',n}^{(j)} = 1 | \mathbf{z}_{1:n}) = \int f(u_{ss',n}^{(j)}, r_{ss',n}^{(j)} = 1 | \mathbf{z}_{1:n}^{(\sim j)}) d\underline{\mathbf{u}}_{ss',n}^{(j)}$ with $\mathbf{z}_{1:n}^{(\sim j)} \triangleq [\mathbf{z}_{1:n-1}^\top \quad [\mathbf{z}_n^{(1)\top} \cdots \mathbf{z}_n^{(j)\top}]]^\top$ and $f(r_{s,n} = 1 | \mathbf{z}_{1:n}) = \int f(\underline{\mathbf{p}}_{s,\text{sfv}}, r_{s,n} = 1 | \mathbf{z}_{1:n}) d\underline{\mathbf{p}}_{s,\text{sfv}}$, and the marginal posterior PDFs $f(u_{ss',n}^{(j)} | r_{ss',n}^{(j)} = 1, \mathbf{z}_{1:n}^{(\sim j)}) = f(u_{ss',n}^{(j)}, r_{ss',n}^{(j)} = 1 | \mathbf{z}_{1:n}^{(\sim j)}) / f(r_{ss',n}^{(j)} = 1 | \mathbf{z}_{1:n})$ and $f(\underline{\mathbf{p}}_{s,\text{sfv}} | r_{s,n} = 1, \mathbf{z}_{1:n}) = f(\underline{\mathbf{p}}_{s,\text{sfv}}, r_{s,n} = 1 | \mathbf{z}_{1:n}) / f(r_{s,n} = 1 | \mathbf{z}_{1:n})$.

$$\begin{aligned}
& f(\mathbf{x}_{0:n}, \mathbf{y}_{0:n}, \boldsymbol{\beta}_{0:n}, \underline{\mathbf{a}}_{1:n}, \bar{\mathbf{a}}_{1:n} | \mathbf{z}_{1:n}) \\
& \propto \underbrace{\left(f(\mathbf{x}_0) \prod_{s=1}^{S_0} f(\mathbf{y}_{s,0}) \prod_{j'=1}^J \prod_{(s,s') \in \mathcal{D}_0^{(j')}} f(\boldsymbol{\beta}_{ss',0}^{(j')}) \right)}_{\text{initial prior PDFs}} \underbrace{\prod_{n'=1}^n f(\mathbf{x}_{n'} | \mathbf{x}_{n'-1})}_{\text{agent state transition}} \underbrace{\left(\prod_{s'=1}^{S_{n'-1}} f(\underline{\mathbf{y}}_{s',n'} | \mathbf{y}_{s',n'-1}) \right)}_{\text{legacy PSFVs' state transition}} \underbrace{\left(\prod_{j'=2}^J \prod_{s'=1}^{S_{n'}^{(j')}} f^{(j)}(\underline{\mathbf{y}}_{s',n'}^{(j')} | \mathbf{y}_{s',n'}^{(j'-1)}) \right)}_{\text{legacy PSFVs' state transition}} \\
& \times \underbrace{\left(\prod_{j=1}^J f(\boldsymbol{\beta}_{00,n'}^{(j)} | \boldsymbol{\beta}_{00,n'-1}^{(j)}) q_{\text{P}}(\mathbf{x}_{n'}, \boldsymbol{\beta}_{00,n'}^{(j)}, \underline{\mathbf{a}}_{00,n'}^{(j)}; \mathbf{z}_{n'}^{(j)}) \prod_{m'=1}^{M_{n'}^{(j)}} \psi(\underline{\mathbf{a}}_{00,n'}^{(j)}, \bar{\mathbf{a}}_{m',n'}^{(j)}) \right)}_{\text{factors related to PAs and LoS PRs}} \\
& \times \underbrace{\prod_{j=1}^J \left(\prod_{s=1}^{S_{n'}^{(j)}} f(\boldsymbol{\beta}_{ss,n'}^{(j)} | \boldsymbol{\beta}_{ss,n'-1}^{(j)}) q_{\text{S}}(\mathbf{x}_{n'}, \underline{\mathbf{y}}_{s,n'}^{(j)}, \boldsymbol{\beta}_{ss,n'}^{(j)}, \underline{\mathbf{a}}_{ss,n'}^{(j)}; \mathbf{z}_{n'}^{(j)}) \prod_{m'=1}^{M_{n'}^{(j)}} \psi(\underline{\mathbf{a}}_{ss,n'}^{(j)}, \bar{\mathbf{a}}_{m',n'}^{(j)}) \right)}_{\text{factors related to legacy PSFVs and single-bounce PRs}} \\
& \times \underbrace{\left(\prod_{s'=1, s' \neq s}^{S_{n'}^{(j)}} f(\boldsymbol{\beta}_{ss',n'}^{(j)} | \boldsymbol{\beta}_{ss',n'-1}^{(j)}) q_{\text{D}}(\mathbf{x}_{n'}, \underline{\mathbf{y}}_{s,n'}^{(j)}, \underline{\mathbf{y}}_{s',n'}^{(j)}, \boldsymbol{\beta}_{ss',n'}^{(j)}, \underline{\mathbf{a}}_{ss',n'}^{(j)}; \mathbf{z}_{n'}^{(j)}) \prod_{m'=1}^{M_{n'}^{(j)}} \psi(\underline{\mathbf{a}}_{ss',n'}^{(j)}, \bar{\mathbf{a}}_{m',n'}^{(j)}) \right)}_{\text{factors related to legacy PSFVs and double-bounce PRs}} \\
& \times \underbrace{\left(\prod_{m=1}^{M_{n'}^{(j)}} \bar{q}_{\text{N}}(\mathbf{x}_{n'}, \bar{\mathbf{y}}_{m,n'}^{(j)}, \bar{\boldsymbol{\beta}}_{m,n'}^{(j)}, \bar{\mathbf{a}}_{m,n'}^{(j)}; \mathbf{z}_{n'}^{(j)}) \right)}_{\text{prior PDFs and factors related to new PSFVs and PRs}} \tag{15}
\end{aligned}$$

A. Existence Detection and State Estimation

The agent state is estimated by means of the minimum mean-square error (MMSE) estimator [37], i.e.,

$$\hat{\mathbf{x}}_n \triangleq \int \mathbf{x}_n f(\mathbf{x}_n | \mathbf{z}_{1:n}) d\mathbf{x}_n. \tag{16}$$

A PR and a PSFV are declared to exist (i.e., detected) if $f(r_{ss',n} = 1 | \mathbf{z}_{1:n}) > p_{\text{pr}}$ and $f(r_{s,n} = 1 | \mathbf{z}_{1:n}) > p_{\text{sfv}}$, where p_{pr} and p_{sfv} are the existence probability thresholds. For existing PSFVs and PRs, their positions and normalized amplitudes are again calculated by the MMSE, yielding

$$\hat{\mathbf{p}}_{s,\text{sfv}} \triangleq \int \mathbf{p}_{s,\text{sfv}} f(\mathbf{p}_{s,\text{sfv}} | r_{s,n} = 1, \mathbf{z}_{1:n}) d\mathbf{p}_{s,\text{sfv}}, \tag{17}$$

$$\hat{u}_{ss',n} \triangleq \int u_{ss',n} f(u_{ss',n} | r_{ss',n} = 1, \mathbf{z}_{1:n}^{(\sim j)}) du_{ss',n}. \tag{18}$$

The posterior PDFs $f(\mathbf{x}_n | \mathbf{z}_{1:n})$, $f(\mathbf{p}_{s,\text{sfv}}, r_{s,n} = 1 | \mathbf{z}_{1:n})$ and $f(u_{ss',n}, r_{ss',n} = 1 | \mathbf{z}_{1:n}^{(\sim j)})$ are marginal PDFs of the joint posterior PDF $f(\mathbf{x}_{0:n}, \mathbf{y}_{0:n}, \boldsymbol{\beta}_{0:n}, \underline{\mathbf{a}}_{1:n}, \bar{\mathbf{a}}_{1:n} | \mathbf{z}_{1:n})$. Since the direct marginalization of the joint posterior PDF is computationally infeasible, we perform message passing using the SPA rules on the factor graph in Fig. 2 representing the joint posterior PDF in (15), which efficiently calculates the beliefs $\hat{f}(\mathbf{x}_n)$, $\hat{f}_s(\mathbf{y}_{s,n})$ and $\hat{f}(\boldsymbol{\beta}_{ss',n}^{(j)})$ approximating these marginal PDFs.

B. Joint Posterior PDF and Factor Graph

Using common assumptions [3], [31], [34], the joint posterior PDF $f(\mathbf{x}_{0:n}, \mathbf{y}_{0:n}, \boldsymbol{\beta}_{0:n}, \underline{\mathbf{a}}_{1:n}, \bar{\mathbf{a}}_{1:n} | \mathbf{z}_{1:n})$ of $\mathbf{x}_{0:n}$, $\mathbf{y}_{0:n}$,

$\boldsymbol{\beta}_{0:n}$, $\underline{\mathbf{a}}_{1:n}$ and $\bar{\mathbf{a}}_{1:n}$ conditioned on the observed (thus fixed) measurements $\mathbf{z}_{1:n}$ is factorized as (15), where the functions $q_{\text{P}}(\mathbf{x}_n, \boldsymbol{\beta}_{00,n}^{(j)}, \underline{\mathbf{a}}_{00,n}^{(j)}; \mathbf{z}_n^{(j)})$, $q_{\text{S}}(\mathbf{x}_n, \underline{\mathbf{y}}_{s,n}^{(j)}, \boldsymbol{\beta}_{ss,n}^{(j)}, \underline{\mathbf{a}}_{ss,n}^{(j)}; \mathbf{z}_n^{(j)})$, $q_{\text{D}}(\mathbf{x}_n, \underline{\mathbf{y}}_{s,n}^{(j)}, \underline{\mathbf{y}}_{s',n}^{(j)}, \boldsymbol{\beta}_{ss',n}^{(j)}, \underline{\mathbf{a}}_{ss',n}^{(j)}; \mathbf{z}_n^{(j)})$ and $\bar{q}_{\text{N}}(\mathbf{x}_n, \bar{\mathbf{y}}_{m,n}^{(j)}, \bar{\boldsymbol{\beta}}_{m,n}^{(j)}, \bar{\mathbf{a}}_{m,n}^{(j)}; \mathbf{z}_n^{(j)})$ will be discussed next.

For the LoS PR related to PA j : the pseudo LHF $q_{\text{P}}(\mathbf{x}_n, \boldsymbol{\beta}_{00,n}^{(j)}, \underline{\mathbf{a}}_{00,n}^{(j)}; \mathbf{z}_n^{(j)}) = q_{\text{P}}(\mathbf{x}_n, \underline{\mathbf{u}}_{00,n}^{(j)}, \underline{\mathbf{r}}_{00,n}^{(j)}, \underline{\mathbf{a}}_{00,n}^{(j)}; \mathbf{z}_n^{(j)})$ is given by

$$\begin{aligned}
& q_{\text{P}}(\mathbf{x}_n, \underline{\mathbf{u}}_{00,n}^{(j)}, \underline{\mathbf{r}}_{00,n}^{(j)} = 1, \underline{\mathbf{a}}_{00,n}^{(j)}; \mathbf{z}_n^{(j)}) \\
& \triangleq \begin{cases} \frac{f_{\text{P}}(\mathbf{z}_{m,n}^{(j)} | \mathbf{p}_n, \underline{\mathbf{u}}_{00,n}^{(j)}) p_{\text{d}}(\underline{\mathbf{u}}_{00,n}^{(j)})}{\mu_{\text{fa}} f_{\text{fa}}(\mathbf{z}_{m,n}^{(j)})}, & \underline{\mathbf{a}}_{00,n}^{(j)} \in \mathcal{M}_n^{(j)} \\ 1 - p_{\text{d}}(\underline{\mathbf{u}}_{00,n}^{(j)}), & \underline{\mathbf{a}}_{00,n}^{(j)} = 0. \end{cases} \tag{19}
\end{aligned}$$

and $q_{\text{P}}(\mathbf{x}_n, \underline{\mathbf{u}}_{00,n}^{(j)}, \underline{\mathbf{r}}_{00,n}^{(j)} = 0, \underline{\mathbf{a}}_{00,n}^{(j)}; \mathbf{z}_n^{(j)}) \triangleq \delta(\underline{\mathbf{a}}_{00,n}^{(j)})$.

For single-bounce PRs: related to PSFV $(s, s') \in \mathcal{D}_{\text{S}}^{(j)}$, the pseudo LHF $q_{\text{S}}(\mathbf{x}_n, \underline{\mathbf{y}}_{s,n}^{(j)}, \boldsymbol{\beta}_{ss,n}^{(j)}, \underline{\mathbf{a}}_{ss,n}^{(j)}; \mathbf{z}_n^{(j)}) = q_{\text{S}}(\mathbf{x}_n, \underline{\mathbf{p}}_{s,\text{sfv}}^{(j)}, \underline{\mathbf{r}}_{s,n}^{(j)}, \underline{\mathbf{u}}_{ss,n}^{(j)}, \underline{\mathbf{r}}_{ss,n}^{(j)}, \underline{\mathbf{a}}_{ss,n}^{(j)}; \mathbf{z}_n^{(j)})$ is given by

$$\begin{aligned}
& q_{\text{S}}(\mathbf{x}_n, \underline{\mathbf{p}}_{s,\text{sfv}}^{(j)}, \underline{\mathbf{r}}_{s,n}^{(j)} = 1, \underline{\mathbf{u}}_{ss,n}^{(j)}, \underline{\mathbf{r}}_{ss,n}^{(j)} = 1, \underline{\mathbf{a}}_{ss,n}^{(j)}; \mathbf{z}_n^{(j)}) \\
& \triangleq \begin{cases} \frac{f_{\text{S}}(\mathbf{z}_{m,n}^{(j)} | \mathbf{p}_n, \underline{\mathbf{p}}_{s,\text{sfv}}^{(j)}, \underline{\mathbf{u}}_{ss,n}^{(j)}) p_{\text{d}}(\underline{\mathbf{u}}_{ss,n}^{(j)})}{\mu_{\text{fa}} f_{\text{fa}}(\mathbf{z}_{m,n}^{(j)})}, & \underline{\mathbf{a}}_{ss,n}^{(j)} \in \mathcal{M}_n^{(j)} \\ 1 - p_{\text{d}}(\underline{\mathbf{u}}_{ss,n}^{(j)}), & \underline{\mathbf{a}}_{ss,n}^{(j)} = 0 \end{cases} \tag{20}
\end{aligned}$$

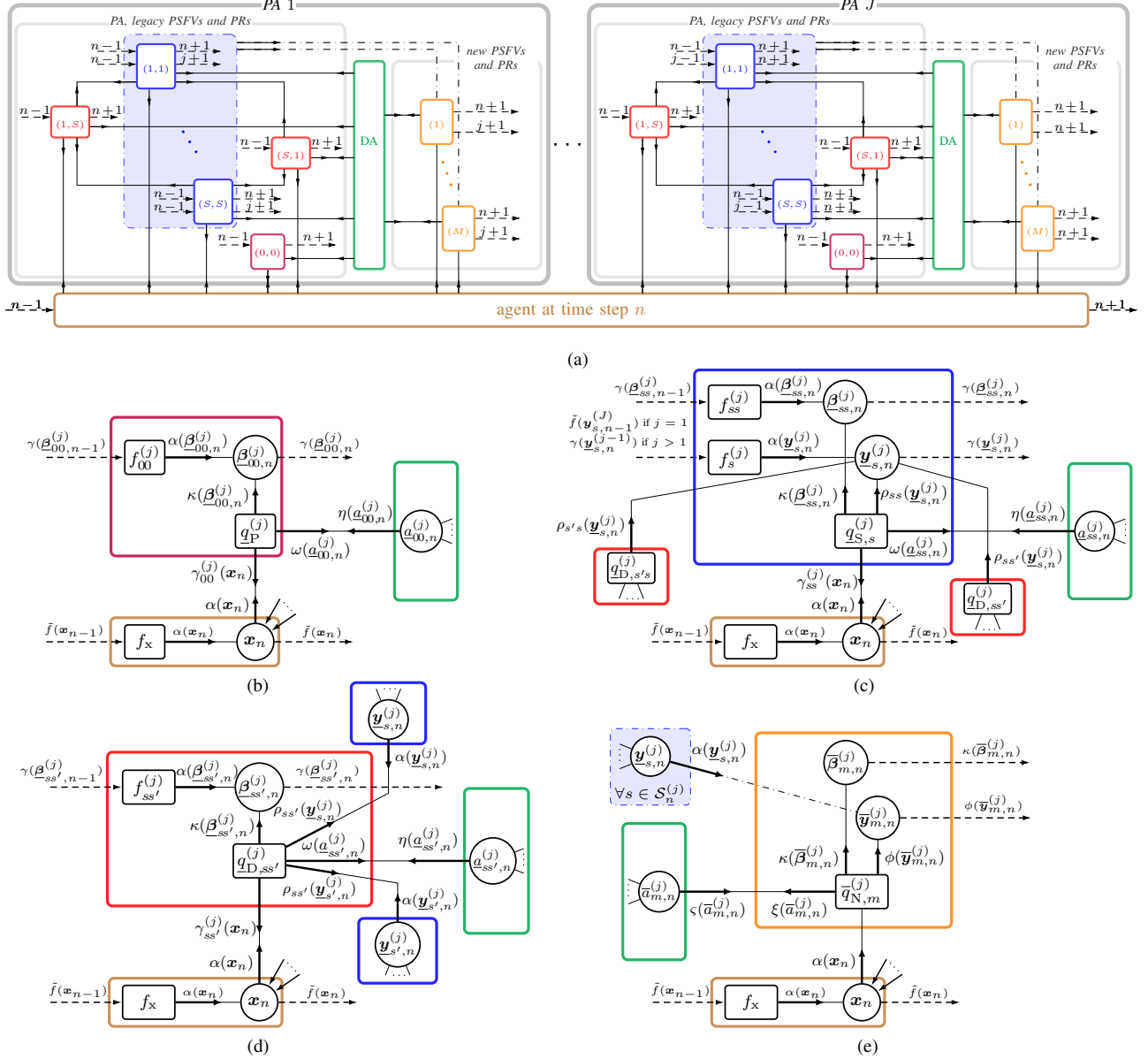


Fig. 2: Factor graph representation of the joint posterior PDF in (15). The black square and circle symbols denote factor nodes and variable nodes, respectively, while the colored boxes represent subgraphs formed by subsets of nodes and edges. The block diagram in (a) illustrates message propagation between the subgraphs, as well as iterations over time and PAs. Detailed views of the variable nodes, factor nodes, and messages related to (b) PAs and LoS PRs, (c) legacy PSFVs and single-bounce PRs, (d) double-bounce PRs, and (e) new PSFVs and new PRs are shown in the corresponding zoomed-in plots. The following shorthand notation is used: $S \triangleq S_n^{(j)}$, $M \triangleq M_n^{(j)}$, $f_x \triangleq f(\mathbf{x}_n | \mathbf{x}_{n-1})$, $f_s^{(j)} \triangleq f(\mathbf{y}_{s,n}^{(j)} | \mathbf{y}_{s,n-1}^{(j)})$, $f_{ss'}^{(j)} \triangleq f(\beta_{ss',n}^{(j)} | \beta_{ss',n-1}^{(j)})$ with $(s, s') \in \mathcal{D}_n^{(j)}$, and $q_P^{(j)}$, $q_{S,s}^{(j)}$, $q_{D,ss'}$, and $\bar{q}_{N,m}^{(j)}$ denote the pseudo LHF nodes of the LoS paths (19), single-bounce paths (20), double-bounce paths (21), and new paths (22), respectively. For a detailed factor graph representation of the DA component, the reader is referred to [7]. In (e), new PSFV states are connected to the legacy PSFV states, reflecting the use of predicted legacy PSFV states for constructing the proposal PDF of new PSFVs supported by double-bounce paths, as detailed in Section V-D.

and $q_S(\mathbf{x}_n, \mathbf{p}_{s,\text{sfv}}^{(j)}, \mathbf{r}_{s,n}^{(j)} = 0, \mathbf{u}_{ss,n}^{(j)}, \mathbf{r}_{ss,n}^{(j)} = 1, \mathbf{a}_{ss,n}^{(j)}; \mathbf{z}_n^{(j)}) = 0$ for the invalid case, i.e., PSFV s does not exist but PR (s, s) exists, otherwise $q_S(\dots) \triangleq \delta(\mathbf{a}_{ss,n}^{(j)})$.

For double-bounce PRs: related to PSFV pair $(s, s') \in \mathcal{D}_n^{(j)}$, the pseudo LHF $q_D(\mathbf{x}_n, \mathbf{y}_{s,n}^{(j)}, \mathbf{y}_{s',n}^{(j)}, \beta_{ss',n}^{(j)}, \mathbf{a}_{ss',n}^{(j)}; \mathbf{z}_n^{(j)}) = q_D(\mathbf{x}_n, \mathbf{p}_{s,\text{sfv}}^{(j)}, \mathbf{r}_{s,n}^{(j)}, \mathbf{p}_{s',\text{sfv}}^{(j)}, \mathbf{r}_{s',n}^{(j)}, \mathbf{u}_{ss',n}^{(j)}, \mathbf{r}_{ss',n}^{(j)}, \mathbf{a}_{ss',n}^{(j)}; \mathbf{z}_n^{(j)})$ is given by

$$q_D(\mathbf{x}_n, \mathbf{p}_{s,\text{sfv}}^{(j)}, \mathbf{p}_{s',\text{sfv}}^{(j)}, \mathbf{u}_{ss',n}^{(j)}, \mathbf{r}_{ss',n}^{(j)}, \mathbf{a}_{ss',n}^{(j)}; \mathbf{z}_n^{(j)})$$

$$\triangleq \begin{cases} f_D(\mathbf{z}_{m,n}^{(j)} | \mathbf{p}_n, \mathbf{p}_{s,\text{sfv}}^{(j)}, \mathbf{p}_{s',\text{sfv}}^{(j)}, \mathbf{u}_{ss',n}^{(j)}) \\ \times \frac{p_d(\mathbf{u}_{ss',n}^{(j)})}{\mu_{\text{fa}} f_{\text{fa}}(\mathbf{z}_{m,n}^{(j)})}, & \mathbf{a}_{ss',n}^{(j)} \in \mathcal{M}_n^{(j)} \\ 1 - p_d(\mathbf{u}_{ss',n}^{(j)}), & \mathbf{a}_{ss',n}^{(j)} = 0 \end{cases} \quad (21)$$

and $q_D(\dots) = 0$ for $(\mathbf{r}_{s,n}^{(j)}, \mathbf{r}_{s',n}^{(j)}, \mathbf{r}_{ss',n}^{(j)}) \in \{(0, 1, 1), (1, 0, 1), (0, 0, 1)\}$ representing invalid cases that path (s, s') exists but one or both the associated surfaces are nonexistent. For other cases, $q_D(\dots) \triangleq \delta(\mathbf{a}_{ss',n}^{(j)})$.

For new PRs: related to new PSFVs, the pseudo LHF $\bar{q}_N(\mathbf{x}_n, \bar{\mathbf{y}}_{m,n}^{(j)}, \bar{\boldsymbol{\beta}}_{m,n}^{(j)}, \bar{a}_{m,n}^{(j)}; \mathbf{z}_n^{(j)}) = \bar{q}_N(\mathbf{x}_n, \bar{\mathbf{p}}_{m,\text{sfv}}^{(j)}, \bar{r}_{m,n}^{(j)}, \bar{u}_{mm,n}^{(j)}, \bar{r}_{mm,n}^{(j)}, \bar{a}_{m,n}^{(j)}; \mathbf{z}_n^{(j)})$ is given by

$$\bar{q}_N(\mathbf{x}_n, \bar{\mathbf{p}}_{m,\text{sfv}}^{(j)}, \bar{r}_{m,n}^{(j)} = 1, \bar{u}_{mm,n}^{(j)}, \bar{r}_{mm,n}^{(j)} = 1, \bar{a}_{m,n}^{(j)}; \mathbf{z}_n^{(j)}) \triangleq \begin{cases} 0, & \bar{a}_{m,n}^{(j)} \in \tilde{\mathcal{D}}_n^{(j)} \\ f_N(\mathbf{z}_{m,n}^{(j)} | \mathbf{p}_n, \bar{\mathbf{p}}_{m,\text{sfv}}^{(j)}, \bar{u}_{mm,n}^{(j)}) \\ \times \frac{\mu_n f_N(\bar{\mathbf{p}}_{m,\text{sfv}}^{(j)}, \bar{u}_{mm,n}^{(j)} | \mathbf{x}_n)}{\mu_{\text{fa}} f_{\text{fa}}(\mathbf{z}_{m,n}^{(j)})}, & \bar{a}_{m,n}^{(j)} = 0 \end{cases} \quad (22)$$

and $\bar{q}_N(\mathbf{x}_n, \bar{\mathbf{p}}_{m,\text{sfv}}^{(j)}, \bar{r}_{m,n}^{(j)} = 0, \bar{u}_{mm,n}^{(j)}, \bar{r}_{mm,n}^{(j)} = 0, \bar{a}_{m,n}^{(j)}; \mathbf{z}_n^{(j)}) \triangleq f_D(\bar{\mathbf{p}}_{m,\text{sfv}}^{(j)}) f_D(\bar{u}_{mm,n}^{(j)})$. For other cases, $\bar{q}_N(\dots) = 0$. Details about the joint prior PDF $f_N(\bar{\mathbf{p}}_{m,\text{sfv}}^{(j)}, \bar{u}_{mm,n}^{(j)} | \mathbf{x}_n)$ and the LHF $f_N(\mathbf{z}_{m,n}^{(j)} | \mathbf{p}_n, \bar{\mathbf{p}}_{m,\text{sfv}}^{(j)}, \bar{u}_{mm,n}^{(j)}) \triangleq f_{\forall s}(\mathbf{z}_{m,n}^{(j)} | \mathbf{p}_n, \bar{\mathbf{p}}_{m,\text{sfv}}^{(j)}, \bar{p}_{s,\text{sfv}}^{(j)}, \bar{u}_{mm,n}^{(j)})$ are provided in Section V-D.

The joint posterior PDF in (15) and its factor graph representation in Fig. 2, the binary check function $\psi(\underline{a}_{ss',n}^{(j)}, \bar{a}_{m,n}^{(j)})$ are in parts in line with [3], [7], [24], [31]. Details of the derivations of the system models, including (15) and the pseudo LHF (19)-(22) are provided in the supplementary material [27, Section II].

V. SUM PRODUCT ALGORITHM

Due to the loops inside the factor graph, we specify the following orders for message computation: (i) messages are sent only forward in time from $n-1$ to n and serially from PA $j-1$ to j ; (ii) iterative message passing is only performed for probabilistic DA, i.e., message passing iteration is performed only once in the loops connecting different PSFVs; (iii) messages are only sent from the agent state variable node to the new PSFV state variable node, not vice versa. Combining the specified orders with the generic SPA rules, the messages and beliefs involved in the factor graph in Fig. 2 are introduced for each time step n and each PA j as follows. For brevity, we provide only the general steps of the SPA algorithm in the following. The derivations of each message are presented in detail in the supplementary material [27, Section II].

A. Prediction

1) *Transition from Time $n-1$ to n* : First, a prediction step from time $n-1$ to n is performed for the agent state, all legacy PSFV states and PR states, leading to the predicted message for the agent state $\alpha(\mathbf{x}_n)$, the predicted messages $\alpha_s(\mathbf{p}_{s,\text{sfv}}, \mathbf{r}_{s,n})$ for all the legacy PSFVs $s \in \mathcal{S}_{n-1}$ and the predicted messages $\alpha_{ss'}(\underline{\boldsymbol{\beta}}_{ss',n}^{(j)}) = \alpha_{ss'}(\underline{\mathbf{u}}_{ss',n}^{(j)}, \mathbf{r}_{ss',n}^{(j)})$ for legacy PRs.

2) *Transition from PA $j-1$ to j* : For $j > 1$ at time n , the predicted messages $\alpha_s(\mathbf{p}_{s,\text{sfv}}, \mathbf{r}_{s,n}^{(j)})$ for former legacy PSFVs $s \in \mathcal{S}_{n-1}^{(j-1)}$ and the predicted messages $\alpha_{S_n^{(j-1)+m}(\mathbf{p}_{S_n^{(j-1)+m,\text{sfv}}, \mathbf{r}_{S_n^{(j-1)+m,n}^{(j)}})$ for former new PSFVs $m \in \mathcal{M}_n^{(j-1)}$ are as in [7].

B. Sequential PA Update

1) *Measurement Evaluation for LoS PRs*: The messages $\omega(\underline{a}_{00,n}^{(j)})$ propagating from the factor node $q_P(\mathbf{x}_n, \underline{\boldsymbol{\beta}}_{00,n}^{(j)}, \underline{a}_{00,n}^{(j)}; \mathbf{z}_n^{(j)})$ to the feature-oriented association variable nodes $\underline{a}_{00,n}^{(j)}$ are calculated.

2) *Measurement Evaluation for Legacy PSFVs*: For $s = s'$, the messages propagating from the factor node $q_S(\mathbf{x}_n, \underline{\mathbf{y}}_{s,n}^{(j)}, \underline{\boldsymbol{\beta}}_{s,n}^{(j)}, \underline{a}_{ss,n}^{(j)}; \mathbf{z}_n^{(j)})$ to the feature-oriented association variable nodes $\underline{a}_{ss,n}^{(j)}$ are given as $\omega(\underline{a}_{ss,n}^{(j)})$. For $s \neq s'$, the messages propagating from the factor node $q_D(\mathbf{x}_n, \underline{\mathbf{y}}_{s,n}^{(j)}, \underline{\mathbf{y}}_{s',n}^{(j)}, \underline{\boldsymbol{\beta}}_{ss',n}^{(j)}, \underline{a}_{ss',n}^{(j)}; \mathbf{z}_n^{(j)})$ to the feature-oriented association variable nodes $\underline{a}_{ss',n}^{(j)}$ are given as $\omega(\underline{a}_{ss',n}^{(j)})$.

3) *Measurement Evaluation for New PSFVs*: For PA j , the messages $\xi(\bar{a}_{m,n}^{(j)})$ sent from $\bar{q}_N(\mathbf{x}_n, \bar{\mathbf{y}}_{m,n}^{(j)}, \bar{\boldsymbol{\beta}}_{m,n}^{(j)}, \bar{a}_{m,n}^{(j)}; \mathbf{z}_n^{(j)})$ to the measurement-oriented association variable nodes $\bar{a}_{m,n}^{(j)}$ are calculated.

4) *Iterative Data Association*: With the messages $\omega(\underline{a}_{ss',n}^{(j)})$ and $\xi(\bar{a}_{m,n}^{(j)})$, the probabilistic DA messages $\eta(\underline{a}_{ss',n}^{(j)})$ and $\zeta(\bar{a}_{m,n}^{(j)})$ are obtained using loopy belief propagation (BP) according to [7], [31].

5) *Measurement Update for The Agent*: For the update of agent state \mathbf{x}_n , only the messages from legacy PSFVs are used. The messages sent from the factor node $q_P(\mathbf{x}_n, \underline{\boldsymbol{\beta}}_{00,n}^{(j)}, \underline{a}_{00,n}^{(j)}; \mathbf{z}_n^{(j)})$ to the agent state variable node \mathbf{x}_n are given as $\gamma_{00}^{(j)}(\mathbf{x}_n)$. For $s = s'$, the messages $\gamma_{ss}^{(j)}(\mathbf{x}_n)$ propagating from the factor node $q_S(\mathbf{x}_n, \underline{\mathbf{y}}_{s,n}^{(j)}, \underline{\boldsymbol{\beta}}_{s,n}^{(j)}, \underline{a}_{ss,n}^{(j)}; \mathbf{z}_n^{(j)})$ to the agent variable node \mathbf{x}_n are calculated. For $s \neq s'$, the messages $\gamma_{ss'}^{(j)}(\mathbf{x}_n)$ propagating from the factor node $q_D(\mathbf{x}_n, \underline{\mathbf{y}}_{s,n}^{(j)}, \underline{\mathbf{y}}_{s',n}^{(j)}, \underline{\boldsymbol{\beta}}_{ss',n}^{(j)}, \underline{a}_{ss',n}^{(j)}; \mathbf{z}_n^{(j)})$ to the agent state variable node \mathbf{x}_n are calculated.

6) *Measurement Update for Legacy PSFVs*: For $s = s'$, the messages $\rho_{ss}(\underline{\mathbf{y}}_{s,n}^{(j)}) = \rho_{ss}(\mathbf{p}_{s,\text{sfv}}, \mathbf{r}_{s,n}^{(j)})$ propagating from the factor node $q_S(\mathbf{x}_n, \underline{\mathbf{y}}_{s,n}^{(j)}, \underline{\boldsymbol{\beta}}_{s,n}^{(j)}, \underline{a}_{ss,n}^{(j)}; \mathbf{z}_n^{(j)})$ to the PSFV variable node $\underline{\mathbf{y}}_{s,n}^{(j)}$ are calculated. For $s \neq s'$, the messages $\rho_{ss'}(\underline{\mathbf{y}}_{s,n}^{(j)}) = \rho_{ss'}(\mathbf{p}_{s,\text{sfv}}, \mathbf{r}_{s,n}^{(j)})$ sent to the PSFV variable node $\underline{\mathbf{y}}_{s,n}^{(j)}$ are also calculated. With $\rho_{ss}(\underline{\mathbf{y}}_{s,n}^{(j)})$ and $\rho_{ss'}(\underline{\mathbf{y}}_{s,n}^{(j)})$, the messages $\gamma(\underline{\mathbf{y}}_{s,n}^{(j)}) \triangleq \gamma(\mathbf{p}_{s,\text{sfv}}, \mathbf{r}_{s,n}^{(j)})$ sent to the next PA are further calculated.

7) *Measurement Update for New PSFVs*: The messages sent from $\bar{q}_N(\mathbf{x}_n, \bar{\mathbf{y}}_{m,n}^{(j)}, \bar{\boldsymbol{\beta}}_{m,n}^{(j)}, \bar{a}_{m,n}^{(j)}; \mathbf{z}_n^{(j)})$ to the variable node $\bar{\mathbf{y}}_{m,n}^{(j)}$ are denoted as $\phi(\bar{\mathbf{y}}_{m,n}^{(j)}) \triangleq \phi(\bar{\mathbf{p}}_{m,\text{sfv}}, \bar{r}_{m,n}^{(j)})$.

8) *Measurement Update for Legacy PRs*: The messages $\kappa(\underline{\boldsymbol{\beta}}_{00,n}^{(j)}) \triangleq \kappa(\underline{\mathbf{u}}_{00,n}^{(j)}, \mathbf{r}_{00,n}^{(j)})$ sent from the factor node $q_P(\mathbf{x}_n, \underline{\boldsymbol{\beta}}_{00,n}^{(j)}, \underline{a}_{00,n}^{(j)}; \mathbf{z}_n^{(j)})$ to the PR node $\underline{\boldsymbol{\beta}}_{00,n}^{(j)}$ are calculated. For $s = s'$, the messages sent from the factor node $q_S(\mathbf{x}_n, \underline{\mathbf{y}}_{s,n}^{(j)}, \underline{\boldsymbol{\beta}}_{s,n}^{(j)}, \underline{a}_{ss,n}^{(j)}; \mathbf{z}_n^{(j)})$ to the PR node $\underline{\boldsymbol{\beta}}_{s,n}^{(j)}$ are given as $\kappa(\underline{\boldsymbol{\beta}}_{ss,n}^{(j)}) \triangleq \kappa(\underline{\mathbf{u}}_{ss,n}^{(j)}, \mathbf{r}_{ss,n}^{(j)})$. For $s \neq s'$, the messages $\kappa(\underline{\boldsymbol{\beta}}_{ss',n}^{(j)}) \triangleq \kappa(\underline{\mathbf{u}}_{ss',n}^{(j)}, \mathbf{r}_{ss',n}^{(j)})$ sent from the factor node $q_D(\mathbf{x}_n, \underline{\mathbf{y}}_{s,n}^{(j)}, \underline{\mathbf{y}}_{s',n}^{(j)}, \underline{\boldsymbol{\beta}}_{ss',n}^{(j)}, \underline{a}_{ss',n}^{(j)}; \mathbf{z}_n^{(j)})$ to the PR node $\underline{\boldsymbol{\beta}}_{ss',n}^{(j)}$ are calculated. Based on the messages above, the messages

$\gamma(\underline{\beta}_{ss',n}^{(j)}) \triangleq \gamma(\underline{u}_{ss',n}^{(j)}, \underline{r}_{ss',n}^{(j)})$ sent to time $n+1$ are further obtained.

9) *Measurement Update for New PRs*: The messages $\kappa(\underline{\beta}_{m,n}^{(j)}) \triangleq \kappa(\underline{u}_{mm,n}^{(j)}, \underline{r}_{mm,n}^{(j)})$ sent from the factor node $\bar{q}_N(\mathbf{x}_n, \bar{\mathbf{y}}_{m,n}^{(j)}, \bar{\beta}_{m,n}^{(j)}, \bar{a}_{m,n}^{(j)}; \mathbf{z}_n^{(j)})$ to the new VA variable node $\bar{\beta}_{m,n}^{(j)}$ are calculated.

C. Belief Calculation

After calculating the messages for all PAs, the belief $\tilde{f}(\mathbf{x}_n)$ of the agent state approximating $f(\mathbf{x}_n | \mathbf{z}_{1:n})$ is given by

$$\tilde{f}(\mathbf{x}_n) = C_n \alpha(\mathbf{x}_n) \prod_{(s,s') \in \mathcal{D}_n^{(j)}} \gamma_{ss'}^{(j)}(\mathbf{x}_n) \prod_{j=1}^J \gamma_{00}^{(j)}(\mathbf{x}_n). \quad (23)$$

The beliefs of legacy PSFVs $\tilde{f}(\underline{\mathbf{y}}_{s,n}^{(j)}) \triangleq \tilde{f}(\underline{\mathbf{p}}_{s,\text{sfv}}^{(j)}, \underline{r}_{s,n}^{(j)})$ with $s \in \mathcal{S}_n^{(j)}$ and of new PSFVs $\tilde{f}(\underline{\mathbf{y}}_{m,n}^{(j)}) \triangleq \tilde{f}(\underline{\mathbf{p}}_{m,\text{sfv}}^{(j)}, \underline{r}_{m,n}^{(j)})$ with $m \in \mathcal{M}_n^{(j)}$ are given by

$$\tilde{f}(\underline{\mathbf{y}}_{s,n}^{(j)}) = \underline{C}_{s,n} \gamma(\underline{\mathbf{y}}_{s,n}^{(j)}), \quad (24)$$

$$\tilde{f}(\underline{\mathbf{y}}_{m,n}^{(j)}) = \bar{C}_{m,n} \phi(\underline{\mathbf{y}}_{m,n}^{(j)}). \quad (25)$$

At each PA j , the beliefs $\tilde{f}(\underline{\beta}_{ss',n}^{(j)}) \triangleq \tilde{f}(\underline{u}_{ss',n}^{(j)}, \underline{r}_{ss',n}^{(j)})$ of legacy VAs $(s, s') \in \tilde{\mathcal{D}}_n^{(j)}$ are given by

$$\tilde{f}(\underline{u}_{ss',n}^{(j)}, \underline{r}_{ss',n}^{(j)}) = \underline{C}_{ss',n}^{(j)} \gamma(\underline{u}_{ss',n}^{(j)}, \underline{r}_{ss',n}^{(j)}) \quad (26)$$

and the beliefs $\tilde{f}(\underline{\beta}_{m,n}^{(j)}) \triangleq \tilde{f}(\underline{u}_{mm,n}^{(j)}, \underline{r}_{mm,n}^{(j)})$ of new PRs are given by

$$\tilde{f}(\underline{\beta}_{m,n}^{(j)}) = \bar{C}_{mm,n}^{(j)} \kappa(\underline{u}_{mm,n}^{(j)}, \underline{r}_{mm,n}^{(j)}). \quad (27)$$

The normalization constants C_n , $\underline{C}_{s,n}$, $\bar{C}_{m,n}$, $\underline{C}_{ss',n}^{(j)}$, $\bar{C}_{mm,n}^{(j)}$ ensure that the beliefs are valid probability distributions, as an example, $\underline{C}_{s,n} = (\int \gamma(\underline{\mathbf{p}}_{s,\text{sfv}}^{(j)}, 1) d\underline{\mathbf{p}}_{s,\text{sfv}}^{(j)} + \gamma_{s,n}^{(j)})^{-1}$.

D. Implementation Aspect and Computational Complexity

As the integrations involved in the message and belief calculations cannot be obtained analytically, we employ a computationally efficient, sequential, particle-based, message-passing implementation, as outlined in [7], [25], [32]. Specifically, we adopt a ‘‘stacked state’’ approach comprising the agent state, the PSFV states, and the PR states, as detailed in [25], [38]. This approach leads to complexity that scales linearly with the number of particles. The supplementary material of [25] provides a comprehensive description of the weight calculations when using ‘‘stacked states’’. SPA performed on loopy factor graph has been shown to converge and provides accurate approximations of marginal posterior PDFs [36], [39]. As the numbers of PSFVs and their associated PRs grow with time, we remove PSFVs with $f(r_{s,n}^{(j)} = 1 | \mathbf{z}_{1:n})$ below a threshold p_{prun} , together with their associated PRs from the state space (‘‘pruned’’) at each PA j to limit computation complexity. Note that only the PRs with existence probabilities above p_{prun} are used for the measurement update of legacy PSFVs in Section V-B6.

The conditional joint prior PDF of each newly detected PSFV state and its associated PR state is factorized as $f_n(\underline{\mathbf{p}}_{m,\text{sfv}}^{(j)}, \underline{u}_{mm,n}^{(j)} | \mathbf{x}_n) = f_n(\underline{\mathbf{p}}_{m,\text{sfv}}^{(j)} | \mathbf{x}_n) f_n(\underline{u}_{mm,n}^{(j)})$. Instead of using the prior PDFs $f_n(\underline{\mathbf{p}}_{m,\text{sfv}}^{(j)} | \mathbf{x}_n)$ and $f_n(\underline{u}_{mm,n}^{(j)})$, we develop alternative proposal PDFs to account for the fact that a new surface could generate both single-bounce paths and double-bounce paths. As an example shown in Fig. 1, the surface 3 is solely supported by a double-bounce path until time step 126 where a single-bounce path shows up. Note that conventional methods mostly use the single-bounce path assumption for initialization of new features. Early detection of new SFVs supported by double-bounce paths enables the use of more measurements associated with these paths, enhancing both mapping and localization performance as shown in Section VI-D. The states of new SFVs and corresponding new VAs are introduced considering following hypotheses, i.e., measurement m can be generated by (i) the single-bounce path from a new PSFV; or (ii) a double-bounce path from the SFV-pair ‘‘legacy PSFV $s \in \mathcal{S}_n^{(j)}$ to the new PSFV’’; or (iii) SFV-pair ‘‘new PSFV to the legacy PSFV $s \in \mathcal{S}_n^{(j)}$ ’’. Specifically, for each measurement $\mathbf{z}_{m,n}^{(j)}$, the initial states $\mathbf{p}_{\text{sfv}}^{\text{ini}}$ and u^{ini} are applied to $f_S(\mathbf{z}_{m,n}^{(j)} | \mathbf{p}_n, \mathbf{p}_{\text{sfv}}^{\text{ini}}, u^{\text{ini}})$ as in (7) to calculate the LHF for single-bounce hypothesis, and to $f_D(\mathbf{z}_{m,n}^{(j)} | \mathbf{p}_n, \underline{\mathbf{p}}_{s,\text{sfv}}^{(j)}, \mathbf{p}_{\text{sfv}}^{\text{ini}}, u^{\text{ini}})$ and $f_D(\mathbf{z}_{m,n}^{(j)} | \mathbf{p}_n, \mathbf{p}_{\text{sfv}}^{\text{ini}}, \underline{\mathbf{p}}_{s,\text{sfv}}^{(j)}, u^{\text{ini}})$ as in (8) for each legacy PSFV $s \in \mathcal{S}_n^{(j)}$ to calculate the LHFs for double-bounce hypotheses. The particles for the states $\mathbf{p}_{\text{sfv}}^{\text{ini}}$ and u^{ini} are obtained by sampling from the initial prior PDFs $f(\mathbf{p}_{\text{sfv}}^{\text{ini}})$ and $f(u^{\text{ini}})$. The new PSFV state $\bar{\mathbf{p}}_{m,\text{sfv}}^{(j)}$ and associated new PR state $\bar{u}_{mm,n}^{(j)}$ needed for (22) are further obtained by resampling the particles representing $\mathbf{p}_{\text{sfv}}^{\text{ini}}$ and u^{ini} based on the proposal PDF, i.e., the aggregated LHF $f_{\forall s}(\mathbf{z}_{m,n}^{(j)} | \mathbf{p}_n, \bar{\mathbf{p}}_{m,\text{sfv}}^{(j)}, \underline{\mathbf{p}}_{s,\text{sfv}}^{(j)}, \bar{u}_{mm,n}^{(j)})$ of all the above LHFs. Thus, the LHF in (22) is given as $f_N(\mathbf{z}_{m,n}^{(j)} | \mathbf{p}_n, \bar{\mathbf{p}}_{m,\text{sfv}}^{(j)}, \bar{u}_{mm,n}^{(j)}) \triangleq f_{\forall s}(\mathbf{z}_{m,n}^{(j)} | \mathbf{p}_n, \bar{\mathbf{p}}_{m,\text{sfv}}^{(j)}, \underline{\mathbf{p}}_{s,\text{sfv}}^{(j)}, \bar{u}_{mm,n}^{(j)})$. Clearly, the double-bounce hypothesis requires a converged state $\underline{\mathbf{p}}_{s,\text{sfv}}^{(j)}$ of the paired legacy PSFV. In general, mapping begins with a combination of single- and double-bounce paths for each surface, as environments containing only double- or higher-order bounce paths are rare. At the beginning, surfaces around the agent are rapidly identified primarily using single-bounce paths. Over time, their states gradually converge and are used to initialize new surfaces supported by double-bounce paths derived from them.

Iterative message passing is performed for probabilistic DA. The computational complexity per DA iteration at the j th processing block is $\mathcal{O}(L_n^{(j)} M_n)$ [3], [7], [31], where $L_n^{(j)} = |\tilde{\mathcal{D}}_n^{(j)}| = 1 + S_n^{(j)2}$ is the number of *PSFV-oriented* association variables $\underline{a}_{ss',n}^{(j)}$ and M_n is the number of *measurement-oriented* association variables $\bar{a}_{m,n}^{(j)}$. The number of iterations required to satisfy the convergence criterion is shown to be bounded [36]. With proper pruning at each processing block, the complexity is further reduced significantly. Moreover, by generating the proposal PDF for new PSFVs as mentioned above, we still follow the assumption ‘‘one measurement–one new PSFV’’ as in [7], therefore the probabilistic DA is not

further complicated due to considering multiple PSFV-pairs for each measurement.

VI. EXPERIMENTAL RESULTS

The proposed method AM-SLAM is validated using both synthetic and real RF measurements. First, using synthetic measurements from a D-MIMO propagation scenario shown in Fig. 1, the performance of AM-SLAM is validated and compared to two reference methods exploiting VAs: (i) the *multipath-based SLAM (MP-SLAM)* from [3] extended with amplitude statistical model [24], [26]; (ii) the *channel SLAM (CH-SLAM)* from [1] excluding the channel estimation stage. We extended MP-SLAM and CH-SLAM to a MIMO setup considering angular statistical models, i.e., ranges, AoDs, AoAs are considered for all paths in all methods. However, the reference methods apply the single-bounce assumption for all VAs when calculating AoDs, leading to mismatch for AoDs of double-bounce paths in LHF, therefore double-bounce measurements are mostly evaluated as FAs in MP-SLAM and CH-SLAM. For consistency with AM-SLAM and MP-SLAM exploiting adaptive variances as shown in Section III-A, CH-SLAM used Fisher information-based variances determined with amplitude measurements $z_{um,n}^{(j)}$. Note that both reference methods assume independent statistics across VAs, hence they do not fuse information about map features across propagation paths like AM-SLAM.

A. Simulation Setup

The following parameters are used for AM-SLAM, MP-SLAM and CH-SLAM unless otherwise stated. The state-transition PDF $f(\mathbf{x}_n|\mathbf{x}_{n-1})$ of the agent state is defined by a linear near constant-velocity motion model [34], i.e., $\mathbf{x}_n = \mathbf{F}\mathbf{x}_{n-1} + \mathbf{\Gamma}\mathbf{v}_n$, where the transition matrices $\mathbf{F} \in \mathbb{R}^{4 \times 4}$ and $\mathbf{\Gamma} \in \mathbb{R}^{4 \times 2}$ are chosen as in [34] with the sampling period ΔT . The driving process $\mathbf{v}_n \in \mathbb{R}^{2 \times 1}$ is independent and identically distributed (iid) across time n , zero-mean and Gaussian with covariance matrix $\sigma_v^2 \mathbf{I}_2$, where σ_v represents the average speed increment along the x or y axis during ΔT and \mathbf{I}_2 is a 2×2 identity matrix. The state-transition PDF of the agent orientation is given as $\Delta\varphi_n = \Delta\varphi_{n-1} + \epsilon_{\varphi,n}$ where the noise $\epsilon_{\varphi,n}$ is zero-mean and Gaussian with variance σ_φ^2 . The state-transition PDF of the PR normalized amplitude $\underline{u}_{ss',n}^{(j)}$ is chosen to be $\underline{u}_{ss',n}^{(j)} = u_{ss',n-1}^{(j)} + \epsilon_{ss',n}$, where the noise $\epsilon_{ss',n}$ is iid across (s,s') $\in \mathcal{D}_n^{(j)}$, j and n , zero-mean, and Gaussian with variance $\sigma_{ss',n}^2$. Geometrically, SFVs represent static reflective surfaces and VAs represent mirror images of static PAs, therefore their positions should remain unchanged over time. However, for the sake of numerical stability and to account for surface nonidealities such as slight curvature, a regularization noise is introduced in the state-transition PDFs of PSFVs in AM-SLAM. The PDFs $f(\underline{\mathbf{p}}_{s,\text{sfv}}^{(j)}|\mathbf{p}_{s,\text{sfv}})$ and $f(\underline{\mathbf{p}}_{s,\text{sfv}}^{(j)}|\mathbf{p}_{s,\text{sfv}}^{(j-1)})$ in (9) and (11) are given as $\underline{\mathbf{p}}_{s,\text{sfv}}^{(j)} = \mathbf{p}_{s,\text{sfv}} + \epsilon_s$ and $\underline{\mathbf{p}}_{s,\text{sfv}}^{(j)} = \mathbf{p}_{s,\text{sfv}}^{(j-1)} + \epsilon_s$, where ϵ_s is iid across s , zero-mean, and Gaussian with variance $\sigma_s^2 \mathbf{I}_2$. Similarly, we also apply a Gaussian regularization noise in the state-transition PDFs of VA position states in MP-SLAM and

CH-SLAM with variance $\sigma_{\text{va}}^2 \mathbf{I}_2$. Furthermore, only the legacy PSFVs that are consecutively detected over 3 time steps are considered for the initialization of new PSFVs.

The samples for the initial agent state are drawn from a 5-D uniform distribution centered at $[\mathbf{p}_0^T \ 0 \ 0 \ \Delta\varphi_0]^T$ where \mathbf{p}_0 and $\Delta\varphi_0$ are the true agent start position and orientation, and the support of position, velocity and orientation components are $[-0.5, 0.5]$ m, $[0.01, 0.01]$ m/s and $[-10^\circ, 10^\circ]$, respectively. The samples representing initial state of new PSFVs $\mathbf{p}_{\text{sfv}}^{\text{ini}}$ are drawn from the PDF $f(\mathbf{p}_{\text{sfv}}^{\text{ini}})$ which is uniform on the region-of-interest (RoI), i.e., $[-15\text{m}, 15\text{m}] \times [-15\text{m}, 15\text{m}]$ centered at the coordinate center. The samples representing the initial normalized amplitude state u^{ini} are drawn from a Gaussian distribution with mean $z_{um,n}^{(j)}$ and variance calculated using the measurement $z_{um,n}$. We performed 100 simulation runs with the following parameters: the mean number of FAs $\mu_{\text{fa}} = 2$, the mean number of new PSFVs $\mu_n = 0.1$ in AM-SLAM, the mean number of new VAs $\mu_n^{\text{va}} = 0.1$ in MP-SLAM, the detection threshold for normalized amplitude measurements $u_{\text{de}} = 6$ dB, the probability of survival $p_s = 0.99$, the pruning threshold $p_{\text{prun}} = 0.1$, the existence detection thresholds for PRs and PSFVs $p_{\text{pr}} = 0.5$ and $p_{\text{sfv}} = 0.5$, 60000 particles for each random variable state, the agent acceleration noise variance $\sigma_v^2 = 9 \cdot 10^{-4}$ m/s², the orientation noise standard deviation $\sigma_\varphi = 7^\circ$, the regularization noise standard deviations for PSFV and VA position states $\sigma_s = 0.01$ m and $\sigma_{\text{va}} = 0.01$ m, the normalized amplitude noise standard deviation $\sigma_{ss',n} = 0.02 \hat{u}_{ss',n-1}^{(j)}$.⁴ For CH-SLAM, we used 2000 particles for the agent and 1000 for the VAs.

The FA measurements originating from the pre-processing stage are modeled by a Poisson point process with mean number μ_{fa} and PDF factorized as $f_{\text{fa}}(z_{m,n}^{(j)}) = f_{\text{fa}}(z_{dm,n}^{(j)})f_{\text{fa}}(z_{\phi_{m,n}}^{(j)})f_{\text{fa}}(z_{\varphi_{m,n}}^{(j)})f_{\text{fa}}(z_{um,n}^{(j)})$, where the individual PDFs corresponding to distances, AoDs and AoAs are uniform on $[0, d_{\text{max}}]$, $[-\pi, \pi]$ and $[-\pi, \pi]$, respectively. For the normalized amplitudes, $f_{\text{fa}}(z_{um,n}^{(j)})$ is given by a truncated Rayleigh PDF with 1/2 scale parameter [24], [40].

B. Performance Metrics

The performance of different methods is measured in terms of their root mean square errors (RMSEs) of the agent position and orientation, and the optimal subpattern assignment (OSPA) error [41] of VAs and SFVs⁵ with cutoff distance 5 m and order 1. The OSPA error is a distance metric that quantifies the difference between a set of estimates and known truths, and it accounts for both the estimation error and cardinality error. In addition, we compute the PCRLBs [29], [42], [43] as a performance benchmark, which explicitly characterizes the localization and mapping error bounds while accounting for data fusion across multiple PAs and propagation paths, as well as system-related factors like array geometry, SNR, and

⁴The heuristic approach to scale the standard deviation $\sigma_{ss',n}$ by the MMSE estimates was chosen considering that the range of normalized amplitude values tends to be very large.

⁵Note that the OSPA error is normalized by the larger cardinality of the comparing sets. Correspondingly, we normalize the error bound with the true number of SFVs.

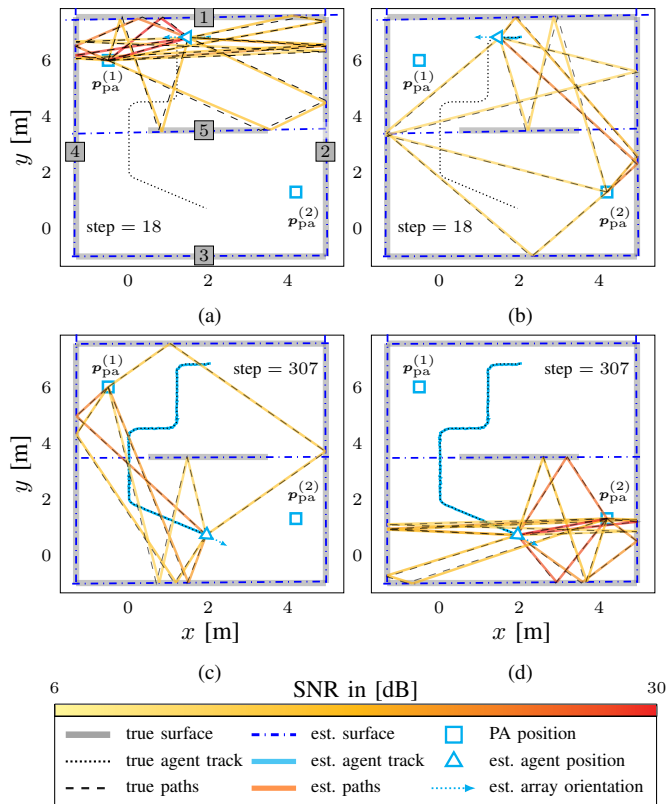


Fig. 3: Results of a simulation run of AM-SLAM for Experiment 1, showing the true and estimated reflective surfaces, propagation paths, and agent positions at time steps $n = 18$ in (a), (b) and $n = 307$ in (c), (d), respectively. In (a), the surfaces are labeled in the same order as in Fig. 1. The line representations of the estimated surfaces are computed from the MMSE estimates of the detected SFVs. Estimated propagation paths are obtained by connecting the MMSE estimate of the agent position, the interaction points on the estimated surfaces, and the PAs, and are compared with the true visible paths at each time step. The color of each estimated path represents its estimated SNR, i.e., the square of the normalized amplitude MMSE estimate.

bandwidth. The mean RMSEs, mean OSPA (MOSPA) errors are obtained at each time by averaging over all converged simulation runs and compared against the position error bound (PEB), orientation error bound (OEB), and mapping error bounds (MEBs) derived in [43]. Furthermore, to illustrate the contribution of different types of propagation paths to the achievable performance, error bounds are reported for three different setups: (i) DB, e.g., PEB(DB), the PEB considering LoSs, single and double-bounce paths. (ii) (SB), the bound considering LoSs, single-bounce paths and (iii) (LoS), the bound considering LoSs only. A simulation run with $\forall n : \|\hat{\mathbf{x}}_n - \mathbf{x}_n\| < 1\text{ m}$ and $\forall s : \|\hat{\mathbf{p}}_{s,\text{sfv}} - \mathbf{p}_{s,\text{sfv}}\| < 1\text{ m}$ is considered as converged.

C. Synthetic Measurements

Measurements $\mathbf{z}_{m,n}^{(j)}$ are synthetically generated according to the scenario shown in Fig. 1, where a D-MIMO system operating at $f_c = 6\text{ GHz}$ with bandwidth of 1 GHz is used. The same 5×5 uniform rectangular array with inter-element spacing of $\lambda/4$ is used at both PAs and the mobile agent. Over time steps, propagation paths experiencing up to double

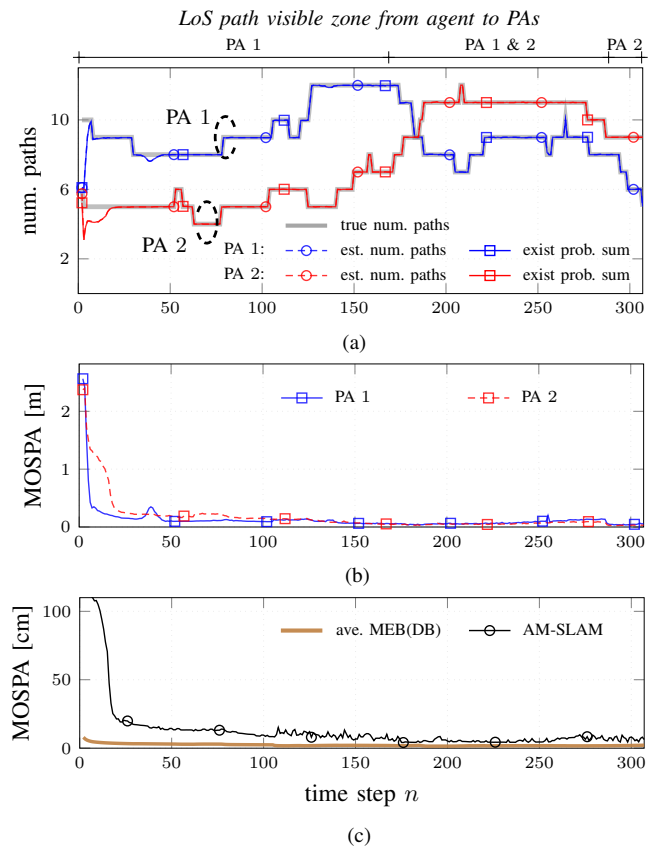


Fig. 4: Performance results of "soft" ray tracing using AM-SLAM for Experiment 1. (a) For each PA, the true number of visible paths, the number of detected paths, and the sum of the estimated existence probabilities of the detected paths are shown. (b) MOSPA errors of the estimated VAs, obtained by geometric transformation of the SFV estimates at each PA. (c) MOSPA errors of the estimated SFVs, including a comparison with the MEBs(DB), averaged over all surfaces. All values are averaged over all simulation runs at each time step.

bounces with time-varying distances, AoAs, AoDs, and normalized amplitudes were synthesized. We assume that the PA orientations are 0° and the true agent orientation is consistent with the direction of movement. The amplitude of each path is assumed to follow free-space path loss and additionally attenuated by 3 dB after each bounce on a surface. The output SNR at 1 m from the PA is assumed to be $\text{SNR}_{1\text{m}} = 30\text{ dB}$, according to which the measurement noise standard deviation is further calculated based on the Fisher information [24], [26], [33]. In each simulation run, noisy measurements are generated according to (2)–(5), i.e., adding noises (determined based on the Fisher information) to the true path parameters, and stacked into the vector $\mathbf{z}_n^{(j)}$. In addition, FA measurements are generated with mean number $\mu_{\text{fa}} = 2$ and added to $\mathbf{z}_n^{(j)}$. In the following, we show results for two synthetic measurement setups: (i) *Experiment 1*: both PA 1 and PA 2 are used, the agent moves from point A to C in Fig. 1, leading to a total of 307 time steps. LoS propagation applies to at least one PA; (ii) *Experiment 2*: only PA 1 is used, the agent moves from point B to D, leading to a total of 312 time steps. Obstructed LoS (OLOs) condition applies after time step 220.

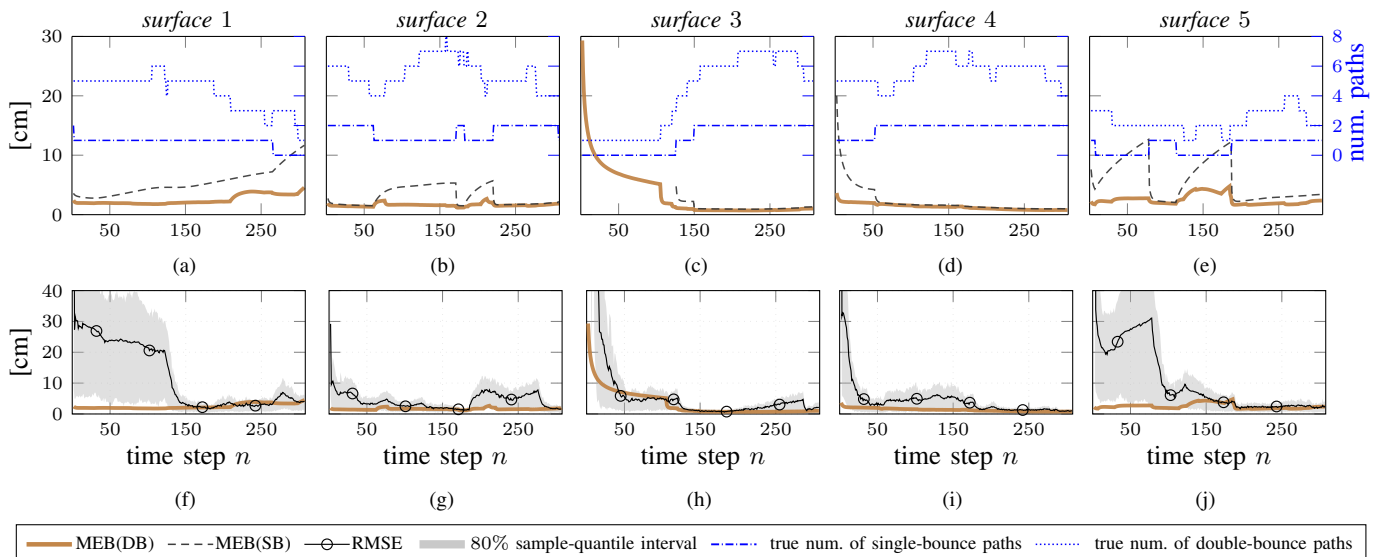


Fig. 5: Performance results of AM-SLAM for Experiment 1. For each surface labeled as $s \in \{1, \dots, 5\}$ in Figs. 1 and 3a, (a)–(e) show the MEBs and the corresponding true numbers of single- and double-bounce paths over time, while (f)–(j) show the RMSEs of the SFV position estimates. The shaded bands around the mean RMSEs indicate the variability of the error samples, corresponding to central 80% quantile intervals [43].

D. Results for Synthetic Measurements

Fig. 3 depicts for one exemplary simulation run of AM-SLAM the MMSE estimates of the agent positions and orientations, the detected reflective surfaces (obtained from the MMSE estimates of SFV positions), as well as the detected PRs. It is shown that AM-SLAM performs accurate ray tracing, the paths at each PA are accurately detected and estimated in terms of their time-varying geometrical parameters and SNRs. Leveraging all PAs and visible MPCs, AM-SLAM accurately localized the agent and rapidly identified all five surfaces including the lower one (surface 3) supported by a single double-bounce path until steps $n > 126$, proving the mapping capability to bypass OLoS conditions. Fig. 4 illustrates more on the “soft” ray tracing. It can be seen that AM-SLAM accurately adapts to the time-varying path visibilities and states at all PAs. Specifically, as shown in Fig. 4a the numbers of detected paths rapidly converge to the true path numbers, and in Fig. 4b the MOSPAs errors of the VA positions rapidly drop below 20 cm at the beginning. The close alignment between the sum of the estimated path existence probabilities and the true number of paths further indicates the strong confidence in the estimates, with individual existence probabilities approaching one.

In the following, we present the statistical performance evaluation⁶. For both experiments, none of the 100 simulation runs diverged for AM-SLAM and MP-SLAM. For CH-SLAM, 5 and 26 runs diverged in Experiment 1 and Experiment 2, respectively⁷. All simulations are conducted on an AMD Ryzen 9 5950X CPU (16 cores, 32 threads; 2.2–3.4 GHz). The average runtimes per time step (MATLAB implementations)

⁶We excluded outliers (unless stated otherwise) with values exceeding 1.5 interquartile ranges above the upper quartile or below the lower quartile [43].

⁷In Experiment 2, for MP-SLAM and CH-SLAM, we only evaluate the estimates up to step 285 for the convergence check, since beyond this step only double-bounce paths exist and all runs for the two methods diverged.

are 2.54 s for AM-SLAM, 0.6 s for MP-SLAM, and 9.43 s for CH-SLAM.

Figs. 5a to 5e show the MEBs(SB) and MEBs(DB) introduced in [43], where the gap between the bounds for each surface highlights the importance of incorporating double- or higher order-bounce paths for mapping, particularly under OLoS conditions and when single-bounce paths are unavailable. It is also shown that the MEBs effectively capture the impacts of individual paths. For instance, for surface 2 the rise in MEB(DB) around time step $n = 220$ indicates a brief disappearance of a double-bounce path. Figs. 5f to 5j further present the RMSEs of SFVs positions and compared against the MEBs(DB), where the associations between the SFVs’ estimates and ground truth were decided using the Hungarian method [44]. In Figs. 5f and 5j, slightly higher RMSEs are observed for surfaces 1 and 5 at the beginning, which arise from the agent’s initial orientation ambiguity leading to the first established surfaces to become stuck in tilted states. This is resolved once the agent undergoes sufficient directional change, specifically after the agent’s first turn at around step 30, the RMSEs start to drop to the MEBs(DB) level. Overall, AM-SLAM converges asymptotically to the MEBs(DB) for individual surfaces. As also depicted in Fig. 4c, the mean MOSPAs of the detected PSFVs rapidly attain the MEBs averaged over all surfaces.

Fig. 6 shows for AM-SLAM, MP-SLAM and CH-SLAM the RMSEs of agent orientation and position, and the comparison against the OEB(DB) and PEB(DB), respectively. As shown in Figs. 6e and 6f for Experiment 1, as the map is rapidly established at the beginning, AM-SLAM efficiently leverages the information from both PAs and all single- and double-bounce paths, attains the OEB(DB) and PEB(DB) with RMSEs quickly dropping below 1° and 1 cm. Note that MP-SLAM and CH-SLAM also converge asymptotically to the PEB(DB) even though they exploit only LoS and single-

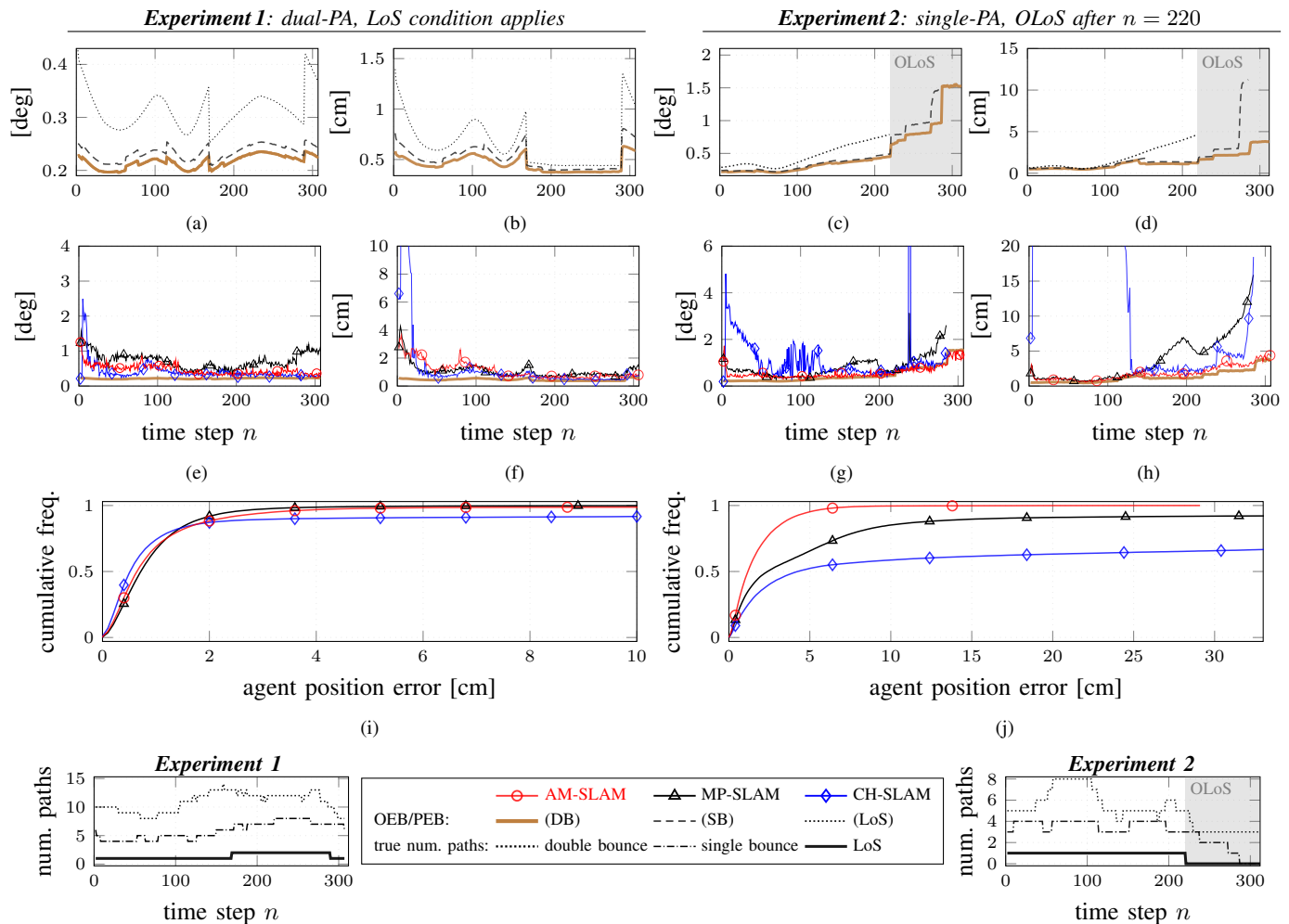


Fig. 6: Performance results of AM-SLAM, MP-SLAM, and CH-SLAM for Experiments 1 and 2 with synthetic measurements. (a)–(d) OEBS and PEBS for different path sets, i.e., LoS, single-bounce (SB), and double-bounce (DB). (e)–(h) RMSEs of the agent orientation and position, including a comparison with the corresponding OEBS(DB) and PEBS(DB). (i)–(j) Cumulative frequencies of the RMSEs (including outliers) of the agent position. In addition, the true numbers of LoS, single-bounce, and double-bounce paths over time are shown for both experiments.

bounce paths, which is due to the contribution of higher-order bounce paths to localization is marginal under MIMO conditions with strong LoSs, as evidenced by the theoretical error bounds in Fig. 6b. In Experiment 2 with the single-PA setup, Figs. 6g and 6h show that AM-SLAM remains tightly aligned with the bounds from the beginning and significantly outperforms MP-SLAM and CH-SLAM under OLoS condition after time step $n = 220$. Even beyond $n = 286$ where only double-bounce paths remain and both MP-SLAM and CH-SLAM completely fail, AM-SLAM still localizes accurately and stays close to the bounds. Figs. 6i and 6j show the cumulative frequencies of the agent errors, including the diverged runs and outliers. The results show that AM-SLAM achieves statistically significant improvements in both accuracy and robustness (fewer instances of large errors), especially in challenging OLoS scenarios, highlighting the performance gain from fusion with double-bounce paths and incorporating amplitude information in the statistical models.

The low mapping and agent RMSEs of AM-SLAM demonstrate the great potential of AM-SLAM for accurate and robust

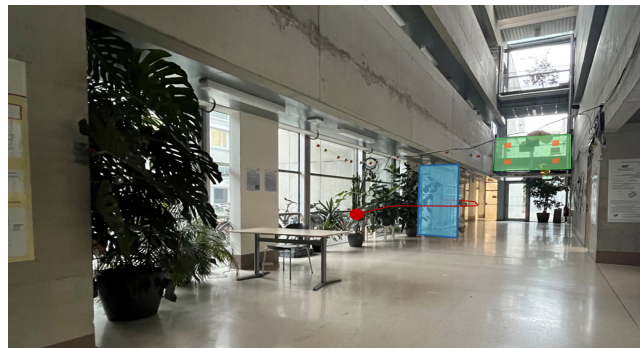


Fig. 7: Overview of the hallway measurement environment at TU Graz, Austria. Ground-truth PA positions and the agent trajectory are shown by brown rectangles and a solid red line, respectively.

sensing. Moreover, the mapping and ray tracing results suggest the broader applicability of the proposed method beyond mapping and localization. AM-SLAM infers the number of visible paths which upper-bounds the rank of MIMO channel matrix and hence the number of independent spatial data streams

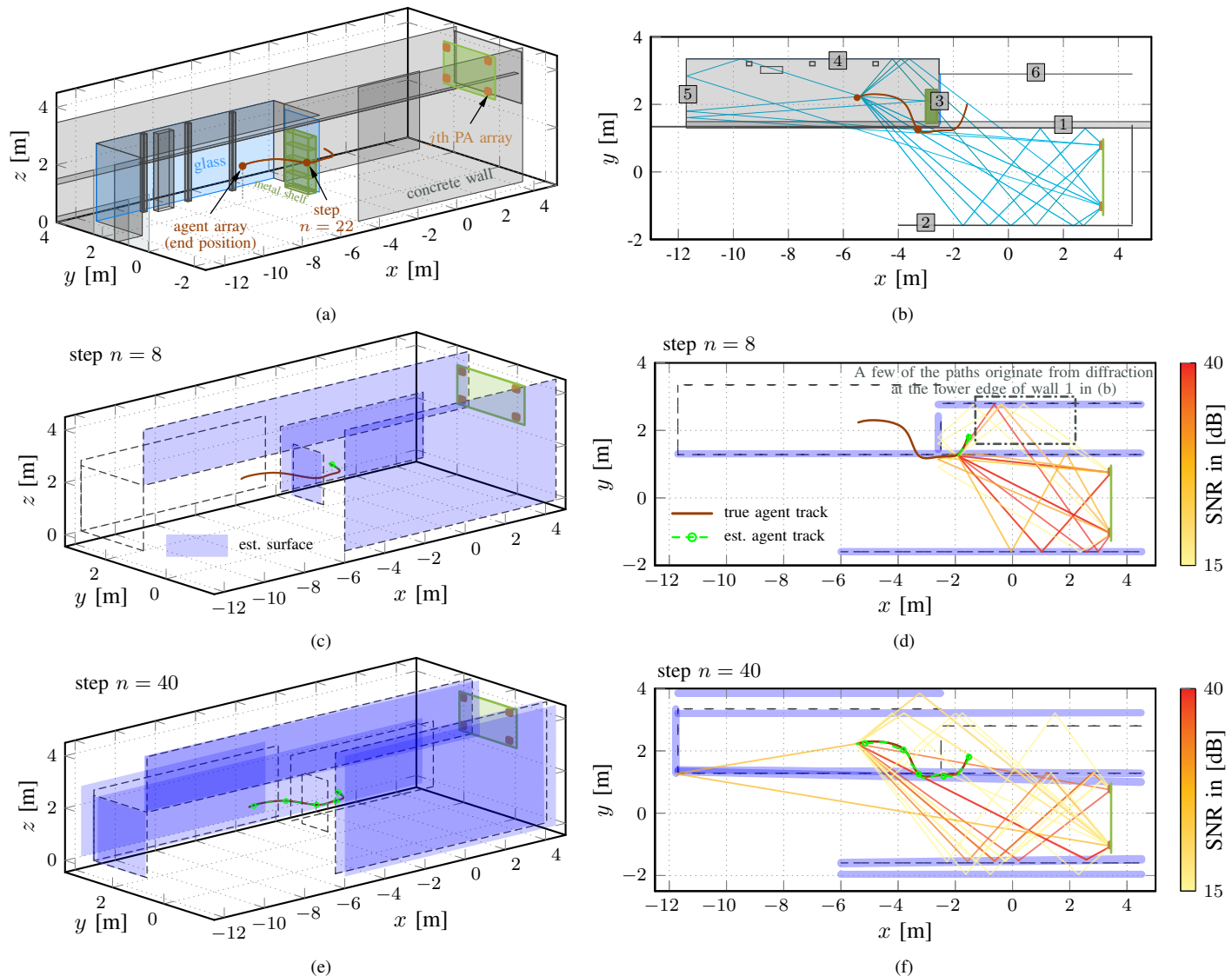


Fig. 8: Real measurement scenario and performance of AM-SLAM. (a) 3D schematic illustration of the hallway scenario (cf. Fig. 7) and the measurement setup. (b) Top view of the environment and the propagation paths up to double bounces generated by ray tracing based on the floor plan at step $n = 40$. Six labeled surfaces indicate the main reflective surfaces in the environment. (c) and (e) Localization and mapping results (detected surfaces) in 3D at steps $n = 8$ and $n = 40$, respectively. (d) and (f) Top views of the corresponding “soft” ray-tracing results. Since AM-SLAM does not estimate surface dimensions, the estimated surfaces are shown using the true surface dimensions solely for visualization purposes.

that can be transmitted over the RF propagation channel. Moreover, it can effectively acquire and predict environment-specific channel state information, and assist applications like OLoS beamforming and beamalignment via MPCs.

E. Results for Real Measurements

We further validate the proposed method using real distributed MIMO synthetic aperture measurements acquired in a hallway scenario at TU Graz, Austria. The environment features multiple concrete and metal-coated glass walls as the primary reflective surfaces, along with rich scattering objects such as metal structures. More details about the measurement campaign can be found in [45]. The channel coefficients between a mobile agent and $J = 4$ distributed PAs were measured with a Rohde & Schwarz ZVA24 vector network analyzer over a bandwidth of 500 MHz centered

around 6.25 GHz. As shown in Fig. 7 and the corresponding schematic depiction in Fig. 8, the PAs were mounted on a bridge between two concrete walls on the second floor, and each PA was equipped with a 4×4 uniform rectangular array. The agent was equipped with a 3×3 uniform rectangular array moved along a trajectory (40 discrete time steps) around a glass wall and metal shelf, from LoS to OLoS conditions (after step $n = 22$). To simulate a strong LoS obstruction in the latter half of the trajectory, the shelf is purposely filled with pyramidal RF absorbers. In LoS conditions, the measurements exhibit an input SNR of approximate 4 dB. Note that the arrays on both agent and PA sides were synthetically formed using mechanical positioners. Accordingly, we extended the proposed algorithm to a 3D uplink formulation with both horizontal and vertical propagation from the agent to the PAs.

At each time step and at each PA, we apply a variational

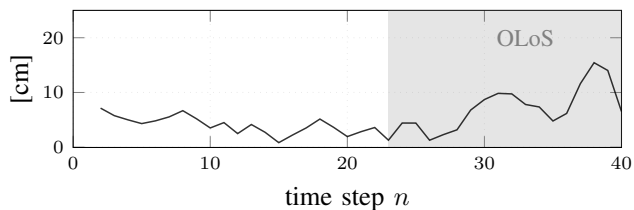


Fig. 9: Performance results of the proposed AM-SLAM for real measurements. Agent position estimation error over time.

sparse Bayesian parametric channel estimation algorithm [14], [35] with detection threshold $u_{de} = 15$ dB to obtain $M_n^{(j)}$ measurement vectors $\mathbf{z}_{m,n}^{(j)}$, consisting of the distance measurement $z_{d,m,n}^{(j)}$, AoD measurements in azimuth $z_{\phi,m,n}^{(j)}$ and elevation $z_{\theta,m,n}^{(j)}$, AoA measurements in azimuth $z_{\varphi,m,n}^{(j)}$ and elevation $z_{\psi,m,n}^{(j)}$, and the normalized amplitude measurement $z_{u,m,n}^{(j)} \in [u_{de}, \infty)$. For the real data, we used the parameter settings as in Section VI-A, except for the following: the orientation noise standard deviation $\sigma_{\varphi} = 9^\circ$, the regularization noise standard deviations for PSFV $\sigma_s = 2$ mm and the normalized amplitude noise standard deviation $\sigma_{ss',n} = 0.01 \hat{u}_{ss',n-1}^{(j)}$.

Fig. 8 depicts for one estimation run of AM-SLAM the estimated agent tracks, the detected reflective surfaces (obtained from the estimates of SFV positions), as well as the detected PRs. It is shown that AM-SLAM quickly establishes the map at the beginning of the trajectory, and identifies all six main reflective surfaces as labeled in Fig. 8b, including surface 3 which is only visible at the beginning of the trajectory. Surface 1 is successfully estimated although it is visible only via double-bounce paths which particularly aid positioning in OLoS conditions. “Ghost” surfaces detected alongside surfaces 4 and 2 arise from complex wall structures (as shown in Fig. 7) that introduce cluttered components in the channel measurements, resulting in short-lived detections of features that are not geometrically meaningful. Figs. 8d and 8f further show the “soft” ray tracing results. The detected paths are mostly consistent with the geometrically predicted paths as shown in Fig. 8b using a known environment geometry. Fig. 9 presents the agent position estimation error versus time n . The results indicate that AM-SLAM accurately localizes the agent, achieving an average agent position estimation error of 5.4 cm, despite OLoS conditions after step $n = 22$.

VII. CONCLUSIONS

In this paper, we introduced a multipath-based SLAM method for D-MIMO systems that performs adaptive data fusion across MPCs and BSs. The main contribution is a novel statistical model that integrates amplitude statistics of propagation paths with an SFV model for representing reflective surfaces, enabling automatic adaptation to time-varying detection probabilities and measurement variances. The detection of SFVs and propagation paths is jointly formulated within a unified Bayesian inference framework, enabling “soft” ray tracing and the estimation of the number and states of SFVs and propagation paths. Furthermore, we develop an improved initialization procedure for emerging surfaces, which enables the reliable introduction of new map features

even when measurements originate solely from double-bounce paths. These aspects result in a highly flexible and robust data fusion approach for multipath-based SLAM in dynamic and complex environments while maintaining moderate computational complexity. Numerical results based on synthetic and real data demonstrate that the proposed method significantly improves localization and mapping performance compared to state-of-the-art multipath-based SLAM methods based on VA features, particularly under OLoS conditions. Our results also indicate that the proposed method can approach the PCRLBs. They furthermore highlight the potential of the proposed framework beyond mapping and localization, for example, in predicting channel state information for integrated sensing and communication systems.

Promising directions for future research include extending the current work to coherent data fusion across PAs while accounting for system impairments, e.g., imperfect time and phase synchronization [29]; employing a sigma point-based implementation [28], [46] and parallel computation on GPUs to achieve real-time performance; extending to multiple measurement-to-feature DA and feature models to account for measurements originating from rough surfaces or other complex structures [20], [23], [47], and using particle flow to improve inference in highly nonlinear system models with high-dimensional states [48]–[50]; extending to a hybrid inference framework, e.g., neural-enhanced belief propagation [51]–[53], which combines model-based and data-driven approaches, allowing statistical models to leverage information learned from raw sensor data; and extending to differentiable ray tracing [54], enabling the learning of differentiable parameters associated with the RF environment and system in a physically interpretable manner.

REFERENCES

- [1] C. Gentner, T. Jost, W. Wang, S. Zhang, A. Dammann, and U. C. Fiebig, “Multipath assisted positioning with simultaneous localization and mapping,” *IEEE Trans. Wireless Commun.*, vol. 15, no. 9, pp. 6104–6117, Sept. 2016.
- [2] X. Li, E. Leitinger, M. Oskarsson, K. Åström, and F. Tufvesson, “Massive MIMO-based localization and mapping exploiting phase information of multipath components,” *IEEE Trans. Wirel. Commun.*, vol. 18, no. 9, pp. 4254–4267, Sept. 2019.
- [3] E. Leitinger, F. Meyer, F. Hlawatsch, K. Witrisal, F. Tufvesson, and M. Z. Win, “A belief propagation algorithm for multipath-based SLAM,” *IEEE Trans. Wireless Commun.*, vol. 18, no. 12, pp. 5613–5629, Dec. 2019.
- [4] R. Mendrzik, F. Meyer, G. Bauch, and M. Z. Win, “Enabling situational awareness in millimeter wave massive MIMO systems,” *IEEE J. Sel. Areas Commun.*, vol. 13, no. 5, pp. 1196–1211, Sept. 2019.
- [5] Y. Ge, O. Kallio, H. Kim, F. Jiang, J. Talvitie, M. Valkama, L. Svensson, S. Kim, and H. Wymeersch, “A computationally efficient EK-PMBM filter for bistatic mmWave radio SLAM,” *IEEE J. Sel. Areas Commun.*, vol. 40, no. 7, pp. 2179–2192, Jul. 2022.
- [6] M. A. Nazari, G. Seco-Granados, P. Johannisson, and H. Wymeersch, “MmWave 6D radio localization with a snapshot observation from a single BS,” *IEEE Trans. Veh. Technol.*, vol. 72, no. 7, pp. 8914–8928, Jul. 2023.
- [7] E. Leitinger, A. Venus, B. Teague, and F. Meyer, “Data fusion for multipath-based SLAM: Combining information from multiple propagation paths,” *IEEE Trans. Signal Process.*, vol. 71, pp. 4011–4028, Sep. 2023.
- [8] X. Li, X. Cai, E. Leitinger, and F. Tufvesson, “A belief propagation algorithm for multipath-based SLAM with multiple map features: A mmWave MIMO application,” in *Proc. IEEE ICC 2024*, Aug. 2024, pp. 269–275.

- [9] M. Liang, E. Leitinger, and F. Meyer, "Direct multipath-based SLAM," *IEEE Trans. Signal Process.*, vol. 74, Mar. 2025.
- [10] A. Richter, "Estimation of radio channel parameters: models and algorithms," Ph.D. dissertation, Ilmenau University of Technology, 2005.
- [11] D. Shutin, W. Wang, and T. Jost, "Incremental sparse Bayesian learning for parameter estimation of superimposed signals," in *Proc. SAMPTA-2013*, no. 1, Sept. 2013, pp. 6–9.
- [12] M. A. Badiu, T. L. Hansen, and B. H. Fleury, "Variational Bayesian inference of line spectra," *IEEE Trans. Signal Process.*, vol. 65, no. 9, pp. 2247–2261, May 2017.
- [13] T. L. Hansen, B. H. Fleury, and B. D. Rao, "Superfast line spectral estimation," *IEEE Trans. Signal Process.*, vol. PP, no. 99, pp. 1–1, 2018.
- [14] S. Grebien, E. Leitinger, K. Witrals, and B. H. Fleury, "Super-resolution estimation of UWB channels including the dense component—an SBL-inspired approach," *IEEE Trans. Wirel. Commun.*, pp. 1–17, Feb. 2024.
- [15] J. Möderl, A. M. Westerkam, A. Venus, and E. Leitinger, "A block-sparse Bayesian learning algorithm with dictionary parameter estimation for multi-sensor data fusion," in *Proc. Fusion-2025, Brazil, Rio de Janeiro*, Jul. 2025.
- [16] F. Meyer and J. L. Williams, "Scalable detection and tracking of geometric extended objects," *IEEE Trans. Signal Process.*, vol. 69, pp. 6283–6298, Oct. 2021.
- [17] H. Kim, K. Granström, L. Gao, G. Battistelli, S. Kim, and H. Wymeersch, "5G mmWave cooperative positioning and mapping using multi-model PHD filter and map fusion," *IEEE Trans. Wireless Commun.*, vol. 19, no. 6, pp. 3782–3795, Mar. 2020.
- [18] X. Chu, Z. Lu, D. Gesbert, L. Wang, X. Wen, M. Wu, and M. Li, "Joint vehicular localization and reflective mapping based on team channel-SLAM," *IEEE Trans. Wireless Commun.*, vol. 21, no. 10, pp. 7957–7974, Apr. 2022.
- [19] J. Yang, C.-K. Wen, S. Jin, and X. Li, "Enabling plug-and-play and crowdsourcing SLAM in wireless communication systems," *IEEE Trans. Wireless Commun.*, vol. 21, no. 3, pp. 1453–1468, Aug. 2022.
- [20] L. Wielandner, A. Venus, T. Wilding, K. Witrals, and E. Leitinger, "MIMO multipath-based SLAM for non-ideal reflective surfaces," in *Proc. Fusion-2024, Venice, Italy*, Jul. 2024.
- [21] Y. Ge, O. Kaltiokallio, Y. Xia, A. F. García-Fernández, H. Kim, J. Talvitie, M. Valkama, H. Wymeersch, and L. Svensson, "Batch SLAM with PMBM data association sampling and graph-based optimization," *IEEE Trans. Signal Process.*, vol. 73, pp. 2139–2153, May 2025.
- [22] E. Leitinger, L. Wielandner, A. Venus, and K. Witrals, "Multipath-based SLAM for cooperative navigation and map fusion," in *Proc. Asilomar-24, Pacific Grove, CA, USA*, Oct. 2024.
- [23] L. Wielandner, A. Venus, T. Wilding, and E. Leitinger, "Multipath-based SLAM for non-ideal reflective surfaces exploiting multiple-measurement data association," *J. Adv. Inf. Fusion*, vol. 18, pp. 59–77, Dec. 2023.
- [24] X. Li, E. Leitinger, A. Venus, and F. Tufvesson, "Sequential detection and estimation of multipath channel parameters using belief propagation," *IEEE Trans. Wirel. Commun.*, vol. 21, no. 10, pp. 8385–8402, Apr. 2022.
- [25] A. Venus, E. Leitinger, S. Tertinek, F. Meyer, and K. Witrals, "Graph-based simultaneous localization and bias tracking," *IEEE Trans. Wirel. Commun.*, vol. 23, no. 10, pp. 13 141–13 158, May 2024.
- [26] E. Leitinger, S. Grebien, and K. Witrals, "Multipath-based SLAM exploiting AoA and amplitude information," in *Proc. IEEE ICCW-19, Shanghai, China*, May 2019, pp. 1–7.
- [27] X. Li, B. Deutschmann, E. Leitinger, and F. Meyer, "Adaptive multipath-based SLAM for distributed MIMO systems: Supporting document," 2025. [Online]. Available: <https://fmeyer.ucsd.edu/TWC-LiDeuLeiMey-2025-SD.pdf>
- [28] H. Kim, K. Granstrom, L. Svensson, S. Kim, and H. Wymeersch, "PMBM-based SLAM filters in 5G mmWave vehicular networks," *IEEE Trans. Veh. Technol.*, pp. 1–1, May 2022.
- [29] A. Fascista, B. J. B. Deutschmann, M. F. Keskin, T. Wilding, A. Coluccia, K. Witrals, E. Leitinger, G. Seco-Granados, and H. Wymeersch, "Joint localization, synchronization and mapping via phase-coherent distributed arrays," *IEEE J. Sel. Top. Signal Process.*, pp. 1–16, Jan. 2025.
- [30] J. Chen, X. Li, R. Whiton, E. Leitinger, and F. Tufvesson, "Robust localization in modern cellular networks using global map features," *IEEE Open J. Signal Process.*, vol. 7, pp. 356–372, Feb. 2026.
- [31] F. Meyer, T. Kropfreiter, J. L. Williams, R. Lau, F. Hlawatsch, P. Braca, and M. Z. Win, "Message passing algorithms for scalable multitarget tracking," *Proc. IEEE*, vol. 106, no. 2, pp. 221–259, Feb. 2018.
- [32] F. Meyer, P. Braca, P. Willett, and F. Hlawatsch, "A scalable algorithm for tracking an unknown number of targets using multiple sensors," *IEEE Trans. Signal Process.*, vol. 65, no. 13, pp. 3478–3493, July 2017.
- [33] T. Wilding, S. Grebien, E. Leitinger, U. Mühlmann, and K. Witrals, "Single-anchor, multipath-assisted indoor positioning with aliased antenna arrays," in *Asilomar-18, Pacific Grove, CA, USA*, Oct. 2018, pp. 525–531.
- [34] Y. Bar-Shalom, P. K. Willett, and X. Tian, *Tracking and Data Fusion: a Handbook of Algorithms*. Storrs, CT, USA: Yaakov Bar-Shalom, 2011.
- [35] J. Möderl, F. Pernkopf, K. Witrals, and E. Leitinger, "Variational inference of structured line spectra exploiting group-sparsity," *IEEE Trans. Signal Process.*, Nov. 2024.
- [36] J. Williams and R. Lau, "Approximate evaluation of marginal association probabilities with belief propagation," *IEEE Trans. Aerosp. Electron. Syst.*, vol. 50, no. 4, pp. 2942–2959, Oct. 2014.
- [37] S. M. Kay, *Fundamentals of Statistical Signal Processing: Estimation Theory*. Upper Saddle River, NJ, USA: Prentice-H, 1993.
- [38] F. Meyer, O. Hlinka, H. Wymeersch, E. Riegler, and F. Hlawatsch, "Distributed localization and tracking of mobile networks including noncooperative objects," *IEEE Trans. Signal Inf. Process. Net.*, vol. 2, no. 1, pp. 57–71, Mar. 2016.
- [39] J. L. Williams and R. A. Lau, "Convergence of loopy belief propagation for data association," in *6th Int. Conf. Intell. Sensors, Sensor Networks and Inf. Process.*, Feb. 2010, pp. 175–180.
- [40] A. Venus, E. Leitinger, S. Tertinek, and K. Witrals, "A graph-based algorithm for robust sequential localization exploiting multipath for obstructed-LOS-bias mitigation," *IEEE Trans. Wirel. Commun.*, vol. 23, no. 2, pp. 1068–1084, Jun. 2024.
- [41] D. Schuhmacher, B.-T. Vo, and B.-N. Vo, "A consistent metric for performance evaluation of multi-object filters," *IEEE Trans. Signal Process.*, vol. 56, no. 8, pp. 3447–3457, Aug. 2008.
- [42] P. Tichavsky, C. Muravchik, and A. Nehorai, "Posterior Cramér-Rao bounds for discrete-time nonlinear filtering," *IEEE Trans. Signal Process.*, vol. 46, no. 5, pp. 1386–1396, May 1998.
- [43] B. J. B. Deutschmann, X. Li, F. Meyer, and E. Leitinger, "Posterior Cramér-Rao bounds on localization and mapping errors in distributed MIMO SLAM," in *Asilomar-25, Pacific Grove, CA, USA*, 2025.
- [44] H. W. Kuhn, "The Hungarian method for the assignment problem," *Naval Research Logistics Quarterly*, vol. 2, no. 1-2, pp. 83–97, Mar. 1955.
- [45] B. J. B. Deutschmann, E. Leitinger, and K. Witrals, "Geometry-based channel estimation, prediction, and fusion," 2025. [Online]. Available: <https://arxiv.org/abs/2503.17868>
- [46] A. Masiero, A. Venus, and E. Leitinger, "A sigma point-based low complexity algorithm for multipath-based SLAM in MIMO systems," in *Proc. Fusion-2025, Jul. 2025*, pp. 1–10.
- [47] S. Zhai, J. Fan, J. Gao, and G. Dai, "Multipath-based SLAM exploiting extended object estimation and classification," *IEEE Trans. Wireless Commun.*, vol. 24, no. 8, pp. 7029–7045, Apr. 2025.
- [48] J. Jang, F. Meyer, E. R. Snyder, S. M. Wiggins, S. Baumann-Pickering, and J. A. Hildebrand, "Bayesian detection and tracking of odontocetes in 3-D from their echolocation clicks," *J. Acoust. Soc.*, vol. 153, no. 5, pp. 2690–2705, May 2023.
- [49] W. Zhang and F. Meyer, "Multisensor multiobject tracking with improved sampling efficiency," *IEEE Trans. Signal Process.*, vol. 72, pp. 2036–2053, Mar. 2024.
- [50] L. Wielandner, E. Leitinger, F. Meyer, and K. Witrals, "Message passing-based 9-D cooperative localization and navigation with embedded particle flow," *IEEE Trans. Signal Inf. Process. Netw.*, vol. 9, pp. 95–109, Jan. 2023.
- [51] M. Liang and F. Meyer, "Neural enhanced belief propagation for multiobject tracking," *IEEE Trans. Signal Process.*, vol. 72, pp. 15–30, Sept. 2023.
- [52] S. Wei, M. Liang, and F. Meyer, "A new architecture for neural enhanced multiobject tracking," in *Proc. FUSION 2024, Jul. 2024*, pp. 1–8.
- [53] A. Venus, E. Leitinger, S. Tertinek, and K. Witrals, "A neural-enhanced factor graph-based algorithm for robust positioning in obstructed LOS situations," *IEEE Open J. Signal Process.*, vol. 5, pp. 29–38, Nov. 2023.
- [54] J. Hoydis, F. A. Aoudia, S. Cammerer, F. Euchner, M. Nimier-David, S. T. Brink, and A. Keller, "Learning radio environments by differentiable ray tracing," *IEEE Trans. Mach. Learn. Commun. Netw.*, vol. 2, pp. 1527–1539, Oct. 2024.

Adaptive Multipath-Based SLAM for Distributed MIMO Systems: Supporting Document

Xuhong Li, Benjamin Deutschmann, Erik Leitinger, and Florian Meyer

This manuscript provides derivations of the statistical models and the sum-product algorithm (SPA) for the publication, “Adaptive Multipath-Based SLAM for Distributed MIMO Systems” by the same authors [S1].

I. STATISTICAL MODEL

In this section, we derive the joint posterior probability density function (PDF) $f(\mathbf{x}_{0:n}, \mathbf{y}_{0:n}, \boldsymbol{\beta}_{0:n}, \mathbf{a}_{1:n}, \bar{\mathbf{a}}_{1:n}, \mathbf{m}_{1:n} | \mathbf{z}_{1:n})$. At first, a few sets are defined as follows: $\mathcal{M}_n^{(j)} \triangleq \{1, \dots, M_n^{(j)}\}$ denotes the sets of measurement indexes, $\mathcal{N}_n^{(j)} \triangleq \{m \in \mathcal{M}_n^{(j)} : \bar{r}_{m,n} = 1, \bar{r}_{mm,n} = 1, \bar{a}_{m,n} = 0\}$ denotes the set of existing new potential surface feature vectors (SFVs) and corresponding potential rays (PRs), $\mathcal{Q}_n^{(j)} \triangleq \{(s, s') \in \tilde{\mathcal{D}}_n^{(j)} : r_{s,n}^{(j)} = 1, r_{s',n}^{(j)} = 1, r_{ss',n}^{(j)} = 1, \underline{a}_{ss',n}^{(j)} \in \mathcal{M}_n^{(j)}\}$ denotes the sets of existing legacy potential SFVs (PSFVs) and corresponding PRs. We further define $\mathcal{M}_{0,n}^{(j)} \triangleq \{0, \mathcal{M}_n^{(j)}\}$.

A. Joint Prior PDF

The joint prior PDF of $\mathbf{x}_{0:n}, \mathbf{y}_{0:n}, \boldsymbol{\beta}_{0:n}, \mathbf{a}_{1:n}, \bar{\mathbf{a}}_{1:n}$ and the number of measurements $\mathbf{m}_{1:n}$ factorizes as

$$\begin{aligned}
 & f(\mathbf{x}_{0:n}, \mathbf{y}_{0:n}, \boldsymbol{\beta}_{0:n}, \mathbf{a}_{1:n}, \bar{\mathbf{a}}_{1:n}, \mathbf{m}_{1:n}) \\
 &= f(\mathbf{x}_{0:n}, \underline{\mathbf{y}}_{0:n}, \bar{\mathbf{y}}_{1:n}, \underline{\boldsymbol{\beta}}_{0:n}, \bar{\boldsymbol{\beta}}_{1:n}, \mathbf{a}_{1:n}, \bar{\mathbf{a}}_{1:n}, \mathbf{m}_{1:n}) \\
 &= \underbrace{\left(f(\mathbf{x}_0) \prod_{s=1}^{S_0} f(\mathbf{y}_{s,0}) \prod_{j'=1}^J \prod_{(s,s') \in \tilde{\mathcal{D}}_0^{(j')}} f(\boldsymbol{\beta}_{ss',0}^{(j')}) \right)}_{\text{initial prior PDFs}} \underbrace{\prod_{n'=1}^n f(\mathbf{x}_{n'} | \mathbf{x}_{n'-1})}_{\text{agent state transition}} \\
 & \times \underbrace{\left(\prod_{s'=1}^{S_{n'-1}} f(\underline{\mathbf{y}}_{s',n'} | \mathbf{y}_{s',n'-1}) \right)}_{\text{legacy PSFVs state transition}} \underbrace{\left(\prod_{j'=2}^J \prod_{s'=1}^{S_{n'}^{(j')}} f^{(j')}(\underline{\mathbf{y}}_{s',n'}^{(j')} | \mathbf{y}_{s',n'}^{(j'-1)}) \right)}_{\text{legacy PRs state transition}} \underbrace{\left(\prod_{j''=1}^J \prod_{(s,s') \in \tilde{\mathcal{D}}_{n'}^{(j'')}} f(\boldsymbol{\beta}_{ss',n'}^{(j'')} | \boldsymbol{\beta}_{ss',n'-1}^{(j'')}) \right)}_{\text{legacy PRs state transition}} \\
 & \times \prod_{j=1}^J f(\bar{\mathbf{p}}_{\text{sfv}}^{(j)}, \bar{\mathbf{u}}_{n'}^{(j)} | \bar{\mathbf{r}}_{n'}^{(j)}, \bar{\bar{\mathbf{r}}}_{n'}^{(j)}, M_{n'}^{(j)}, \mathbf{x}_{n'}) p(\bar{\mathbf{r}}_{n'}^{(j)}, \bar{\bar{\mathbf{r}}}_{n'}^{(j)}, \mathbf{a}_{n'}^{(j)}, \bar{\mathbf{a}}_{n'}^{(j)}, M_{n'}^{(j)} | \underline{\mathbf{y}}_{n'}^{(j)}, \underline{\boldsymbol{\beta}}_{n'}^{(j)}, \mathbf{x}_{n'}). \tag{1}
 \end{aligned}$$

The joint prior PDF of new PSFVs and new PRs $f(\bar{\mathbf{p}}_{\text{sfv}}^{(j)}, \bar{\mathbf{u}}_{n'}^{(j)} | \bar{\mathbf{r}}_{n'}^{(j)}, \bar{\bar{\mathbf{r}}}_{n'}^{(j)}, M_{n'}^{(j)}, \mathbf{x}_{n'})$ and the joint conditional prior probability mass function (PMF) $p(\bar{\mathbf{r}}_{n'}^{(j)}, \bar{\bar{\mathbf{r}}}_{n'}^{(j)}, \mathbf{a}_{n'}^{(j)}, \bar{\mathbf{a}}_{n'}^{(j)}, M_{n'}^{(j)} | \underline{\mathbf{y}}_{n'}^{(j)}, \underline{\boldsymbol{\beta}}_{n'}^{(j)}, \mathbf{x}_{n'})$ are further defined as follows.

The joint prior PDF of new PSFVs and new PRs $f(\bar{\mathbf{p}}_{\text{sfv}}^{(j)}, \bar{\mathbf{u}}_{n'}^{(j)} | \bar{\mathbf{r}}_{n'}^{(j)}, \bar{\bar{\mathbf{r}}}_{n'}^{(j)}, M_{n'}^{(j)}, \mathbf{x}_{n'})$ is given as

$$f(\bar{\mathbf{p}}_{\text{sfv}}^{(j)}, \bar{\mathbf{u}}_{n'}^{(j)} | \bar{\mathbf{r}}_{n'}^{(j)}, \bar{\bar{\mathbf{r}}}_{n'}^{(j)}, M_{n'}^{(j)}, \mathbf{x}_{n'}) = \prod_{m \in \mathcal{N}_n^{(j)}} f_{\text{n}}(\bar{\mathbf{p}}_{m,\text{sfv}}^{(j)}, \bar{\mathbf{u}}_{mm,n}^{(j)} | \mathbf{x}_n) \prod_{m' \in \mathcal{M}_n^{(j)} \setminus \mathcal{N}_n^{(j)}} f_{\text{D}}(\bar{\mathbf{p}}_{m',\text{sfv}}^{(j)}) f_{\text{D}}(\bar{\mathbf{u}}_{m'm',n}^{(j)}). \tag{2}$$

The joint conditional prior PMF $p(\bar{\mathbf{r}}_n^{(j)}, \bar{\mathbf{r}}_n^{(j)}, \underline{\mathbf{a}}_n^{(j)}, \bar{\mathbf{a}}_n^{(j)}, M_n^{(j)} | \underline{\mathbf{y}}_n^{(j)}, \underline{\boldsymbol{\beta}}_n^{(j)}, \mathbf{x}_n)$ is given as

$$\begin{aligned}
& p(\bar{\mathbf{r}}_n^{(j)}, \bar{\mathbf{r}}_n^{(j)}, \underline{\mathbf{a}}_n^{(j)}, \bar{\mathbf{a}}_n^{(j)}, M_n^{(j)} | \underline{\mathbf{y}}_n^{(j)}, \underline{\boldsymbol{\beta}}_n^{(j)}, \mathbf{x}_n) \\
&= \chi_{\bar{\mathbf{r}}_n^{(j)}, \bar{\mathbf{r}}_n^{(j)}, \underline{\mathbf{a}}_n^{(j)}, M_n^{(j)}} \underbrace{\left(\prod_{m \in \mathcal{N}_n^{(j)}} \Gamma_{\underline{\mathbf{a}}_n^{(j)}}(\bar{\mathbf{r}}_{m,n}^{(j)}, \bar{\mathbf{r}}_{mm,n}^{(j)}) \right)}_{\text{exclusion functions}} \underbrace{\left(\prod_{(s,s') \in \bar{\mathcal{D}}_n^{(j)}} \Gamma_{\underline{\mathbf{a}}_n^{(j)}}(r_{s,n}^{(j)}, r_{s',n}^{(j)}, r_{ss',n}^{(j)}) \right)}_{\text{exclusion functions}} \\
&\times \underbrace{\prod_{(s,s') \in \bar{\mathcal{D}}_n^{(j)}} \prod_{m=1}^{M_n^{(j)}} \psi(\underline{a}_{ss',n}^{(j)}, \bar{a}_{m,n}^{(j)})}_{\text{binary check functions}} \left(\prod_{(s,s') \in \mathcal{Q}_n^{(j)}} p_d(\underline{u}_{ss',n}^{(j)}) \right) \left(\prod_{(s,s') \in \bar{\mathcal{D}}_n^{(j)} \setminus \mathcal{Q}_n^{(j)}} 1(\underline{a}_{ss',n}^{(j)}) - p_{d,ss'}(\underline{u}_{ss',n}^{(j)}) \right). \quad (3)
\end{aligned}$$

where the normalization constant $\chi_{\bar{\mathbf{r}}_n^{(j)}, \bar{\mathbf{r}}_n^{(j)}, \underline{\mathbf{a}}_n^{(j)}, M_n^{(j)}}$ is defined inline with [S2], the binary check function $\psi(\underline{a}_{ss',n}^{(j)}, \bar{a}_{m,n}^{(j)})$ checks if the PSFV-oriented association variable $\underline{a}_{ss',n}^{(j)}$ and the measurement-oriented association variable $\bar{a}_{m,n}^{(j)}$ describe the same association event.

Based on the existence/non-existence relations between PSFVs and corresponding PRs, several invalid cases are defined. The joint prior PDF is enforce to be zero for these cases using the exclusion functions $\Gamma_{\underline{\mathbf{a}}_n^{(j)}}(r_{s,n}^{(j)}, r_{s',n}^{(j)}, r_{ss',n}^{(j)})$ and $\Gamma_{\underline{\mathbf{a}}_n^{(j)}}(\bar{\mathbf{r}}_{m,n}^{(j)}, \bar{\mathbf{r}}_{mm,n}^{(j)})$. Fundamentally, a PSFV models a potentially existing environmental object and PRs model signal interacting processes on this object, thus their existence/non-existence status are related as follows: (i) a nonexistent reflective surface cannot generate any propagation paths, i.e., from $r_{s,n} = 0$ follows $r_{ss',n} = 0 \forall (s, s')$; (ii) an existing surface does not necessarily interact with any radio frequency (RF) signals and therefore generate propagation paths, i.e., if $r_{s,n} = 1$, then $r_{ss',n} \in \{1, 0\}$; (iii) a path exists if and only if the interacting surfaces all exist, i.e., from $r_{ss',n} = 1$ follows $r_{s,n} = 1$ and $r_{s',n} = 1$. Accordingly, the invalid cases and exclusion functions are defined in what follows.

For physical anchors (PAs) and corresponding line-of-sight (LoS) PR: $(s, s') = (0, 0)$, the exclusion function $\Gamma_{\underline{\mathbf{a}}_n^{(j)}}(r_{s,n}^{(j)}, r_{s',n}^{(j)}, r_{ss',n}^{(j)}) = \Gamma_{\underline{\mathbf{a}}_n^{(j)}}(r_{00,n}^{(j)})$ is given as

$$\Gamma_{\underline{\mathbf{a}}_n^{(j)}}(r_{00,n}^{(j)}) = \begin{cases} 1, & r_{00,n}^{(j)} = 1, \underline{a}_{00,n}^{(j)} \in \mathcal{M}_n^{(j)} & \Rightarrow \text{Eq. (19) in [S1]} \\ 1, & r_{00,n}^{(j)} = 1, \underline{a}_{00,n}^{(j)} = 0 \\ 1, & r_{00,n}^{(j)} = 0, \underline{a}_{00,n}^{(j)} = 0 \\ 0, & r_{00,n}^{(j)} = 0, \underline{a}_{00,n}^{(j)} \in \mathcal{M}_n^{(j)} & \Rightarrow \text{invalid case ①} \end{cases} \quad (4)$$

where the *invalid case for LoS PR* indicates a nonexistent LoS path is associated to a measurement.

For legacy PSFVs and corresponding single-bounce PRs: $s = s' \wedge (s, s') \neq (0, 0)$, the exclusion function $\Gamma_{\underline{\mathbf{a}}_n^{(j)}}(r_{s,n}^{(j)}, r_{s',n}^{(j)}, r_{ss',n}^{(j)}) = \Gamma_{\underline{\mathbf{a}}_n^{(j)}}(r_{s,n}^{(j)}, r_{ss',n}^{(j)})$ is given as

$$\Gamma_{\underline{\mathbf{a}}_n^{(j)}}(r_{s,n}^{(j)}, r_{ss',n}^{(j)}) = \begin{cases} 1, & r_{s,n}^{(j)} = 1, r_{ss',n}^{(j)} = 1, \underline{a}_{ss',n}^{(j)} \in \mathcal{M}_{0,n}^{(j)} & \Rightarrow \text{Eq. (20) in [S1]} \\ 1, & \forall r_{s,n}^{(j)}, r_{ss',n}^{(j)} = 0, \underline{a}_{ss',n}^{(j)} = 0 \\ 0, & \forall r_{s,n}^{(j)}, r_{ss',n}^{(j)} = 0, \underline{a}_{ss',n}^{(j)} \in \mathcal{M}_n^{(j)} \\ 0, & r_{s,n}^{(j)} = 0, r_{ss',n}^{(j)} = 1, \underline{a}_{ss',n}^{(j)} \in \mathcal{M}_{0,n}^{(j)} & \Rightarrow \text{invalid cases ②} \end{cases} \quad (5)$$

where the *invalid cases for single-bounce PRs* indicate: (i) a nonexistent single-bounce path is associated to a measurement; (ii) surface is nonexistent but the associated single-bounce path exists.

For legacy PSFVs and corresponding double-bounce PRs: $s \neq s' \wedge (s, s') \neq (0, 0)$, the exclusion function $\Gamma_{\underline{\mathbf{a}}_n^{(j)}}(r_{s,n}^{(j)}, r_{s',n}^{(j)}, r_{ss',n}^{(j)})$ is given as

$$\Gamma_{\underline{\mathbf{a}}_n^{(j)}}(r_{s,n}^{(j)}, r_{s',n}^{(j)}, r_{ss',n}^{(j)}) = \begin{cases} 1, & r_{s,n}^{(j)} = 1, r_{s',n}^{(j)} = 1, r_{ss',n}^{(j)} = 1, \underline{a}_{ss',n}^{(j)} \in \mathcal{M}_{0,n}^{(j)} & \Rightarrow \text{Eq. (21) in [S1]} \\ 1, & \forall (r_{s,n}^{(j)}, r_{ss',n}^{(j)}), r_{ss',n}^{(j)} = 0, \underline{a}_{ss',n}^{(j)} = 0 \\ 0, & \forall (r_{s,n}^{(j)}, r_{ss',n}^{(j)}), r_{ss',n}^{(j)} = 0, \underline{a}_{ss',n}^{(j)} \in \mathcal{M}_n^{(j)} \\ 0, & (r_{s,n}^{(j)} = 0) \vee (r_{s',n}^{(j)} = 0), r_{ss',n}^{(j)} = 1, \underline{a}_{ss',n}^{(j)} \in \mathcal{M}_{0,n}^{(j)} & \Rightarrow \text{invalid cases ③} \end{cases} \quad (6)$$

where the *invalid cases for double-bounce PRs* indicate: (i) a nonexistent double-bounce path is associated to a measurement; (ii) one or both surfaces are nonexistent but the associated double-bounce path exists.

For new PSFVs and corresponding PRs: the exclusion function $\Gamma_{\underline{a}_n^{(j)}}(\bar{r}_{m,n}^{(j)}, \bar{r}_{mm,n}^{(j)})$ is defined as

$$\Gamma_{\underline{a}_n^{(j)}}(\bar{r}_{m,n}^{(j)}, \bar{r}_{mm,n}^{(j)}) = \begin{cases} 1, & \bar{r}_{m,n}^{(j)} = 1, \bar{r}_{mm,n}^{(j)} = 1, \underline{a}_{ss',n}^{(j)} = 0 \Rightarrow \text{Eq. (22) in [S1]} \\ 1, & \bar{r}_{m,n}^{(j)} = 0, \bar{r}_{mm,n}^{(j)} = 0, \underline{a}_{ss',n}^{(j)} \in \mathcal{M}_{0,n}^{(j)} \\ 0, & \text{otherwise} \Rightarrow \text{invalid cases } \textcircled{4} \end{cases} \quad (7)$$

where the **invalid cases for new PRs** indicate: the exclusive presence of a new PSFV and its corresponding new PR, meaning one exists while the other does not.

We further define the function $p_{d,ss'}(\underline{u}_{ss',n}^{(j)})$ providing the detection probabilities constrained by the corresponding PSFV and PR existence probabilities, given as

$$p_{d,ss'}(\underline{u}_{ss',n}^{(j)}) \triangleq \begin{cases} r_{00,n}^{(j)} p_d(\underline{u}_{00,n}^{(j)}), & (s, s') = (0, 0) \\ r_{s,n}^{(j)} r_{ss,n}^{(j)} p_d(\underline{u}_{ss,n}^{(j)}), & s = s' \wedge (s, s') \neq (0, 0) \\ r_{s,n}^{(j)} r_{s',n}^{(j)} r_{-ss',n}^{(j)} p_d(\underline{u}_{ss',n}^{(j)}), & s \neq s' \wedge (s, s') \neq (0, 0). \end{cases} \quad (8)$$

The product of the joint prior PDF (2) and the joint conditional prior PMF (3) can be written up to the normalization constant as

$$\begin{aligned} & f(\bar{\mathbf{p}}_{\text{sfv}}^{(j)}, \bar{\mathbf{u}}_n^{(j)} | \bar{\mathbf{r}}_n^{(j)}, \bar{\bar{\mathbf{r}}}_n^{(j)}, M_n^{(j)}, \mathbf{x}_n) p(\bar{\mathbf{r}}_n^{(j)}, \bar{\bar{\mathbf{r}}}_n^{(j)}, \underline{\mathbf{a}}_n^{(j)}, \bar{\mathbf{a}}_n^{(j)}, M_n^{(j)} | \underline{\mathbf{y}}_n^{(j)}, \underline{\boldsymbol{\beta}}_n^{(j)}, \mathbf{x}_n) \\ & \propto \prod_{(s,s') \in \tilde{\mathcal{D}}_n^{(j)}} \prod_{m=1}^{M_n^{(j)}} \psi(\underline{a}_{ss',n}^{(j)}, \bar{a}_{m,n}^{(j)}) \\ & \times \underbrace{\left(\prod_{(s,s') \in \tilde{\mathcal{D}}_n^{(j)}} \Gamma_{\underline{a}_n^{(j)}}(r_{s,n}^{(j)}, r_{s',n}^{(j)}, r_{-ss',n}^{(j)}) \prod_{(s,s') \in \mathcal{Q}_n^{(j)}} \frac{p_d(\underline{u}_{ss',n}^{(j)})}{\mu_{\text{fa}}} \prod_{(s,s') \in \tilde{\mathcal{D}}_n^{(j)} \setminus \mathcal{Q}_n^{(j)}} (1(\underline{a}_{ss',n}^{(j)}) - p_{d,ss'}(\underline{u}_{ss',n}^{(j)})) \right)}_{\text{factors related to PAs, legacy PSFVs and their corresponding PRs}} \\ & \times \underbrace{\left(\prod_{m \in \mathcal{N}_n^{(j)}} \frac{\mu_n f_n(\bar{\mathbf{p}}_{m,\text{sfv}}^{(j)}, \bar{u}_{mm,n}^{(j)} | \mathbf{x}_n)}{\mu_{\text{fa}}} \Gamma_{\underline{a}_n^{(j)}}(\bar{r}_{m,n}^{(j)}, \bar{r}_{mm,n}^{(j)}) \prod_{m' \in \mathcal{M}_n^{(j)} \setminus \mathcal{N}_n^{(j)}} f_D(\bar{\mathbf{p}}_{m',\text{sfv}}^{(j)}) f_D(\bar{u}_{m'm',n}^{(j)}) \right)}_{\text{factors related to the new PSFVs and corresponding PRs}}. \end{aligned} \quad (9)$$

After integrating the definitions of the binary check function $\psi(\underline{a}_{ss',n}^{(j)}, \bar{a}_{m,n}^{(j)})$, the exclusion functions $\Gamma_{\underline{a}_n^{(j)}}(r_{s,n}^{(j)}, r_{s',n}^{(j)}, r_{-ss',n}^{(j)})$ and $\Gamma_{\underline{a}_n^{(j)}}(\bar{r}_{m,n}^{(j)}, \bar{r}_{mm,n}^{(j)})$, and with some simple manipulations, Eq. (9) can be further written as

$$\begin{aligned} & f(\bar{\mathbf{p}}_{\text{sfv}}^{(j)}, \bar{\mathbf{u}}_n^{(j)} | \bar{\mathbf{r}}_n^{(j)}, \bar{\bar{\mathbf{r}}}_n^{(j)}, M_n^{(j)}, \mathbf{x}_n) p(\bar{\mathbf{r}}_n^{(j)}, \bar{\bar{\mathbf{r}}}_n^{(j)}, \underline{\mathbf{a}}_n^{(j)}, \bar{\mathbf{a}}_n^{(j)}, M_n^{(j)} | \underline{\mathbf{y}}_n^{(j)}, \underline{\boldsymbol{\beta}}_n^{(j)}, \mathbf{x}_n) \\ & \propto \left(\prod_{m'=1}^{M_n^{(j)}} \psi(\underline{a}_{00,n}^{(j)}, \bar{a}_{m',n}^{(j)}) \prod_{j=1}^J q_{\text{P1}}(\boldsymbol{\beta}_{00,n}^{(j)}, \underline{a}_{00,n}^{(j)}) \right) \\ & \times \left(\prod_{m'=1}^{M_n^{(j)}} \psi(\underline{a}_{ss,n}^{(j)}, \bar{a}_{m',n}^{(j)}) \prod_{s=1}^{S_n^{(j)}} q_{\text{S1}}(\underline{\mathbf{y}}_{s,n}^{(j)}, \underline{\boldsymbol{\beta}}_{ss,n}^{(j)}, \underline{a}_{ss,n}^{(j)}) \right) \\ & \times \left(\prod_{m'=1}^{M_n^{(j)}} \psi(\underline{a}_{ss',n}^{(j)}, \bar{a}_{m',n}^{(j)}) \prod_{s'=1, s \neq s'}^{S_n^{(j)}} q_{\text{D1}}(\underline{\mathbf{y}}_{s,n}^{(j)}, \underline{\mathbf{y}}_{s',n}^{(j)}, \underline{\boldsymbol{\beta}}_{ss',n}^{(j)}, \underline{a}_{ss',n}^{(j)}) \right) \\ & \times \left(\prod_{m=1}^{M_n^{(j)}} \bar{q}_{\text{N1}}(\bar{\mathbf{y}}_{m,n}^{(j)}, \bar{\boldsymbol{\beta}}_{m,n}^{(j)}, \bar{a}_{m,n}^{(j)}) \right). \end{aligned} \quad (10)$$

The function $q_{\text{P1}}(\boldsymbol{\beta}_{00,n}^{(j)}, \underline{a}_{00,n}^{(j)}) = q_{\text{P1}}(\underline{u}_{00,n}^{(j)}, r_{00,n}^{(j)}, \underline{a}_{00,n}^{(j)})$ for PAs integrating the definition of the exclusion function

$\Gamma_{\underline{a}_n^{(j)}}(\underline{r}_{00,n}^{(j)})$ is given by

$$q_{\text{P1}}(\underline{u}_{00,n}^{(j)}, \underline{r}_{00,n}^{(j)} = 1, \underline{a}_{00,n}^{(j)}) \triangleq \begin{cases} \frac{p_d(\underline{u}_{00,n}^{(j)})}{\mu_{\text{fa}}}, & \underline{a}_{00,n}^{(j)} \in \mathcal{M}_n^{(j)} \\ 1 - p_d(\underline{u}_{00,n}^{(j)}), & \underline{a}_{00,n}^{(j)} = 0, \end{cases} \quad (11)$$

$q_{\text{P1}}(\underline{u}_{00,n}^{(j)}, \underline{r}_{00,n}^{(j)} = 0, \underline{a}_{00,n}^{(j)} = 0) = 1$, and $q_{\text{P1}}(\underline{u}_{00,n}^{(j)}, \underline{r}_{00,n}^{(j)} = 0, \underline{a}_{00,n}^{(j)} = m) = 0$ for the *invalid case* ①.

The function $q_{\text{S1}}(\underline{y}_{s,n}^{(j)}, \underline{\beta}_{ss,n}^{(j)}, \underline{a}_{ss,n}^{(j)}) = q_{\text{S1}}(\underline{r}_{s,n}^{(j)}, \underline{u}_{ss,n}^{(j)}, \underline{r}_{ss,n}^{(j)}, \underline{a}_{ss,n}^{(j)})$ integrating the definition of the exclusion function $\Gamma_{\underline{a}_n^{(j)}}(\underline{r}_{s,n}^{(j)}, \underline{r}_{ss,n}^{(j)})$ is given by

$$q_{\text{S1}}(\underline{r}_{s,n}^{(j)} = 1, \underline{u}_{ss,n}^{(j)}, \underline{r}_{ss,n}^{(j)} = 1, \underline{a}_{ss,n}^{(j)}) \triangleq \begin{cases} \frac{p_d(\underline{u}_{ss,n}^{(j)})}{\mu_{\text{fa}}}, & \underline{a}_{ss,n}^{(j)} \in \mathcal{M}_n^{(j)} \\ 1 - p_d(\underline{u}_{ss,n}^{(j)}), & \underline{a}_{ss,n}^{(j)} = 0, \end{cases} \quad (12)$$

$q_{\text{S1}}(\underline{r}_{s,n}^{(j)}, \underline{u}_{ss,n}^{(j)}, \underline{r}_{ss,n}^{(j)} = 0, \underline{a}_{ss,n}^{(j)} = 0) = 1$, and $q_{\text{S1}}(\underline{r}_{s,n}^{(j)}, \underline{u}_{ss,n}^{(j)}, \underline{r}_{ss,n}^{(j)} = 0, \underline{a}_{ss,n}^{(j)} = m) = 0$ and $q_{\text{S1}}(\underline{r}_{s,n}^{(j)} = 0, \underline{u}_{ss,n}^{(j)}, \underline{r}_{ss,n}^{(j)} = 1, \underline{a}_{ss,n}^{(j)}) = 0$ for the *invalid cases* ②.

The function $q_{\text{D1}}(\underline{y}_{s,n}^{(j)}, \underline{y}_{s',n}^{(j)}, \underline{\beta}_{ss',n}^{(j)}, \underline{a}_{ss',n}^{(j)}) = q_{\text{D1}}(\underline{r}_{s,n}^{(j)}, \underline{r}_{s',n}^{(j)}, \underline{u}_{ss',n}^{(j)}, \underline{r}_{ss',n}^{(j)}, \underline{a}_{ss',n}^{(j)})$ integrating the definition of the exclusion function $\Gamma_{\underline{a}_n^{(j)}}(\underline{r}_{s,n}^{(j)}, \underline{r}_{s',n}^{(j)}, \underline{r}_{ss',n}^{(j)})$ is given by

$$q_{\text{D1}}(\underline{r}_{s,n}^{(j)} = 1, \underline{r}_{s',n}^{(j)} = 1, \underline{u}_{ss',n}^{(j)}, \underline{r}_{ss',n}^{(j)} = 1, \underline{a}_{ss',n}^{(j)}) \triangleq \begin{cases} \frac{p_d(\underline{u}_{ss',n}^{(j)})}{\mu_{\text{fa}}}, & \underline{a}_{ss',n}^{(j)} \in \mathcal{M}_n^{(j)} \\ 1 - p_d(\underline{u}_{ss',n}^{(j)}), & \underline{a}_{ss',n}^{(j)} = 0, \end{cases} \quad (13)$$

$q_{\text{D1}}(\underline{r}_{s,n}^{(j)}, \underline{r}_{s',n}^{(j)}, \underline{u}_{ss',n}^{(j)}, \underline{r}_{ss',n}^{(j)} = 0, \underline{a}_{ss',n}^{(j)} = 0) = 1$, and $q_{\text{D1}}(\dots) = 0$ for $\{\underline{r}_{s,n}^{(j)}, \underline{r}_{s',n}^{(j)}, \underline{r}_{ss',n}^{(j)}\} \in \{(0, 1, 1), (1, 0, 1), (0, 0, 1)\}$ and $q_{\text{D1}}(\underline{r}_{s,n}^{(j)}, \underline{r}_{s',n}^{(j)}, \underline{u}_{ss',n}^{(j)}, \underline{r}_{ss',n}^{(j)} = 0, \underline{a}_{ss',n}^{(j)} = m) = 0$ represent the *invalid cases* ③.

The function $\bar{q}_{\text{N1}}(\underline{y}_{m,n}^{(j)}, \underline{\beta}_{m,n}^{(j)}, \underline{a}_{m,n}^{(j)}) = \bar{q}_{\text{N1}}(\bar{r}_{m,n}^{(j)}, \bar{u}_{mm,n}^{(j)}, \bar{r}_{mm,n}^{(j)}, \bar{a}_{m,n}^{(j)})$ integrating the definition of the exclusion function $\Gamma_{\underline{a}_n^{(j)}}(\bar{r}_{m,n}^{(j)}, \bar{r}_{mm,n}^{(j)})$ is given by

$$\bar{q}_{\text{N1}}(\bar{r}_{m,n}^{(j)} = 1, \bar{u}_{mm,n}^{(j)}, \bar{r}_{mm,n}^{(j)} = 1, \bar{a}_{m,n}^{(j)}) \triangleq \begin{cases} 0, & \bar{a}_{m,n}^{(j)} \in \tilde{\mathcal{D}}_n^{(j)} \\ \frac{\mu_n f_n(\bar{\mathcal{P}}_{m,\text{sfv}}^{(j)}, \bar{u}_{mm,n}^{(j)} | \mathbf{x}_n)}{\mu_{\text{fa}}}, & \bar{a}_{m,n}^{(j)} = 0, \end{cases} \quad (14)$$

$\bar{q}_{\text{N1}}(\bar{r}_{m,n}^{(j)} = 0, \bar{u}_{mm,n}^{(j)}, \bar{r}_{mm,n}^{(j)} = 0, \bar{a}_{m,n}^{(j)}) \triangleq f_{\text{D}}(\bar{\mathcal{P}}_{m',\text{sfv}}^{(j)}) f_{\text{D}}(\bar{u}_{m',n}^{(j)})$, otherwise $\bar{q}_{\text{N1}}(\dots) = 0$ for the *invalid cases* ④.

Finally, by inserting (10) into (1), the joint prior PDF can be rewritten as

$$\begin{aligned} & f(\mathbf{x}_{0:n}, \mathbf{y}_{0:n}, \underline{\beta}_{0:n}, \underline{a}_{1:n}, \bar{\mathbf{a}}_{1:n}, \mathbf{m}_{1:n}) \\ & \propto \left(f(\mathbf{x}_0) \prod_{s=1}^{S_0} f(\mathbf{y}_{s,0}) \prod_{j'=1}^J \prod_{(s,s') \in \tilde{\mathcal{D}}_0^{(j')}} f(\underline{\beta}_{ss',0}^{(j')}) \right) \prod_{n'=1}^n f(\mathbf{x}_{n'} | \mathbf{x}_{n'-1}) \left(\prod_{m'=1}^{M_n^{(j)}} \psi(\underline{a}_{00,n}^{(j)}, \bar{a}_{m',n}^{(j)}) \prod_{j=1}^J q_{\text{P1}}(\underline{\beta}_{00,n}^{(j)}, \underline{a}_{00,n}^{(j)}) \right) \\ & \times \underbrace{\left(\prod_{s'=1}^{S_{n'-1}} f(\underline{y}_{s',n'} | \underline{y}_{s',n'-1}) \right)}_{\text{legacy PSFVs state transition}} \underbrace{\left(\prod_{j'=2}^J \prod_{s'=1}^{S_{n'}^{(j')}} f^{(j)}(\underline{y}_{s',n'}^{(j')} | \underline{y}_{s',n'-1}^{(j'-1)}) \right)}_{\text{legacy PRs state transition}} \left(\prod_{j''=1}^J \prod_{(s,s') \in \tilde{\mathcal{D}}_{n'}^{(j'')}} f(\underline{\beta}_{ss',n'}^{(j'')} | \underline{\beta}_{ss',n'-1}^{(j'')}) \right) \\ & \times \left(\prod_{m'=1}^{M_n^{(j)}} \psi(\underline{a}_{ss,n}^{(j)}, \bar{a}_{m',n}^{(j)}) \prod_{s=1}^{S_n^{(j)}} q_{\text{S1}}(\underline{y}_{s,n}^{(j)}, \underline{\beta}_{ss,n}^{(j)}, \underline{a}_{ss,n}^{(j)}) \left(\prod_{m'=1}^{M_n^{(j)}} \psi(\underline{a}_{ss',n}^{(j)}, \bar{a}_{m',n}^{(j)}) \right) \right) \\ & \times \prod_{s'=1, s \neq s'}^{S_n^{(j)}} q_{\text{D1}}(\underline{y}_{s,n}^{(j)}, \underline{y}_{s',n}^{(j)}, \underline{\beta}_{ss',n}^{(j)}, \underline{a}_{ss',n}^{(j)}) \left(\prod_{m=1}^{M_n^{(j)}} \bar{q}_{\text{N2}}(\mathbf{x}_n, \bar{\mathbf{y}}_{m,n}^{(j)}, \bar{\underline{\beta}}_{m,n}^{(j)}, \bar{a}_{m,n}^{(j)}; \mathbf{z}_n^{(j)}) \right). \end{aligned} \quad (15)$$

B. Joint Likelihood Function

Following [S2], the joint likelihood function $f(\mathbf{z}_{1:n}|\mathbf{x}_{0:n}, \mathbf{y}_{0:n}, \boldsymbol{\beta}_{0:n}, \underline{\mathbf{a}}_{1:n}, \bar{\mathbf{a}}_{1:n}, \mathbf{m}_{1:n})$ can be written as

$$\begin{aligned} & f(\mathbf{z}_{1:n}|\mathbf{x}_{0:n}, \mathbf{y}_{0:n}, \boldsymbol{\beta}_{0:n}, \underline{\mathbf{a}}_{1:n}, \bar{\mathbf{a}}_{1:n}, \mathbf{m}_{1:n}) \\ & \propto \prod_{n'=1}^n \prod_{j=1}^J \left(\underbrace{q_{\text{P}2}(\mathbf{x}_n, \underline{\boldsymbol{\beta}}_{00,n}^{(j)}, \underline{\mathbf{a}}_{00,n}^{(j)}; \mathbf{z}_n^{(j)})}_{\triangleq q_{\text{P}1}(\dots)} \prod_{s=1}^{S_{n'}-1} \underbrace{q_{\text{S}2}(\mathbf{x}_n, \underline{\mathbf{y}}_{s,n}^{(j)}, \underline{\boldsymbol{\beta}}_{ss,n}^{(j)}, \underline{\mathbf{a}}_{ss,n}^{(j)}; \mathbf{z}_n^{(j)})}_{\triangleq q_{\text{S}1}(\dots)} \right. \\ & \quad \left. \times \prod_{s'=1, s' \neq s}^{S_n^{(j)}} \underbrace{q_{\text{D}}(\mathbf{x}_n, \underline{\mathbf{y}}_{s,n}^{(j)}, \underline{\mathbf{y}}_{s',n}^{(j)}, \underline{\boldsymbol{\beta}}_{ss',n}^{(j)}, \underline{\mathbf{a}}_{ss',n}^{(j)}; \mathbf{z}_n^{(j)})}_{\triangleq q_{\text{D}1}(\dots)} \right) \left(\prod_{m=1}^{M_n^{(j)}} \underbrace{\bar{q}_{\text{N}2}(\bar{\mathbf{y}}_{m,n}^{(j)}, \bar{\boldsymbol{\beta}}_{m,n}^{(j)}, \bar{\mathbf{a}}_{m,n}^{(j)})}_{\triangleq \bar{q}_{\text{N}1}(\dots)} \right). \end{aligned} \quad (16)$$

The definitions of the functions $q_{\text{P}2}(\dots)$, $q_{\text{S}2}(\dots)$, $q_{\text{D}2}(\dots)$ and $\bar{q}_{\text{N}2}(\dots)$, together with a summary of the functions $q_{\text{P}1}(\dots)$, $q_{\text{S}1}(\dots)$, $q_{\text{D}1}(\dots)$ and $\bar{q}_{\text{N}1}(\dots)$ are provided in the following table.

C. Joint Posterior PDF

Assume that the measurements are observed and thus fixed. By using Bayes rule and common assumptions, the joint posterior PDF is obtained as

$$\begin{aligned} & f(\mathbf{x}_{0:n}, \mathbf{y}_{0:n}, \boldsymbol{\beta}_{0:n}, \underline{\mathbf{a}}_{1:n}, \bar{\mathbf{a}}_{1:n}, \mathbf{m}_{1:n} | \mathbf{z}_{1:n}) \\ & = \sum_{M'_1=0}^{\infty} \sum_{M'_2=0}^{\infty} \cdots \sum_{M'_n=0}^{\infty} f(\mathbf{z}_{1:n} | \mathbf{x}_{0:n}, \mathbf{y}_{0:n}, \boldsymbol{\beta}_{0:n}, \underline{\mathbf{a}}_{1:n}, \bar{\mathbf{a}}_{1:n}, \mathbf{m}'_{1:n}) f(\mathbf{x}_{0:n}, \mathbf{y}_{0:n}, \boldsymbol{\beta}_{0:n}, \underline{\mathbf{a}}_{1:n}, \bar{\mathbf{a}}_{1:n}, \mathbf{m}'_{1:n}). \end{aligned} \quad (17)$$

By substituting the joint prior PDF with (15) and the joint likelihood function with (16), the joint posterior PDF can be written as

$$\begin{aligned} & f(\mathbf{x}_{0:n}, \mathbf{y}_{0:n}, \boldsymbol{\beta}_{0:n}, \underline{\mathbf{a}}_{1:n}, \bar{\mathbf{a}}_{1:n} | \mathbf{z}_{1:n}) \\ & \propto \left(f(\mathbf{x}_0) \prod_{s=1}^{S_0} f(\mathbf{y}_{s,0}) \prod_{j''=1}^J \prod_{(s,s') \in \bar{\mathcal{D}}_0^{(j'')}} f(\boldsymbol{\beta}_{ss',0}^{(j'')}) \right) \prod_{n'=1}^n f(\mathbf{x}_{n'} | \mathbf{x}_{n'-1}) \left(\prod_{s'=1}^{S_{n'}-1} f(\underline{\mathbf{y}}_{s',n'} | \mathbf{y}_{s',n'-1}) \right) \left(\prod_{j'=2}^J \prod_{s'=1}^{S_{n'}^{(j')}} f^{(j)}(\underline{\mathbf{y}}_{s',n'}^{(j')} | \mathbf{y}_{s',n'}^{(j'-1)}) \right) \\ & \quad \times \left(\prod_{j=1}^J f(\underline{\boldsymbol{\beta}}_{00,n'}^{(j)} | \boldsymbol{\beta}_{00,n'-1}^{(j)}) \underbrace{q_{\text{P}}(\mathbf{x}_{n'}, \underline{\boldsymbol{\beta}}_{00,n'}^{(j)}, \underline{\mathbf{a}}_{00,n'}^{(j)}; \mathbf{z}_{n'}^{(j)})}_{\triangleq q_{\text{P}1}(\dots) q_{\text{P}2}(\dots)} \prod_{m'=1}^{M_{n'}^{(j)}} \psi(\underline{\mathbf{a}}_{00,n'}^{(j)}, \bar{\mathbf{a}}_{m',n'}^{(j)}) \right) \\ & \quad \times \prod_{j=1}^J \left(\prod_{s=1}^{S_{n'}^{(j)}} f(\underline{\boldsymbol{\beta}}_{ss,n'}^{(j)} | \boldsymbol{\beta}_{ss,n'-1}^{(j)}) \underbrace{q_{\text{S}}(\mathbf{x}_{n'}, \underline{\mathbf{y}}_{s,n'}^{(j)}, \underline{\boldsymbol{\beta}}_{ss,n'}^{(j)}, \underline{\mathbf{a}}_{ss,n'}^{(j)}; \mathbf{z}_{n'}^{(j)})}_{\triangleq q_{\text{S}1}(\dots) q_{\text{S}2}(\dots)} \prod_{m'=1}^{M_{n'}^{(j)}} \psi(\underline{\mathbf{a}}_{ss,n'}^{(j)}, \bar{\mathbf{a}}_{m',n'}^{(j)}) \right) \\ & \quad \times \left(\prod_{s'=1, s' \neq s}^{S_{n'}^{(j)}} f(\underline{\boldsymbol{\beta}}_{ss',n'}^{(j)} | \boldsymbol{\beta}_{ss',n'-1}^{(j)}) \underbrace{q_{\text{D}}(\mathbf{x}_{n'}, \underline{\mathbf{y}}_{s,n'}^{(j)}, \underline{\mathbf{y}}_{s',n'}^{(j)}, \underline{\boldsymbol{\beta}}_{ss',n'}^{(j)}, \underline{\mathbf{a}}_{ss',n'}^{(j)}; \mathbf{z}_{n'}^{(j)})}_{\triangleq q_{\text{D}1}(\dots) q_{\text{D}2}(\dots)} \prod_{m'=1}^{M_{n'}^{(j)}} \psi(\underline{\mathbf{a}}_{ss',n'}^{(j)}, \bar{\mathbf{a}}_{m',n'}^{(j)}) \right) \\ & \quad \times \left(\prod_{m=1}^{M_{n'}^{(j)}} \underbrace{\bar{q}_{\text{N}}(\mathbf{x}_{n'}, \bar{\mathbf{y}}_{m,n'}^{(j)}, \bar{\boldsymbol{\beta}}_{m,n'}^{(j)}, \bar{\mathbf{a}}_{m,n'}^{(j)}; \mathbf{z}_{n'}^{(j)})}_{\triangleq \bar{q}_{\text{N}1}(\dots) \bar{q}_{\text{N}2}(\dots)} \right). \end{aligned} \quad (18)$$

Summary of exclusion functions and pseudo LHF's

cases	exclusion function	pseudo LHF part1	pseudo LHF part2	pseudo LHF
<p>For PAs and LoSs PRs i.e., $(s, s') = (0, 0)$</p> <p>$T_{00,n}^{(j)} = 1, \underline{q}_{00,n}^{(j)} \in \mathcal{M}_n^{(j)}$</p> <p>$T_{00,n}^{(j)} = 1, \underline{q}_{00,n}^{(j)} = 0$</p> <p>$T_{00,n}^{(j)} = 0, \underline{q}_{00,n}^{(j)} = 0$</p> <p>$T_{00,n}^{(j)} = 0, \underline{q}_{00,n}^{(j)} \in \mathcal{M}_n^{(j)}$</p>	<p>$T_{\underline{q}_n^{(j)}}(T_{00,n}^{(j)})$</p> <p>1</p> <p>1</p> <p>1</p> <p>0</p>	<p>$q_{p1}(\dots)$</p> <p>$\frac{pd(\underline{u}_{00,n}^{(j)})}{\mu_{fa}}$</p> <p>$1 - pd(\underline{u}_{00,n}^{(j)})$</p> <p>1</p> <p>0</p>	<p>$q_{p2}(\dots)$</p> <p>$\frac{fp(z_{m,n}^{(j)} \mathbf{P}_n, \underline{u}_{00,n}^{(j)})}{fa(z_{m,n}^{(j)})}$</p> <p>1</p> <p>1</p> <p>0</p>	<p>$q_p(\dots) \triangleq q_{p1}(\dots)q_{p2}(\dots)$</p> <p>$\frac{fp(z_{m,n}^{(j)} \mathbf{P}_n, \underline{u}_{00,n}^{(j)})pd(\underline{u}_{00,n}^{(j)})}{\mu_{fa}fa(z_{m,n}^{(j)})}$</p> <p>$1 - pd(\underline{u}_{00,n}^{(j)})$</p> <p>1</p> <p>0</p>
<p>For legacy PSFV's and single-bounce PRs i.e., $s = s' \wedge (s, s') \neq (0, 0)$</p> <p>$T_{s'n}^{(j)} = 1, \underline{q}_{ss'n}^{(j)} \in \mathcal{M}_n^{(j)}$</p> <p>$T_{s'n}^{(j)} = 1, \underline{q}_{ss'n}^{(j)} = 1, \underline{q}_{ss'n}^{(j)} = 0$</p> <p>$T_{s'n}^{(j)} = 1, \underline{q}_{ss'n}^{(j)} = 1, \underline{q}_{ss'n}^{(j)} = 0$</p> <p>$T_{s'n}^{(j)} = 0, \underline{q}_{ss'n}^{(j)} = 0$</p> <p>$T_{s'n}^{(j)} = 0, \underline{q}_{ss'n}^{(j)} \in \mathcal{M}_n^{(j)}$</p> <p>$T_{s'n}^{(j)} = 0, \underline{q}_{ss'n}^{(j)} = 1, \underline{q}_{ss'n}^{(j)} \in \mathcal{M}_{0,n}^{(j)}$</p>	<p>$T_{\underline{q}_n^{(j)}}(T_{s'n}^{(j)}, T_{ss'n}^{(j)})$</p> <p>1</p> <p>1</p> <p>1</p> <p>0</p> <p>0</p>	<p>$q_{s1}(\dots)$</p> <p>$\frac{pd(\underline{u}_{ss'n}^{(j)})}{\mu_{fa}}$</p> <p>$1 - pd(\underline{u}_{ss'n}^{(j)})$</p> <p>1</p> <p>0</p> <p>0</p>	<p>$q_{s2}(\dots)$</p> <p>$\frac{fs(z_{m,n}^{(j)} \mathbf{P}_n, \underline{p}_{s,sfV}^{(j)}, \underline{u}_{ss'n}^{(j)})}{fa(z_{m,n}^{(j)})}$</p> <p>1</p> <p>1</p> <p>0</p> <p>0</p>	<p>$q_s(\dots) \triangleq q_{s1}(\dots)q_{s2}(\dots)$</p> <p>$\frac{fs(z_{m,n}^{(j)} \mathbf{P}_n, \underline{p}_{s,sfV}^{(j)}, \underline{u}_{ss'n}^{(j)})pd(\underline{u}_{ss'n}^{(j)})}{\mu_{fa}fa(z_{m,n}^{(j)})}$</p> <p>$1 - pd(\underline{u}_{ss'n}^{(j)})$</p> <p>1</p> <p>0</p> <p>0</p>
<p>For legacy PSFV's and double-bounce PRs i.e., $s \neq s' \wedge (s, s') \neq (0, 0)$</p> <p>$T_{s'n}^{(j)} = 1, \underline{q}_{ss'n}^{(j)} = 1, \underline{q}_{ss'n}^{(j)} \in \mathcal{M}_n^{(j)}$</p> <p>$T_{s'n}^{(j)} = 1, \underline{q}_{ss'n}^{(j)} = 1, \underline{q}_{ss'n}^{(j)} = 1, \underline{q}_{ss'n}^{(j)} = 0$</p> <p>$V(T_{s'n}^{(j)}, T_{ss'n}^{(j)})$</p> <p>$V(T_{s'n}^{(j)}, T_{ss'n}^{(j)})$</p> <p>$V(T_{s'n}^{(j)}, T_{ss'n}^{(j)})$</p> <p>$(T_{s'n}^{(j)} = 0) \vee (T_{s'n}^{(j)} = 0), T_{ss'n}^{(j)} = 1, \underline{q}_{ss'n}^{(j)} \in \mathcal{M}_{0,n}^{(j)}$</p>	<p>$T_{\underline{q}_n^{(j)}}(T_{s'n}^{(j)}, T_{ss'n}^{(j)}, T_{ss'n}^{(j)})$</p> <p>1</p> <p>1</p> <p>1</p> <p>0</p> <p>0</p>	<p>$\underline{q}_{D1}(\dots)$</p> <p>$\frac{pd(\underline{u}_{ss'n}^{(j)})}{\mu_{fa}}$</p> <p>$1 - pd(\underline{u}_{ss'n}^{(j)})$</p> <p>1</p> <p>0</p> <p>0</p>	<p>$\underline{q}_{D2}(\dots)$</p> <p>$\frac{fd(z_{m,n}^{(j)} \mathbf{P}_n, \underline{p}_{s,sfV}^{(j)}, \underline{p}_{s,sfV}^{(j)}, \underline{u}_{ss'n}^{(j)})}{fa(z_{m,n}^{(j)})}$</p> <p>1</p> <p>1</p> <p>0</p> <p>0</p>	<p>$\underline{q}_D(\dots) \triangleq \underline{q}_{D1}(\dots)\underline{q}_{D2}(\dots)$</p> <p>$\frac{fd(z_{m,n}^{(j)} \mathbf{P}_n, \underline{p}_{s,sfV}^{(j)}, \underline{p}_{s,sfV}^{(j)}, \underline{u}_{ss'n}^{(j)})pd(\underline{u}_{ss'n}^{(j)})}{\mu_{fa}fa(z_{m,n}^{(j)})}$</p> <p>$1 - pd(\underline{u}_{ss'n}^{(j)})$</p> <p>1</p> <p>0</p> <p>0</p>

Summary of exclusion functions and pseudo LHF's

cases	exclusion function	pseudo LHF part1	pseudo LHF part2	pseudo LHF
For new PSFVs and new PRs	$\Gamma_{\underline{q}_n^{(j)}}(\bar{r}_{m,n}^{(j)}, \bar{r}_{m,m,n}^{(j)})$	$q_{N1}(\dots)$	$q_{N2}(\dots)$	$q_N(\dots) \triangleq q_{N1}(\dots)q_{N2}(\dots)$
$\bar{r}_{m,n}^{(j)} = 1, \bar{r}_{m,m,n}^{(j)} = 1, \underline{q}_{ss',n}^{(j)} = 0$	1	$\frac{\mu_n f_n(\bar{\mathbf{p}}_{m,\text{stfv}}^{(j)}, \bar{u}_{mm,n}^{(j)} \mathbf{x}_n)}{\mu_{fa}}$	$\frac{f(\mathbf{z}_{m,n}^{(j)} \mathbf{p}_n, \bar{\mathbf{p}}_{m,\text{stfv}}^{(j)}, \underline{\mathbf{p}}_{Y_{ss},\text{stfv}}^{(j)}, \bar{u}_{mm,n}^{(j)})}{f_{fa}(\mathbf{z}_{m,n}^{(j)})}$	$\frac{f(\mathbf{z}_{m,n}^{(j)} \mathbf{p}_n, \bar{\mathbf{p}}_{m,\text{stfv}}^{(j)}, \underline{\mathbf{p}}_{Y_{ss},\text{stfv}}^{(j)}, \bar{u}_{mm,n}^{(j)}) \mu_n f_n(\bar{\mathbf{p}}_{m,\text{stfv}}^{(j)}, \bar{u}_{mm,n}^{(j)} \mathbf{x}_n)}{\mu_{fa} f_{fa}(\mathbf{z}_{m,n}^{(j)})}$
$\bar{r}_{m,n}^{(j)} = 0, \bar{r}_{m,m,n}^{(j)} = 0, \underline{q}_{ss',n}^{(j)} \in \mathcal{M}_{0,n}^{(j)}$	1	$f_D(\bar{\mathbf{p}}_{m',\text{stfv}}^{(j)}) f_D(\bar{u}_{m',m',n}^{(j)})$	1	$f_D(\bar{\mathbf{p}}_{m',\text{stfv}}^{(j)}) f_D(\bar{u}_{m',m',n}^{(j)})$
otherwise	0	0	0	0

II. SUM-PRODUCT ALGORITHM

Due to the loops inside the factor graph, we specify the following orders for message computation: (i) messages are sent forward both in time from $n-1$ to n and serially from PA $j-1$ to j ; (ii) iterative message passing is only performed for probabilistic data association (DA), i.e., message passing iteration is performed only once in the loops connecting different PSFVs; (iii) messages are only sent from the agent state variable node to the new PSFV state variable node, not vice versa. Combining the specified orders with the generic SPA rules for calculating messages and beliefs yields the following calculations at each time n and each PA j :

A. Prediction

1) *Transition from Time $n-1$ to n* : First, a prediction step from time $n-1$ to n is performed for the agent state, all legacy PSFV states and PR states. The predicted messages for the agent state are given by

$$\alpha(\mathbf{x}_n) = \int f(\mathbf{x}_n | \mathbf{x}_{n-1}) \tilde{f}(\mathbf{x}_{n-1}) d\mathbf{x}_{n-1}. \quad (19)$$

For all the legacy PSFVs $s \in \mathcal{S}_{n-1}$, the predicted messages are given by

$$\alpha(\underline{\mathbf{p}}_{s,\text{sfv}}, \underline{r}_{s,n}) = \sum_{r_{s,n-1} \in \{0,1\}} \int f(\underline{\mathbf{p}}_{s,\text{sfv}}, \underline{r}_{s,n} | \underline{\mathbf{p}}_{s,\text{sfv}}, r_{s,n-1}) \tilde{f}(\underline{\mathbf{p}}_{s,\text{sfv}}, r_{s,n-1}) d\underline{\mathbf{p}}_{s,\text{sfv}}. \quad (20)$$

By inserting (9) and (10) in [S1], we further obtain

$$\alpha(\underline{\mathbf{p}}_{s,\text{sfv}}, \underline{r}_{s,n} = 1) = p_s \int f(\underline{\mathbf{p}}_{s,\text{sfv}} | \underline{\mathbf{p}}_{s,\text{sfv}}) \tilde{f}(\underline{\mathbf{p}}_{s,\text{sfv}}, 1) d\underline{\mathbf{p}}_{s,\text{sfv}} \quad (21)$$

for existing PSFVs and $\alpha(\underline{\mathbf{p}}_{s,\text{sfv}}, \underline{r}_{s,n} = 0) = \alpha_{s,n} f_D(\underline{\mathbf{p}}_{s,\text{sfv}})$ for nonexistent PSFVs with

$$\alpha_{s,n} = (1 - p_s) \int \tilde{f}(\underline{\mathbf{p}}_{s,\text{sfv}}, 1) d\underline{\mathbf{p}}_{s,\text{sfv}} + \tilde{f}_{s,n-1}. \quad (22)$$

and $\tilde{f}_{s,n-1} = \int \tilde{f}(\underline{\mathbf{p}}_{s,\text{sfv}}, 0) d\underline{\mathbf{p}}_{s,\text{sfv}}$ approximating the nonexistent probability of legacy PSFV s at the previous time. Similarly, the predicted messages $\alpha(\underline{\beta}_{ss',n}^{(j)}) = \alpha(\underline{u}_{ss',n}^{(j)}, \underline{r}_{ss',n}^{(j)})$ for legacy PRs are obtained as

$$\alpha(\underline{u}_{ss',n}^{(j)}, \underline{r}_{ss',n}^{(j)}) = \sum_{r_{ss',n-1}^{(j)} \in \{0,1\}} \int f(\underline{u}_{ss',n}^{(j)}, \underline{r}_{ss',n}^{(j)} | \underline{u}_{ss',n-1}^{(j)}, r_{ss',n-1}^{(j)}) \tilde{f}(\underline{u}_{ss',n-1}^{(j)}, r_{ss',n-1}^{(j)}) d\underline{u}_{ss',n-1}^{(j)}. \quad (23)$$

By inserting (13) and (14) in [S1], we further obtain

$$\alpha(\underline{u}_{ss',n}^{(j)}, \underline{r}_{ss',n}^{(j)} = 1) = p_s \int f(\underline{u}_{ss',n}^{(j)} | \underline{u}_{ss',n-1}^{(j)}) \tilde{f}(\underline{u}_{ss',n-1}^{(j)}, 1) d\underline{u}_{ss',n-1}^{(j)} \quad (24)$$

for existing PRs and $\alpha(\underline{u}_{ss',n}^{(j)}, \underline{r}_{ss',n}^{(j)} = 0) = \alpha_{ss',n}^{(j)} f_D(\underline{u}_{ss',n}^{(j)})$ for nonexistent PRs with

$$\alpha_{ss',n}^{(j)} = (1 - p_s) \int \tilde{f}(\underline{u}_{ss',n-1}^{(j)}, 1) d\underline{u}_{ss',n-1}^{(j)} + \tilde{f}_{ss',n-1}^{(j)} \quad (25)$$

and $\tilde{f}_{ss',n-1}^{(j)} = \int \tilde{f}(\underline{u}_{ss',n-1}^{(j)}, 0) d\underline{u}_{ss',n-1}^{(j)}$ approximating the nonexistent probability of legacy PR (s, s') at the previous time $n-1$. The beliefs of the agent state $\tilde{f}(\mathbf{x}_{n-1})$, of the PSFV states $\tilde{f}(\underline{\mathbf{p}}_{s,\text{sfv}}, r_{s,n-1})$, and of the PR states $\tilde{f}(\underline{u}_{ss',n-1}^{(j)}, r_{ss',n-1}^{(j)})$ are obtained at time $n-1$.

2) *Transition from PA $j-1$ to j* : For $j > 1$, the predicted messages $\alpha(\underline{\mathbf{p}}_{s,\text{sfv}}^{(j)}, \underline{r}_{s,n}^{(j)})$ for the former legacy PSFVs $s \in \mathcal{S}_n^{(j-1)}$ and the predicted messages $\alpha(\underline{\mathbf{p}}_{S_n^{(j-1)}+m,\text{sfv}}^{(j)}, \underline{r}_{S_n^{(j-1)}+m,n}^{(j)})$ for the former new PSFVs $m \in \mathcal{M}_n^{(j-1)}$ are inline with [S2].

B. Sequential PA Update

1) *Measurement Evaluation for the LoS Path:* The messages $\omega(\underline{a}_{00,n}^{(j)})$ propagate from the j th PA related factor node $q_P(\mathbf{x}_n, \underline{\beta}_{00,n}^{(j)}, \underline{a}_{00,n}^{(j)}; \mathbf{z}_n^{(j)})$ to the feature-oriented association variable nodes $\underline{a}_{00,n}^{(j)}$ are given by

$$\begin{aligned}
\omega(\underline{a}_{00,n}^{(j)}) &= \sum_{r_{00,n}^{(j)} \in \{0,1\}} \iint \alpha(\mathbf{x}_n) \alpha(\underline{u}_{00,n}^{(j)}, r_{00,n}^{(j)}) q_P(\mathbf{x}_n, \underline{u}_{00,n}^{(j)}, r_{00,n}^{(j)}, \underline{a}_{00,n}^{(j)}; \mathbf{z}_n^{(j)}) d\mathbf{x}_n du_{00,n}^{(j)} \\
&= \iint \alpha(\mathbf{x}_n) \alpha(\underline{u}_{00,n}^{(j)}, 1) q_P(\mathbf{x}_n, \underline{u}_{00,n}^{(j)}, 1, \underline{a}_{00,n}^{(j)}; \mathbf{z}_n^{(j)}) d\mathbf{x}_n du_{00,n}^{(j)} \\
&\quad + 1(\underline{a}_{00,n}^{(j)}) \iint \alpha(\mathbf{x}_n) \alpha(\underline{u}_{00,n}^{(j)}, 0) d\mathbf{x}_n du_{00,n}^{(j)} \\
&= \iint \alpha(\mathbf{x}_n) \alpha(\underline{u}_{00,n}^{(j)}, 1) q_P(\mathbf{x}_n, \underline{u}_{00,n}^{(j)}, 1, \underline{a}_{00,n}^{(j)}; \mathbf{z}_n^{(j)}) d\mathbf{x}_n du_{00,n}^{(j)} + 1(\underline{a}_{00,n}^{(j)}) \alpha_{00,n}^{(j)}. \tag{26}
\end{aligned}$$

2) *Measurement Evaluation for Legacy PSFVs:*

a) *Single-bounce propagation path:* For $s = s'$, the messages $\omega(\underline{a}_{ss,n}^{(j)})$ propagate from the single-bounce PR related factor node $q_S(\mathbf{x}_n, \underline{\mathbf{y}}_{s,n}^{(j)}, \underline{\beta}_{ss,n}^{(j)}, \underline{a}_{ss,n}^{(j)}; \mathbf{z}_n^{(j)})$ to the feature-oriented association variable nodes $\underline{a}_{ss,n}^{(j)}$ are given by

$$\begin{aligned}
\omega(\underline{a}_{ss,n}^{(j)}) &= \sum_{r_{ss,n}^{(j)} \in \{0,1\}} \sum_{r_{s',n}^{(j)} \in \{0,1\}} \iiint \alpha(\mathbf{x}_n) \alpha(\underline{\mathbf{p}}_{s,\text{sfv}}^{(j)}, r_{s,n}^{(j)}) \\
&\quad \times \alpha(\underline{u}_{ss,n}^{(j)}, r_{ss,n}^{(j)}) q_S(\mathbf{x}_n, \underline{\mathbf{p}}_{s,\text{sfv}}^{(j)}, r_{s,n}^{(j)}, \underline{u}_{ss,n}^{(j)}, r_{ss,n}^{(j)}, \underline{a}_{ss,n}^{(j)}; \mathbf{z}_n^{(j)}) d\mathbf{x}_n d\underline{\mathbf{p}}_{s,\text{sfv}}^{(j)} du_{ss,n}^{(j)} \\
&= \iiint \alpha(\mathbf{x}_n) \alpha(\underline{\mathbf{p}}_{s,\text{sfv}}^{(j)}, 1) \alpha(\underline{u}_{ss,n}^{(j)}, 1) q_S(\mathbf{x}_n, \underline{\mathbf{p}}_{s,\text{sfv}}^{(j)}, 1, \underline{u}_{ss,n}^{(j)}, 1, \underline{a}_{ss,n}^{(j)}; \mathbf{z}_n^{(j)}) d\mathbf{x}_n d\underline{\mathbf{p}}_{s,\text{sfv}}^{(j)} du_{ss,n}^{(j)} \\
&\quad + 1(\underline{a}_{ss,n}^{(j)}) \alpha_{ss,n}^{(j)} \underbrace{\left(\alpha_{s,n}^{(j)} + \int \alpha(\underline{\mathbf{p}}_{s,\text{sfv}}^{(j)}, 1) d\underline{\mathbf{p}}_{s,\text{sfv}}^{(j)} \right)}_{=1} \\
&= \iiint \alpha(\mathbf{x}_n) \alpha(\underline{\mathbf{p}}_{s,\text{sfv}}^{(j)}, 1) \alpha(\underline{u}_{ss,n}^{(j)}, 1) q_S(\mathbf{x}_n, \underline{\mathbf{p}}_{s,\text{sfv}}^{(j)}, 1, \underline{u}_{ss,n}^{(j)}, 1, \underline{a}_{ss,n}^{(j)}; \mathbf{z}_n^{(j)}) d\mathbf{x}_n d\underline{\mathbf{p}}_{s,\text{sfv}}^{(j)} du_{ss,n}^{(j)} \\
&\quad + 1(\underline{a}_{ss,n}^{(j)}) \alpha_{ss,n}^{(j)}. \tag{27}
\end{aligned}$$

b) *Double-bounce propagation path:* For $s \neq s'$, the messages $\omega(\underline{a}_{ss',n}^{(j)})$ propagate from the double-bounce PR related factor node $q_D(\mathbf{x}_n, \underline{\mathbf{y}}_{s,n}^{(j)}, \underline{\mathbf{y}}_{s',n}^{(j)}, \underline{\mathbf{u}}_{ss',n}^{(j)}, \underline{a}_{ss',n}^{(j)}; \mathbf{z}_n^{(j)})$ to the feature-oriented association variable nodes $\underline{a}_{ss',n}^{(j)}$ are

given by

$$\begin{aligned}
& \omega(\underline{a}_{ss',n}^{(j)}) \\
&= \sum_{r_{ss,n}^{(j)} \in \{0,1\}} \sum_{r_{s,n}^{(j)} \in \{0,1\}} \sum_{r_{s',n}^{(j)} \in \{0,1\}} \iiint \alpha(\mathbf{x}_n) \alpha(\underline{\mathbf{p}}_{s,\text{sfv}}^{(j)}, r_{s,n}^{(j)}) \alpha(\underline{\mathbf{p}}_{s',\text{sfv}}^{(j)}, r_{s',n}^{(j)}) \alpha(\underline{\mathbf{u}}_{ss',n}^{(j)}, r_{ss',n}^{(j)}) \\
& \quad \times q_{\text{D}}(\mathbf{x}_n, \underline{\mathbf{p}}_{s,\text{sfv}}^{(j)}, r_{s,n}^{(j)}, \underline{\mathbf{p}}_{s',\text{sfv}}^{(j)}, r_{s',n}^{(j)}, \underline{\mathbf{u}}_{ss',n}^{(j)}, r_{ss',n}^{(j)}, \underline{\mathbf{a}}_{ss',n}^{(j)}; \mathbf{z}_n^{(j)}) d\mathbf{x}_n d\underline{\mathbf{p}}_{s,\text{sfv}}^{(j)} d\underline{\mathbf{p}}_{s',\text{sfv}}^{(j)} d\underline{\mathbf{u}}_{ss',n}^{(j)} \\
&= \iiint \alpha(\mathbf{x}_n) \alpha(\underline{\mathbf{p}}_{s,\text{sfv}}^{(j)}, 1) \alpha(\underline{\mathbf{p}}_{s',\text{sfv}}^{(j)}, 1) \alpha(\underline{\mathbf{u}}_{ss',n}^{(j)}, 1) q_{\text{D}}(\mathbf{x}_n, \underline{\mathbf{p}}_{s,\text{sfv}}^{(j)}, 1, \underline{\mathbf{p}}_{s',\text{sfv}}^{(j)}, 1, \underline{\mathbf{u}}_{ss',n}^{(j)}, 1, \underline{\mathbf{a}}_{ss',n}^{(j)}; \mathbf{z}_n^{(j)}) \\
& \quad \times d\mathbf{x}_n d\underline{\mathbf{p}}_{s,\text{sfv}}^{(j)} d\underline{\mathbf{p}}_{s',\text{sfv}}^{(j)} d\underline{\mathbf{u}}_{ss',n}^{(j)} + 1(\underline{\mathbf{a}}_{ss',n}^{(j)}) \alpha_{ss',n}^{(j)} \alpha_{s',n}^{(j)} \underbrace{\left(\alpha_{s,n}^{(j)} + \int \alpha(\underline{\mathbf{p}}_{s,\text{sfv}}^{(j)}, 1) d\underline{\mathbf{p}}_{s,\text{sfv}}^{(j)} \right)}_{=1} \\
& \quad + 1(\underline{\mathbf{a}}_{ss',n}^{(j)}) \alpha_{ss',n}^{(j)} \underbrace{\left(\alpha_{s,n}^{(j)} + \int \alpha(\underline{\mathbf{p}}_{s,\text{sfv}}^{(j)}, 1) d\underline{\mathbf{p}}_{s,\text{sfv}}^{(j)} \right)}_{=1} \int \alpha(\underline{\mathbf{p}}_{s',\text{sfv}}^{(j)}, 1) d\underline{\mathbf{p}}_{s',\text{sfv}}^{(j)} \\
&= \iiint \alpha(\mathbf{x}_n) \alpha(\underline{\mathbf{p}}_{s,\text{sfv}}^{(j)}, 1) \alpha(\underline{\mathbf{p}}_{s',\text{sfv}}^{(j)}, 1) \alpha(\underline{\mathbf{u}}_{ss',n}^{(j)}, 1) q_{\text{D}}(\mathbf{x}_n, \underline{\mathbf{p}}_{s,\text{sfv}}^{(j)}, 1, \underline{\mathbf{p}}_{s',\text{sfv}}^{(j)}, 1, \underline{\mathbf{u}}_{ss',n}^{(j)}, 1, \underline{\mathbf{a}}_{ss',n}^{(j)}; \mathbf{z}_n^{(j)}) \\
& \quad \times d\mathbf{x}_n d\underline{\mathbf{p}}_{s,\text{sfv}}^{(j)} d\underline{\mathbf{p}}_{s',\text{sfv}}^{(j)} d\underline{\mathbf{u}}_{ss',n}^{(j)} + 1(\underline{\mathbf{a}}_{ss',n}^{(j)}) \alpha_{ss',n}^{(j)} \underbrace{\left(\alpha_{s',n}^{(j)} + \int \alpha(\underline{\mathbf{p}}_{s',\text{sfv}}^{(j)}, 1) d\underline{\mathbf{p}}_{s',\text{sfv}}^{(j)} \right)}_{=1}. \tag{28}
\end{aligned}$$

Finally, we obtain

$$\begin{aligned}
\omega(\underline{a}_{ss',n}^{(j)}) &= 1(\underline{\mathbf{a}}_{ss',n}^{(j)}) \alpha_{ss',n}^{(j)} + \iiint \alpha(\mathbf{x}_n) \alpha(\underline{\mathbf{p}}_{s,\text{sfv}}^{(j)}, 1) \alpha(\underline{\mathbf{p}}_{s',\text{sfv}}^{(j)}, 1) \alpha(\underline{\mathbf{u}}_{ss',n}^{(j)}, 1) \\
& \quad \times q_{\text{D}}(\mathbf{x}_n, \underline{\mathbf{p}}_{s,\text{sfv}}^{(j)}, 1, \underline{\mathbf{p}}_{s',\text{sfv}}^{(j)}, 1, \underline{\mathbf{u}}_{ss',n}^{(j)}, 1, \underline{\mathbf{a}}_{ss',n}^{(j)}; \mathbf{z}_n^{(j)}) d\mathbf{x}_n d\underline{\mathbf{p}}_{s,\text{sfv}}^{(j)} d\underline{\mathbf{p}}_{s',\text{sfv}}^{(j)} d\underline{\mathbf{u}}_{ss',n}^{(j)}. \tag{29}
\end{aligned}$$

3) *Measurement Evaluation for New PSFVs*: For PA j , the messages $\xi(\bar{a}_{m,n}^{(j)})$ sent from the new PSFV and new PR related factor node $\bar{q}_{\text{N}}(\mathbf{x}_n, \bar{\mathbf{y}}_{m,n}^{(j)}, \bar{\boldsymbol{\beta}}_{m,n}^{(j)}, \bar{a}_{m,n}^{(j)}; \mathbf{z}_n^{(j)})$ to the measurement-oriented association variable nodes $\bar{a}_{m,n}^{(j)}$ are given by

$$\xi(\bar{a}_{m,n}^{(j)}) = \sum_{\bar{r}_{m,n}^{(j)} \in \{0,1\}} \sum_{\bar{r}_{mm,n}^{(j)} \in \{0,1\}} \iiint \alpha(\mathbf{x}_n) \bar{q}_{\text{N}}(\mathbf{x}_n, \bar{\mathbf{p}}_{m,\text{sfv}}^{(j)}, \bar{r}_{m,n}^{(j)}, \bar{u}_{mm,n}^{(j)}, \bar{r}_{mm,n}^{(j)}, \bar{a}_{m,n}^{(j)}; \mathbf{z}_n^{(j)}) d\mathbf{x}_n d\bar{\mathbf{p}}_{m,\text{sfv}}^{(j)} d\bar{u}_{mm,n}^{(j)}. \tag{30}$$

Specifically, $\xi(\bar{a}_{m,n}^{(j)}) = 1$ for $\bar{a}_{m,n}^{(j)} \in \tilde{\mathcal{D}}_n^{(j)}$, and for $\bar{a}_{m,n}^{(j)} = 0$,

$$\xi(\bar{a}_{m,n}^{(j)}) = \frac{\mu_n}{\mu_{\text{fa}} f_{\text{fa}}(\mathbf{z}_{m,n}^{(j)})} \iiint \alpha(\mathbf{x}_n) f_{\text{N}}(\bar{\mathbf{p}}_{m,\text{sfv}}^{(j)}, \bar{u}_{mm,n}^{(j)} | \mathbf{x}_n) f(\mathbf{z}_{m,n}^{(j)} | \mathbf{p}_n, \bar{\mathbf{p}}_{m,\text{sfv}}^{(j)}, \bar{u}_{mm,n}^{(j)}) d\mathbf{x}_n d\bar{\mathbf{p}}_{m,\text{sfv}}^{(j)} d\bar{u}_{mm,n}^{(j)} + 1. \tag{31}$$

4) *Iterative Data Association*: With the messages $\omega(\underline{a}_{ss',n}^{(j)})$ and $\xi(\bar{a}_{m,n}^{(j)})$, the probabilistic DA messages $\eta(\underline{a}_{ss',n}^{(j)})$ and $\varsigma(\bar{a}_{m,n}^{(j)})$ are obtained using loopy belief propagation (BP) according to [S2], [S3].

5) *Measurement Update for Agent*: For the update of agent state \mathbf{x}_n , only the messages from legacy PSFVs are used.

a) *LoS propagation path*: The messages $\gamma_{00}^{(j)}(\mathbf{x}_n)$ sent from the factor node $q_{\text{P}}(\mathbf{x}_n, \underline{\boldsymbol{\beta}}_{00,n}^{(j)}, \underline{a}_{00,n}^{(j)}; \mathbf{z}_n^{(j)})$ to the agent variable node \mathbf{x}_n are obtained as

$$\gamma_{00}^{(j)}(\mathbf{x}_n) = \sum_{\underline{a}_{00,n}^{(j)} \in \mathcal{M}_{0,n}^{(j)}} \eta(\underline{a}_{00,n}^{(j)}) \int \alpha(\underline{\mathbf{u}}_{00,n}^{(j)}, 1) q_{\text{P}}(\mathbf{x}_n, \underline{\mathbf{u}}_{00,n}^{(j)}, 1, \underline{\mathbf{a}}_{00,n}^{(j)}; \mathbf{z}_n^{(j)}) d\underline{\mathbf{u}}_{00,n}^{(j)} + \eta(\underline{a}_{00,n}^{(j)} = 0) \alpha_{00,n}^{(j)} \tag{32}$$

with $\mathcal{M}_{0,n}^{(j)} \triangleq \{0, \mathcal{M}_n^{(j)}\}$.

b) *Single-bounce propagation path:* For $s = s'$, the messages $\gamma_{ss}^{(j)}(\mathbf{x}_n)$ propagate from the single-bounce PR related factor node $q_S(\mathbf{x}_n, \mathbf{y}_{s,n}^{(j)}, \boldsymbol{\beta}_{ss,n}^{(j)}, \underline{a}_{ss,n}^{(j)}; \mathbf{z}_n^{(j)})$ to the agent variable node \mathbf{x}_n are obtained as

$$\begin{aligned} \gamma_{ss}^{(j)}(\mathbf{x}_n) &= \sum_{\underline{r}_{ss,n}^{(j)} \in \{0,1\}} \sum_{\underline{r}_{s,n}^{(j)} \in \{0,1\}} \sum_{\underline{a}_{ss,n}^{(j)} \in \mathcal{M}_{0,n}^{(j)}} \eta(\underline{a}_{ss,n}^{(j)}) \iint \alpha(\underline{\mathbf{p}}_{s,\text{sfv}}^{(j)}, \underline{r}_{s,n}^{(j)}) \alpha(\underline{\mathbf{u}}_{ss,n}^{(j)}, \underline{r}_{ss,n}^{(j)}) \\ &\quad \times q_S(\mathbf{x}_n, \underline{\mathbf{p}}_{s,\text{sfv}}^{(j)}, \underline{r}_{s,n}^{(j)}, \underline{\mathbf{u}}_{ss,n}^{(j)}, \underline{r}_{ss,n}^{(j)}, \underline{a}_{ss,n}^{(j)}; \mathbf{z}_n^{(j)}) d\underline{\mathbf{p}}_{s,\text{sfv}}^{(j)} d\underline{\mathbf{u}}_{ss,n}^{(j)} \\ &\quad + \eta(\underline{a}_{ss,n}^{(j)} = 0) \alpha_{ss,n}^{(j)} \left(\underbrace{\alpha_{s,n}^{(j)} + \int \alpha(\underline{\mathbf{p}}_{s,\text{sfv}}^{(j)}, 1) d\underline{\mathbf{p}}_{s,\text{sfv}}^{(j)}}_{=1} \right). \end{aligned} \quad (33)$$

Finally, we obtain

$$\begin{aligned} \gamma_{ss}^{(j)}(\mathbf{x}_n) &= \sum_{\underline{a}_{ss,n}^{(j)} \in \mathcal{M}_{0,n}^{(j)}} \eta(\underline{a}_{ss,n}^{(j)}) \iint \alpha(\underline{\mathbf{p}}_{s,\text{sfv}}^{(j)}, 1) \alpha(\underline{\mathbf{u}}_{ss,n}^{(j)}, 1) q_S(\mathbf{x}_n, \underline{\mathbf{p}}_{s,\text{sfv}}^{(j)}, 1, \underline{\mathbf{u}}_{ss,n}^{(j)}, 1, \underline{a}_{ss,n}^{(j)}; \mathbf{z}_n^{(j)}) d\underline{\mathbf{p}}_{s,\text{sfv}}^{(j)} d\underline{\mathbf{u}}_{ss,n}^{(j)} \\ &\quad + \eta(\underline{a}_{ss,n}^{(j)} = 0) \alpha_{ss,n}^{(j)}. \end{aligned} \quad (34)$$

c) *Double-bounce propagation path:* For $s \neq s'$, the messages $\gamma_{ss'}^{(j)}(\mathbf{x}_n)$ propagate from double-bounce PR related factor node $q_D(\mathbf{x}_n, \mathbf{y}_{s,n}^{(j)}, \mathbf{y}_{s',n}^{(j)}, \underline{\mathbf{u}}_{ss',n}^{(j)}, \underline{a}_{ss',n}^{(j)}; \mathbf{z}_n^{(j)})$ to the agent variable node \mathbf{x}_n are obtained as

$$\begin{aligned} \gamma_{ss'}^{(j)}(\mathbf{x}_n) &= \sum_{\underline{r}_{ss',n}^{(j)} \in \{0,1\}} \sum_{\underline{r}_{s,n}^{(j)} \in \{0,1\}} \sum_{\underline{r}_{s',n}^{(j)} \in \{0,1\}} \sum_{\underline{a}_{ss',n}^{(j)} \in \mathcal{M}_{0,n}^{(j)}} \eta(\underline{a}_{ss',n}^{(j)}) \iiint \alpha(\underline{\mathbf{p}}_{s,\text{sfv}}^{(j)}, \underline{r}_{s,n}^{(j)}) \alpha(\underline{\mathbf{p}}_{s',\text{sfv}}^{(j)}, \underline{r}_{s',n}^{(j)}) \\ &\quad \times \alpha(\underline{\mathbf{u}}_{ss',n}^{(j)}, \underline{r}_{ss',n}^{(j)}) q_D(\mathbf{x}_n, \underline{\mathbf{p}}_{s,\text{sfv}}^{(j)}, 1, \underline{\mathbf{p}}_{s',\text{sfv}}^{(j)}, 1, \underline{\mathbf{u}}_{ss',n}^{(j)}, \underline{r}_{ss',n}^{(j)}, \underline{a}_{ss',n}^{(j)}; \mathbf{z}_n^{(j)}) d\underline{\mathbf{p}}_{s,\text{sfv}}^{(j)} d\underline{\mathbf{p}}_{s',\text{sfv}}^{(j)} d\underline{\mathbf{u}}_{ss',n}^{(j)} \\ &= \sum_{\underline{a}_{ss',n}^{(j)} \in \mathcal{M}_{0,n}^{(j)}} \eta(\underline{a}_{ss',n}^{(j)}) \iiint \alpha(\underline{\mathbf{p}}_{s,\text{sfv}}^{(j)}, 1) \alpha(\underline{\mathbf{p}}_{s',\text{sfv}}^{(j)}, 1) \alpha(\underline{\mathbf{u}}_{ss',n}^{(j)}, 1) \\ &\quad \times q_D(\mathbf{x}_n, \underline{\mathbf{p}}_{s,\text{sfv}}^{(j)}, 1, \underline{\mathbf{p}}_{s',\text{sfv}}^{(j)}, 1, \underline{\mathbf{u}}_{ss',n}^{(j)}, 1, \underline{a}_{ss',n}^{(j)}; \mathbf{z}_n^{(j)}) d\underline{\mathbf{p}}_{s,\text{sfv}}^{(j)} d\underline{\mathbf{p}}_{s',\text{sfv}}^{(j)} d\underline{\mathbf{u}}_{ss',n}^{(j)} \\ &\quad + \eta(\underline{a}_{ss',n}^{(j)} = 0) \left(\alpha_{ss',n}^{(j)} \alpha_{s',n}^{(j)} \underbrace{\left(\alpha_{s,n}^{(j)} + \int \alpha(\underline{\mathbf{p}}_{s,\text{sfv}}^{(j)}, 1) d\underline{\mathbf{p}}_{s,\text{sfv}}^{(j)} \right)}_{=1} \right) \\ &\quad + \alpha_{ss',n}^{(j)} \underbrace{\left(\alpha_{s,n}^{(j)} + \int \alpha(\underline{\mathbf{p}}_{s,\text{sfv}}^{(j)}, 1) d\underline{\mathbf{p}}_{s,\text{sfv}}^{(j)} \right)}_{=1} \int \alpha(\underline{\mathbf{p}}_{s',\text{sfv}}^{(j)}, 1) d\underline{\mathbf{p}}_{s',\text{sfv}}^{(j)}. \end{aligned} \quad (35)$$

Finally, we obtain

$$\begin{aligned} \gamma_{ss'}^{(j)}(\mathbf{x}_n) &= \eta(\underline{a}_{ss',n}^{(j)} = 0) \alpha_{ss',n}^{(j)} + \sum_{\underline{a}_{ss',n}^{(j)} \in \mathcal{M}_{0,n}^{(j)}} \eta(\underline{a}_{ss',n}^{(j)}) \iiint \alpha(\underline{\mathbf{p}}_{s,\text{sfv}}^{(j)}, 1) \alpha(\underline{\mathbf{p}}_{s',\text{sfv}}^{(j)}, 1) \alpha(\underline{\mathbf{u}}_{ss',n}^{(j)}, 1) \\ &\quad \times q_D(\mathbf{x}_n, \underline{\mathbf{p}}_{s,\text{sfv}}^{(j)}, 1, \underline{\mathbf{p}}_{s',\text{sfv}}^{(j)}, 1, \underline{\mathbf{u}}_{ss',n}^{(j)}, 1, \underline{a}_{ss',n}^{(j)}; \mathbf{z}_n^{(j)}) d\underline{\mathbf{p}}_{s,\text{sfv}}^{(j)} d\underline{\mathbf{p}}_{s',\text{sfv}}^{(j)} d\underline{\mathbf{u}}_{ss',n}^{(j)}. \end{aligned} \quad (36)$$

6) Measurement Update for Legacy PSFVs:

a) *Single-bounce propagation path:* For $s = s'$, the messages $\rho_{ss}(\mathbf{y}_{s,n}^{(j)})$ propagate from the factor node $q_S(\mathbf{x}_n, \mathbf{y}_{s,n}^{(j)}, \boldsymbol{\beta}_{ss,n}^{(j)}, \underline{a}_{ss,n}^{(j)}; \mathbf{z}_n^{(j)})$ to the PSFV variable node $\mathbf{y}_{s,n}^{(j)}$ are obtained as

$$\begin{aligned} &\rho_{ss}(\underline{\mathbf{p}}_{s,\text{sfv}}^{(j)}, \underline{r}_{s,n}^{(j)}) \\ &= \sum_{\underline{r}_{ss,n}^{(j)} \in \{0,1\}} \sum_{\underline{a}_{ss,n}^{(j)} \in \mathcal{M}_{0,n}^{(j)}} \eta(\underline{a}_{ss,n}^{(j)}) \iint \alpha(\mathbf{x}_n) \alpha(\underline{\mathbf{u}}_{ss,n}^{(j)}, \underline{r}_{ss,n}^{(j)}) q_S(\mathbf{x}_n, \underline{\mathbf{p}}_{s,\text{sfv}}^{(j)}, \underline{r}_{s,n}^{(j)}, \underline{\mathbf{u}}_{ss,n}^{(j)}, \underline{r}_{ss,n}^{(j)}, \underline{a}_{ss,n}^{(j)}; \mathbf{z}_n^{(j)}) d\mathbf{x}_n d\underline{\mathbf{u}}_{ss,n}^{(j)}. \end{aligned} \quad (37)$$

We further obtain the messages for existing legacy PSFVs as

$$\begin{aligned}
\rho_{ss}(\underline{\mathbf{p}}_{s,\text{sfv}}^{(j)}, 1) &= \sum_{\underline{a}_{ss,n}^{(j)} \in \mathcal{M}_{0,n}^{(j)}} \eta(\underline{a}_{ss,n}^{(j)}) \iint \alpha(\mathbf{x}_n) \alpha(\underline{u}_{ss,n}^{(j)}, 1) \underline{q}_S(\mathbf{x}_n, \underline{\mathbf{p}}_{s,\text{sfv}}^{(j)}, 1, \underline{u}_{ss,n}^{(j)}, 1, \underline{a}_{ss,n}^{(j)}; \mathbf{z}_n^{(j)}) d\mathbf{x}_n d\underline{u}_{ss,n}^{(j)} \\
&\quad + \eta(\underline{a}_{ss,n}^{(j)} = 0) \iint \alpha(\mathbf{x}_n) \alpha(\underline{u}_{ss,n}^{(j)}, 0) d\mathbf{x}_n d\underline{u}_{ss,n}^{(j)} \\
&= \sum_{\underline{a}_{ss,n}^{(j)} \in \mathcal{M}_{0,n}^{(j)}} \eta(\underline{a}_{ss,n}^{(j)}) \iint \alpha(\mathbf{x}_n) \alpha(\underline{u}_{ss,n}^{(j)}, 1) \underline{q}_S(\mathbf{x}_n, \underline{\mathbf{p}}_{s,\text{sfv}}^{(j)}, 1, \underline{u}_{ss,n}^{(j)}, 1, \underline{a}_{ss,n}^{(j)}; \mathbf{z}_n^{(j)}) d\mathbf{x}_n d\underline{u}_{ss,n}^{(j)} \\
&\quad + \eta(\underline{a}_{ss,n}^{(j)} = 0) \alpha_{ss,n}^{(j)},
\end{aligned} \tag{38}$$

and the messages $\rho_{ss}(\underline{\mathbf{p}}_{s,\text{sfv}}^{(j)}, 0) \triangleq \rho_{ss}^{(j)}$ for nonexistent legacy PSFVs as

$$\begin{aligned}
\rho_{ss}(\underline{\mathbf{p}}_{s,\text{sfv}}^{(j)}, 0) &= \eta(\underline{a}_{ss,n}^{(j)} = 0) \iint \alpha(\mathbf{x}_n) \alpha(\underline{u}_{ss,n}^{(j)}, 0) d\mathbf{x}_n d\underline{u}_{ss,n}^{(j)} \\
&= \eta(\underline{a}_{ss,n}^{(j)} = 0) \alpha_{ss,n}^{(j)}.
\end{aligned} \tag{39}$$

b) Double-bounce propagation path: For $s \neq s'$, the messages $\rho_{ss'}(\mathbf{y}_{s,n}^{(j)})$ from the factor node $\underline{q}_D(\mathbf{x}_n, \mathbf{y}_{s,n}^{(j)}, \mathbf{y}_{s',n}^{(j)}, \underline{\beta}_{ss',n}^{(j)}, \underline{a}_{ss',n}^{(j)}; \mathbf{z}_n^{(j)})$ to the PSFV variable node $\mathbf{y}_{s,n}^{(j)}$ are obtained as

$$\begin{aligned}
\rho_{ss'}(\underline{\mathbf{p}}_{s,\text{sfv}}^{(j)}, \underline{r}_{s,n}^{(j)}) &= \sum_{\underline{r}_{ss',n}^{(j)} \in \{0,1\}} \sum_{\underline{r}_{s',n}^{(j)} \in \{0,1\}} \sum_{\underline{a}_{ss',n}^{(j)} \in \mathcal{M}_{0,n}^{(j)}} \eta(\underline{a}_{ss',n}^{(j)}) \iiint \alpha(\mathbf{x}_n) \alpha(\underline{\mathbf{p}}_{s',\text{sfv}}^{(j)}, \underline{r}_{s',n}^{(j)}) \alpha(\underline{u}_{ss',n}^{(j)}, \underline{r}_{s',n}^{(j)}) \\
&\quad \times \underline{q}_D(\mathbf{x}_n, \underline{\mathbf{p}}_{s,\text{sfv}}^{(j)}, \underline{r}_{s,n}^{(j)}, \underline{\mathbf{p}}_{s',\text{sfv}}^{(j)}, \underline{r}_{s',n}^{(j)}, \underline{u}_{ss',n}^{(j)}, \underline{r}_{s',n}^{(j)}, \underline{a}_{ss',n}^{(j)}; \mathbf{z}_n^{(j)}) d\mathbf{x}_n d\underline{\mathbf{p}}_{s',\text{sfv}}^{(j)} d\underline{u}_{ss',n}^{(j)}.
\end{aligned} \tag{40}$$

We further obtain the messages for existing legacy PSFVs as

$$\begin{aligned}
\rho_{ss'}(\underline{\mathbf{p}}_{s,\text{sfv}}^{(j)}, 1) &= \sum_{\underline{a}_{ss',n}^{(j)} \in \mathcal{M}_{0,n}^{(j)}} \eta(\underline{a}_{ss',n}^{(j)}) \iiint \alpha(\mathbf{x}_n) \alpha(\underline{\mathbf{p}}_{s',\text{sfv}}^{(j)}, 1) \alpha(\underline{u}_{ss',n}^{(j)}, 1) \\
&\quad \times \underline{q}_D(\mathbf{x}_n, \underline{\mathbf{p}}_{s,\text{sfv}}^{(j)}, 1, \underline{\mathbf{p}}_{s',\text{sfv}}^{(j)}, 1, \underline{u}_{ss',n}^{(j)}, 1, \underline{a}_{ss',n}^{(j)}; \mathbf{z}_n^{(j)}) d\mathbf{x}_n d\underline{\mathbf{p}}_{s',\text{sfv}}^{(j)} d\underline{u}_{ss',n}^{(j)} \\
&\quad + \eta(\underline{a}_{ss',n}^{(j)} = 0) \alpha_{ss',n}^{(j)} \underbrace{\left(\alpha_{s',n}^{(j)} + \int \alpha(\underline{\mathbf{p}}_{s',\text{sfv}}^{(j)}, 1) d\underline{\mathbf{p}}_{s',\text{sfv}}^{(j)} \right)}_{=1} \\
&= \sum_{\underline{a}_{ss',n}^{(j)} \in \mathcal{M}_{0,n}^{(j)}} \eta(\underline{a}_{ss',n}^{(j)}) \iiint \alpha(\mathbf{x}_n) \alpha(\underline{\mathbf{p}}_{s',\text{sfv}}^{(j)}, 1) \alpha(\underline{u}_{ss',n}^{(j)}, 1) \\
&\quad \times \underline{q}_D(\mathbf{x}_n, \underline{\mathbf{p}}_{s,\text{sfv}}^{(j)}, 1, \underline{\mathbf{p}}_{s',\text{sfv}}^{(j)}, 1, \underline{u}_{ss',n}^{(j)}, 1, \underline{a}_{ss',n}^{(j)}; \mathbf{z}_n^{(j)}) d\mathbf{x}_n d\underline{\mathbf{p}}_{s',\text{sfv}}^{(j)} d\underline{u}_{ss',n}^{(j)} \\
&\quad + \eta(\underline{a}_{ss',n}^{(j)} = 0) \alpha_{ss',n}^{(j)},
\end{aligned} \tag{41}$$

and the messages $\rho_{ss'}(\underline{\mathbf{p}}_{s,\text{sfv}}^{(j)}, 0) \triangleq \rho_{ss'}^{(j)}$ for nonexistent legacy PSFVs as

$$\begin{aligned}
\rho_{ss'}(\underline{\mathbf{p}}_{s,\text{sfv}}^{(j)}, 0) &= \eta(\underline{a}_{ss',n}^{(j)} = 0) \alpha_{ss',n}^{(j)} \underbrace{\left(\alpha_{s',n}^{(j)} + \int \alpha(\underline{\mathbf{p}}_{s',\text{sfv}}^{(j)}, 1) d\underline{\mathbf{p}}_{s',\text{sfv}}^{(j)} \right)}_{=1} \\
&= \eta(\underline{a}_{ss',n}^{(j)} = 0) \alpha_{ss',n}^{(j)}.
\end{aligned} \tag{42}$$

The messages sent to the next PA $\gamma(\underline{\mathbf{y}}_{s,n}^{(j)}) \triangleq \gamma(\underline{\mathbf{p}}_{s,\text{sfv}}^{(j)}, \underline{\mathbf{r}}_{s,n}^{(j)})$ are given as

$$\gamma(\underline{\mathbf{p}}_{s,\text{sfv}}^{(j)}, 1) = \alpha(\underline{\mathbf{p}}_{s,\text{sfv}}^{(j)}, 1) \rho_{ss}(\underline{\mathbf{p}}_{s,\text{sfv}}^{(j)}, 1) \prod_{s'=1, s' \neq s}^{S_n^{(j)}} \rho_{ss'}(\underline{\mathbf{p}}_{s,\text{sfv}}^{(j)}, 1), \quad (43)$$

$$\gamma(\underline{\mathbf{p}}_{s,\text{sfv}}^{(j)}, 0) \triangleq \gamma_{s,n}^{(j)} = \alpha(\underline{\mathbf{p}}_{s,\text{sfv}}^{(j)}, 0) \rho_{ss}^{(j)} \prod_{s'=1, s' \neq s}^{S_n^{(j)}} \rho_{ss'}^{(j)}. \quad (44)$$

7) *Measurement Update for New PSFVs*: The messages $\phi(\underline{\mathbf{y}}_{m,n}^{(j)}) \triangleq \phi(\underline{\mathbf{p}}_{m,\text{sfv}}^{(j)}, \bar{\mathbf{r}}_{m,n}^{(j)})$ sent from $\bar{q}_N(\mathbf{x}_n, \underline{\mathbf{y}}_{m,n}^{(j)}, \bar{\boldsymbol{\beta}}_{m,n}^{(j)}, \bar{a}_{m,n}^{(j)}; \mathbf{z}_n^{(j)})$ to the new PR variable node $\bar{\mathbf{y}}_{m,n}^{(j)}$ are given as follows with $\bar{\mathcal{D}}_{0,n}^{(j)} \triangleq \{0, \tilde{\mathcal{D}}_n^{(j)}\}$,

$$\begin{aligned} & \phi(\underline{\mathbf{p}}_{m,\text{sfv}}^{(j)}, \bar{\mathbf{r}}_{m,n}^{(j)}) \\ &= \sum_{\bar{\mathbf{r}}_{mm,n}^{(j)} \in \{0,1\}} \sum_{\bar{a}_{m,n}^{(j)} \in \bar{\mathcal{D}}_{0,n}^{(j)}} \varsigma(\bar{a}_{m,n}^{(j)}) \iint \alpha(\mathbf{x}_n) \bar{q}_N(\mathbf{x}_n, \underline{\mathbf{p}}_{m,\text{sfv}}^{(j)}, \bar{\mathbf{r}}_{m,n}^{(j)}, \bar{u}_{mm,n}^{(j)}, \bar{\mathbf{r}}_{mm,n}^{(j)}, \bar{a}_{m,n}^{(j)}; \mathbf{z}_n^{(j)}) d\mathbf{x}_n d\bar{u}_{mm,n}^{(j)}. \end{aligned} \quad (45)$$

We further obtain the messages $\phi(\underline{\mathbf{p}}_{m,\text{sfv}}^{(j)}, 1)$ for existing new PSFVs as

$$\phi(\underline{\mathbf{p}}_{m,\text{sfv}}^{(j)}, 1) = \varsigma(\bar{a}_{m,n}^{(j)} = 0) \iint \alpha(\mathbf{x}_n) \bar{q}_N(\mathbf{x}_n, \underline{\mathbf{p}}_{m,\text{sfv}}^{(j)}, 1, \bar{u}_{mm,n}^{(j)}, 1, 0; \mathbf{z}_n^{(j)}) d\mathbf{x}_n d\bar{u}_{mm,n}^{(j)}, \quad (46)$$

and the messages $\phi(\underline{\mathbf{p}}_{m,\text{sfv}}^{(j)}, 0) \triangleq \phi_{m,n}^{(j)}$ for nonexistent new PSFVs as

$$\begin{aligned} \phi(\underline{\mathbf{p}}_{m,\text{sfv}}^{(j)}, 0) &= \sum_{\bar{a}_{m,n}^{(j)} \in \bar{\mathcal{D}}_{0,n}^{(j)}} \varsigma(\bar{a}_{m,n}^{(j)}) \underbrace{\left(\iint \alpha(\mathbf{x}_n) f_D(\underline{\mathbf{p}}_{m,\text{sfv}}^{(j)}) f_D(\bar{u}_{mm,n}^{(j)}) d\mathbf{x}_n d\bar{u}_{mm,n}^{(j)} \right)}_{=1} \\ &= \sum_{\bar{a}_{m,n}^{(j)} \in \bar{\mathcal{D}}_{0,n}^{(j)}} \varsigma(\bar{a}_{m,n}^{(j)}). \end{aligned} \quad (47)$$

8) *Measurement Update for Legacy PRs*:

a) *LoS propagation path*: The messages $\kappa(\underline{\boldsymbol{\beta}}_{00,n}^{(j)}) \triangleq \kappa(\underline{\mathbf{u}}_{00,n}^{(j)}, \underline{\mathbf{r}}_{00,n}^{(j)})$ sent from the LoS PR related factor node $\underline{q}_P(\mathbf{x}_n, \underline{\boldsymbol{\beta}}_{00,n}^{(j)}, \underline{\mathbf{a}}_{00,n}^{(j)}; \mathbf{z}_n^{(j)})$ to the LoS PR state variable node $\underline{\boldsymbol{\beta}}_{00,n}^{(j)}$ are obtained as

$$\kappa(\underline{\mathbf{u}}_{00,n}^{(j)}, 1) = \sum_{\underline{\mathbf{a}}_{00,n}^{(j)} \in \mathcal{M}_{0,n}^{(j)}} \eta(\underline{\mathbf{a}}_{00,n}^{(j)}) \int \alpha(\mathbf{x}_n) \underline{q}_P(\mathbf{x}_n, \underline{\mathbf{u}}_{00,n}^{(j)}, 1, \underline{\mathbf{a}}_{00,n}^{(j)}; \mathbf{z}_n^{(j)}) d\mathbf{x}_n, \quad (48)$$

$$\kappa(\underline{\mathbf{u}}_{00,n}^{(j)}, 0) \triangleq \kappa_{00,n}^{(j)} = \eta(\underline{\mathbf{a}}_{00,n}^{(j)} = 0) \int \alpha(\mathbf{x}_n) \delta(\underline{\mathbf{a}}_{00,n}^{(j)} = 0) d\mathbf{x}_n = \eta(\underline{\mathbf{a}}_{00,n}^{(j)} = 0). \quad (49)$$

b) *Single-bounce propagation path*: For $s = s'$, the messages $\kappa(\underline{\boldsymbol{\beta}}_{ss,n}^{(j)}) \triangleq \kappa(\underline{\mathbf{u}}_{ss,n}^{(j)}, \underline{\mathbf{r}}_{ss,n}^{(j)})$ sent from the single-bounce PR related factor node $\underline{q}_S(\mathbf{x}_n, \underline{\mathbf{y}}_{s,n}^{(j)}, \underline{\boldsymbol{\beta}}_{ss,n}^{(j)}, \underline{\mathbf{a}}_{ss,n}^{(j)}; \mathbf{z}_n^{(j)})$ to the single-bounce PR state variable node $\underline{\boldsymbol{\beta}}_{ss,n}^{(j)}$ are obtained as

$$\begin{aligned} \kappa(\underline{\mathbf{u}}_{ss,n}^{(j)}, 1) &= \sum_{\underline{\mathbf{r}}_{s,n}^{(j)} \in \{0,1\}} \sum_{\underline{\mathbf{a}}_{ss,n}^{(j)} \in \mathcal{M}_{0,n}^{(j)}} \eta(\underline{\mathbf{a}}_{ss,n}^{(j)}) \iint \alpha(\mathbf{x}_n) \alpha(\underline{\mathbf{p}}_{s,\text{sfv}}^{(j)}, \underline{\mathbf{r}}_{s,n}^{(j)}) \\ &\quad \times \underline{q}_S(\mathbf{x}_n, \underline{\mathbf{p}}_{s,\text{sfv}}^{(j)}, \underline{\mathbf{r}}_{s,n}^{(j)}, \underline{\mathbf{u}}_{ss,n}^{(j)}, \underline{\mathbf{r}}_{ss,n}^{(j)}, \underline{\mathbf{a}}_{ss,n}^{(j)}; \mathbf{z}_n^{(j)}) d\mathbf{x}_n d\underline{\mathbf{p}}_{s,\text{sfv}}^{(j)}. \end{aligned} \quad (50)$$

We further obtain the messages for existing legacy PRs as

$$\kappa(\underline{\mathbf{u}}_{ss,n}^{(j)}, 1) = \sum_{\underline{\mathbf{a}}_{ss,n}^{(j)} \in \mathcal{M}_{0,n}^{(j)}} \eta(\underline{\mathbf{a}}_{ss,n}^{(j)}) \iint \alpha(\mathbf{x}_n) \alpha_s(\underline{\mathbf{p}}_{s,\text{sfv}}^{(j)}, 1) \underline{q}_S(\mathbf{x}_n, \underline{\mathbf{p}}_{s,\text{sfv}}^{(j)}, 1, \underline{\mathbf{u}}_{ss,n}^{(j)}, 1, \underline{\mathbf{a}}_{ss,n}^{(j)}; \mathbf{z}_n^{(j)}) d\mathbf{x}_n d\underline{\mathbf{p}}_{s,\text{sfv}}^{(j)}, \quad (51)$$

and the messages $\kappa(\underline{u}_{ss,n}^{(j)}, 0) \triangleq \kappa_{ss,n}^{(j)}$ for nonexistent legacy PRs as

$$\kappa(\underline{u}_{ss,n}^{(j)}, 0) = \eta(\underline{a}_{ss,n}^{(j)} = 0) \underbrace{\left(\alpha_{s,n}^{(j)} + \int \alpha(\underline{p}_{s,\text{sfv}}^{(j)}, 1) d\underline{p}_{s,\text{sfv}}^{(j)} \right)}_{=1} = \eta(\underline{a}_{ss,n}^{(j)} = 0). \quad (52)$$

c) *Double-bounce propagation path:* For $s \neq s'$, the messages $\kappa(\underline{\beta}_{ss',n}^{(j)}) \triangleq \kappa(\underline{u}_{ss',n}^{(j)}, \underline{r}_{ss',n}^{(j)})$ sent from the double-bounce PR related factor node $q_D(\mathbf{x}_n, \underline{y}_{s,n}^{(j)}, \underline{y}_{s',n}^{(j)}, \underline{\beta}_{ss',n}^{(j)}, \underline{a}_{ss',n}^{(j)}; \mathbf{z}_n^{(j)})$ to the legacy PR state variable node $\underline{\beta}_{ss',n}^{(j)}$ are obtained as

$$\begin{aligned} \kappa(\underline{u}_{ss',n}^{(j)}, \underline{r}_{ss',n}^{(j)}) &= \sum_{\underline{r}_{s,n}^{(j)} \in \{0,1\}} \sum_{\underline{r}_{s',n}^{(j)} \in \{0,1\}} \sum_{\underline{a}_{ss',n}^{(j)} \in \mathcal{M}_{0,n}^{(j)}} \eta(\underline{a}_{ss',n}^{(j)}) \iiint \alpha(\mathbf{x}_n) \alpha(\underline{p}_{s,\text{sfv}}^{(j)}, \underline{r}_{s,n}^{(j)}) \alpha(\underline{p}_{s',\text{sfv}}^{(j)}, \underline{r}_{s',n}^{(j)}) \\ &\times q_D(\mathbf{x}_n, \underline{p}_{s,\text{sfv}}^{(j)}, \underline{r}_{s,n}^{(j)}, \underline{p}_{s',\text{sfv}}^{(j)}, \underline{r}_{s',n}^{(j)}, \underline{u}_{ss',n}^{(j)}, \underline{r}_{ss',n}^{(j)}, \underline{a}_{ss',n}^{(j)}; \mathbf{z}_n^{(j)}) d\mathbf{x}_n d\underline{p}_{s,\text{sfv}}^{(j)} d\underline{p}_{s',\text{sfv}}^{(j)}. \end{aligned} \quad (53)$$

We further obtain the messages $\kappa(\underline{u}_{ss',n}^{(j)}, 1)$ for existing legacy PRs as

$$\begin{aligned} \kappa(\underline{u}_{ss',n}^{(j)}, 1) &= \sum_{\underline{a}_{ss',n}^{(j)} \in \mathcal{M}_{0,n}^{(j)}} \eta(\underline{a}_{ss',n}^{(j)}) \iiint \alpha(\mathbf{x}_n) \alpha(\underline{p}_{s,\text{sfv}}^{(j)}, 1) \alpha(\underline{p}_{s',\text{sfv}}^{(j)}, 1) \\ &\times q_D(\mathbf{x}_n, \underline{p}_{s,\text{sfv}}^{(j)}, 1, \underline{p}_{s',\text{sfv}}^{(j)}, 1, \underline{u}_{ss',n}^{(j)}, 1, \underline{a}_{ss',n}^{(j)}; \mathbf{z}_n^{(j)}) d\mathbf{x}_n d\underline{p}_{s,\text{sfv}}^{(j)} d\underline{p}_{s',\text{sfv}}^{(j)}, \end{aligned} \quad (54)$$

and the messages $\kappa(\underline{u}_{ss',n}^{(j)}, 0) \triangleq \kappa_{ss',n}^{(j)}$ for nonexistent legacy PRs as

$$\begin{aligned} \kappa(\underline{u}_{ss',n}^{(j)}, 0) &= \eta(\underline{a}_{ss',n}^{(j)} = 0) \underbrace{\left(\int \alpha(\underline{p}_{s,\text{sfv}}^{(j)}, 1) d\underline{p}_{s,\text{sfv}}^{(j)} \int \alpha(\underline{p}_{s',\text{sfv}}^{(j)}, 1) d\underline{p}_{s',\text{sfv}}^{(j)} + \alpha_{s,n}^{(j)} \int \alpha(\underline{p}_{s',\text{sfv}}^{(j)}, 1) d\underline{p}_{s',\text{sfv}}^{(j)} \right.} \\ &\quad \left. + \alpha_{s',n}^{(j)} \int \alpha(\underline{p}_{s,\text{sfv}}^{(j)}, 1) d\underline{p}_{s,\text{sfv}}^{(j)} + \alpha_{s,n}^{(j)} \alpha_{s',n}^{(j)} \right)}_{=1} \\ &= \eta(\underline{a}_{ss',n}^{(j)} = 0). \end{aligned} \quad (55)$$

Based on the messages above, the messages $\gamma(\underline{\beta}_{ss',n}^{(j)}) \triangleq \gamma(\underline{u}_{ss',n}^{(j)}, \underline{r}_{ss',n}^{(j)})$ sent to the next time step $n+1$ are computed as

$$\gamma(\underline{u}_{ss',n}^{(j)}, 1) = \alpha(\underline{u}_{ss',n}^{(j)}, 1) \kappa(\underline{u}_{ss',n}^{(j)}, 1), \quad (56)$$

$$\gamma(\underline{u}_{ss',n}^{(j)}, 0) = \alpha(\underline{u}_{ss',n}^{(j)}, 0) \kappa(\underline{u}_{ss',n}^{(j)}, 0). \quad (57)$$

9) *Measurement Update for New PRs:* The messages $\kappa(\underline{\beta}_{mm,n}^{(j)}) \triangleq \kappa(\underline{u}_{mm,n}^{(j)}, \underline{r}_{mm,n}^{(j)})$ sent from the factor node $\bar{q}_N(\mathbf{x}_n, \underline{y}_{m,n}^{(j)}, \underline{\beta}_{m,n}^{(j)}, \underline{a}_{m,n}^{(j)}; \mathbf{z}_n^{(j)})$ to the new PR variable node $\underline{\beta}_{mm,n}^{(j)}$ are given by

$$\begin{aligned} \kappa(\underline{u}_{mm,n}^{(j)}, 1) &= \sum_{\underline{r}_{m,n}^{(j)} \in \{0,1\}} \sum_{\underline{a}_{m,n}^{(j)} \in \tilde{\mathcal{D}}_{0,n}^{(j)}} \varsigma(\underline{a}_{m,n}^{(j)}) \iiint \alpha(\mathbf{x}_n) \\ &\times \bar{q}_N(\mathbf{x}_n, \underline{p}_{m,\text{sfv}}^{(j)}, \underline{r}_{m,n}^{(j)}, \underline{u}_{mm,n}^{(j)}, \underline{r}_{mm,n}^{(j)}, \underline{a}_{m,n}^{(j)}; \mathbf{z}_n^{(j)}) d\mathbf{x}_n d\underline{p}_{m,\text{sfv}}^{(j)}. \end{aligned} \quad (58)$$

We further obtain the messages $\kappa(\underline{u}_{mm,n}^{(j)}, 1)$ for existing new PRs as

$$\kappa(\underline{u}_{mm,n}^{(j)}, 1) = \varsigma(\underline{a}_{m,n}^{(j)} = 0) \iiint \alpha(\mathbf{x}_n) \bar{q}_N(\mathbf{x}_n, \underline{p}_{m,\text{sfv}}^{(j)}, 1, \underline{u}_{mm,n}^{(j)}, 1, 0; \mathbf{z}_n^{(j)}) d\mathbf{x}_n d\underline{p}_{m,\text{sfv}}^{(j)}, \quad (59)$$

and the messages $\kappa(\underline{u}_{mm,n}^{(j)}, 0) \triangleq \kappa_{mm,n}^{(j)}$ for nonexistent new PRs as

$$\begin{aligned} \kappa(\underline{u}_{mm,n}^{(j)}, 0) &= \sum_{\bar{a}_{m,n}^{(j)} \in \bar{\mathcal{D}}_{0,n}^{(j)}} \varsigma(\bar{a}_{m,n}^{(j)}) \underbrace{\left(\iint \alpha(\mathbf{x}_n) f_{\mathcal{D}}(\bar{\mathbf{p}}_{m,\text{sfv}}^{(j)}) d\mathbf{x}_n d\bar{\mathbf{p}}_{m,\text{sfv}}^{(j)} \right)}_{=1} \\ &= \sum_{\bar{a}_{m,n}^{(j)} \in \bar{\mathcal{D}}_{0,n}^{(j)}} \varsigma(\bar{a}_{m,n}^{(j)}). \end{aligned} \quad (60)$$

C. Belief Calculation

After calculating the messages for all PAs, the belief $\tilde{f}(\mathbf{x}_n)$ of the agent state approximating $f(\mathbf{x}_n | \mathbf{z}_{1:n})$ is given by

$$\tilde{f}(\mathbf{x}_n) = C_n \alpha(\mathbf{x}_n) \prod_{(s,s') \in \mathcal{D}_n^{(j)}} \gamma_{ss'}^{(j)}(\mathbf{x}_n) \prod_{j=1}^J \gamma_{00}^{(j)}(\mathbf{x}_n), \quad (61)$$

with the normalization constant

$$C_n = \left(\int \alpha(\mathbf{x}_n) \prod_{(s,s') \in \mathcal{D}_n^{(j)}} \gamma_{ss'}^{(j)}(\mathbf{x}_n) \prod_{j=1}^J \gamma_{00}^{(j)}(\mathbf{x}_n) d\mathbf{x}_n \right)^{-1}. \quad (62)$$

The beliefs of legacy PSFVs $\tilde{f}(\underline{\mathbf{y}}_{s,n}^{(j)}) \triangleq \tilde{f}(\underline{\mathbf{p}}_{s,\text{sfv}}^{(j)}, \underline{\mathbf{r}}_{s,n}^{(j)})$ with $s \in \mathcal{S}_n^{(j)}$ are given by

$$\tilde{f}(\underline{\mathbf{y}}_{s,n}^{(j)}) = \underline{C}_{s,n} \gamma(\underline{\mathbf{y}}_{s,n}^{(j)}) \quad (63)$$

with the normalization constant $\underline{C}_{s,n} = \left(\int \gamma(\underline{\mathbf{y}}_{s,n}^{(j)}) d\underline{\mathbf{y}}_{s,n}^{(j)} \right)^{-1}$. Similarly, the beliefs of new PSFVs $\tilde{f}(\underline{\mathbf{y}}_{m,n}^{(j)}) \triangleq \tilde{f}(\underline{\mathbf{p}}_{m,\text{sfv}}^{(j)}, \underline{\mathbf{r}}_{m,n}^{(j)})$ with $m \in \mathcal{M}_n^{(j)}$ are given by

$$\tilde{f}(\underline{\mathbf{y}}_{m,n}^{(j)}) = \bar{C}_{m,n} \phi(\underline{\mathbf{y}}_{m,n}^{(j)}), \quad (64)$$

with the normalization constant $\bar{C}_{m,n} = \left(\int \phi(\underline{\mathbf{y}}_{m,n}^{(j)}) d\underline{\mathbf{y}}_{m,n}^{(j)} \right)^{-1}$.

At each PA j , the beliefs $\tilde{f}(\underline{\beta}_{ss',n}^{(j)}) \triangleq \tilde{f}(\underline{\mathbf{u}}_{ss',n}^{(j)}, \underline{\mathbf{r}}_{ss',n}^{(j)})$ of legacy PRs $(s, s') \in \tilde{\mathcal{D}}_n^{(j)}$ are given by

$$\tilde{f}(\underline{\beta}_{ss',n}^{(j)}) = \underline{C}_{ss',n}^{(j)} \gamma(\underline{\beta}_{ss',n}^{(j)}), \quad (65)$$

with the normalization constant $\underline{C}_{ss',n}^{(j)} = \left(\int \gamma(\underline{\beta}_{ss',n}^{(j)}) d\underline{\beta}_{ss',n}^{(j)} \right)^{-1}$. Similarly, the beliefs $\tilde{f}(\underline{\beta}_{mm,n}^{(j)}) \triangleq \tilde{f}(\underline{\mathbf{u}}_{mm,n}^{(j)}, \underline{\mathbf{r}}_{mm,n}^{(j)})$ of new PRs are given by

$$\tilde{f}(\underline{\beta}_{mm,n}^{(j)}) = \bar{C}_{mm,n}^{(j)} \kappa(\underline{\beta}_{mm,n}^{(j)}), \quad (66)$$

with the normalization constant $\bar{C}_{mm,n}^{(j)} = \left(\int \kappa(\underline{\beta}_{mm,n}^{(j)}) d\underline{\beta}_{mm,n}^{(j)} \right)^{-1}$. The normalization constants C_n , $\underline{C}_{s,n}$, $\bar{C}_{m,n}$, $\underline{C}_{ss',n}^{(j)}$, $\bar{C}_{mm,n}^{(j)}$ ensure that the beliefs are valid probability distributions.

As the integrations involved in the message and belief calculations cannot be obtained analytically, we employ a computationally efficient, sequential, particle-based, message-passing implementation, as outlined in [S2], [S4], [S5]. Specifically, we adopt a ‘‘stacked state’’ approach comprising the agent state, the PSFV states, and the PR states, as detailed in [S5], [S6]. This approach leads to complexity that scales linearly with the number of particles. The supplementary material of [S5] provides a comprehensive description of the weight calculations when using ‘‘stacked states’’.

REFERENCES

- [S1] X. Li, B. Deuschmann, E. Leitinger, and F. Meyer, "Adaptive multipath-based SLAM for distributed MIMO systems," 2025, arXiv. [Online]. Available: <https://arxiv.org/abs/2506.21798>
- [S2] E. Leitinger, A. Venus, B. Teague, and F. Meyer, "Data fusion for multipath-based SLAM: Combining information from multiple propagation paths," *IEEE Trans. Signal Process.*, vol. 71, pp. 4011–4028, Sep. 2023.
- [S3] F. Meyer, T. Kropfreiter, J. L. Williams, R. Lau, F. Hlawatsch, P. Braca, and M. Z. Win, "Message passing algorithms for scalable multitarget tracking," *Proc. IEEE*, vol. 106, no. 2, pp. 221–259, Feb. 2018.
- [S4] F. Meyer, P. Braca, P. Willett, and F. Hlawatsch, "A scalable algorithm for tracking an unknown number of targets using multiple sensors," *IEEE Trans. Signal Process.*, vol. 65, no. 13, pp. 3478–3493, July 2017.
- [S5] A. Venus, E. Leitinger, S. Tertinek, F. Meyer, and K. Witrisal, "Graph-based simultaneous localization and bias tracking," *IEEE Trans. Wirel. Commun.*, vol. 23, no. 10, pp. 13 141–13 158, May 2024.
- [S6] F. Meyer, O. Hlinka, H. Wymeersch, E. Riegler, and F. Hlawatsch, "Distributed localization and tracking of mobile networks including noncooperative objects," *IEEE Trans. Signal Inf. Process. Net.*, vol. 2, no. 1, pp. 57–71, Mar. 2016.